STATE OF NEVADA
AGENCY FOR NUCLEAR PROJECTS
NUCLEAR WASTE PROJECT

DOE/NV/10461--T77

NWPO-TR-023-95

INVESTIGATION OF THE IMPACT OF SPARSE DATA ON THE USE OF GEOSTATISTICAL APPROACHES

by

Gregg W. Lamorey and Elizabeth A. Jacobson
Water Resources Center
Desert Research Institute
University and Community College System of Nevada

October 1995

The Nevada Agency for Nuclear Projects/Nuclear Waste Project Office (NWPO) was created by the Nevada Legislature to oversee federal high-level nuclear waste activities in the State. Since 1985, it has dealt largely with the U.S. Department of Energy's siting of a high-level nuclear waste repository at Yucca Mountain in southern Nevada. As part of its oversight role, NWPO has contracted for studies of various technical questions at the Yucca Mountain Project.

DISCLAIMER

EXECUTIVE SUMMARY

The hydrogeologic flow system at Yucca Mountain, both saturated and unsaturated conditions, will have to be fully understood prior to emplacement of waste in any repository. Flow and transport modeling based on the conceptual model of the flow system should lead to a better understanding of the system, as well as yield pre-emplacement predictions of the possible performance of the repository. The hydrologic properties needed to understand both the saturated and unsaturated flow at Yucca Mountain are expected to be based on small-scale measurements (i.e., laboratory-scale measurements or hydraulic testing of boreholes) and extrapolated to evaluate field-scale problems (Site Characterization Plan, Yucca Mountain Site, 1988, page 8.3.1.2-67). The suggested approach to assess the extrapolation error is the use of geostatistical methods that require the estimation of spatial correlation in the data, usually calculated from a semivariogram. This information is used, in turn, to generate realizations for a Monte Carlo analysis of the model uncertainty produced by the extrapolation errors.

The quantity of data available to determine the spatial correlation of hydrologic properties at Yucca Mountain will be sparse and this will lead to uncertainties about the correlation length and overall variance in the data. In many hydrologic studies, the variance of the data increases with the collection of additional data because of the increased probability of sampling either larger or smaller values of the hydrologic property. An investigation of the impact of sparse data on the estimation of correlation length and variance using geostatistical approaches will indicate the degree of reliability of the estimates. The results of the investigation may also be used to suggest the level of characterization necessary for a desired level of reliability in the estimates of correlation length and variance. Once the spatial correlation of the hydrologic properties is established, this information will be used to extrapolate values between the measurement points to generate a field-scale description of the properties for input to modeling studies.

The uncertainty in model output caused by the extrapolation error can be assessed by generating many "realizations" of the field-scale properties and conducting a statistical analysis of the corresponding model outputs, called a Monte Carlo analysis. The number of realizations that are required to reproduce the input statistics is dependent on the sampling method. Pure random sampling could require a very large number of realizations (e.g., 600 to 1000) to guarantee that values are obtained from the tails of the statistical distribution (i.e., large and small values). A sampling method called Latin Hypercube sampling produces values from the entire statistical distribution with a fewer number of realizations (e.g., 100). Although the Latin Hypercube sampling method was not initially developed for use with spatially correlated properties, it has been applied to transmissivities that varied in space. However, this is only one application and additional research is needed before this approach can have widespread use.

The research presented in the following three papers was conducted by the Water Resources Center (WRC), Desert Research Institute (DRI) in support of the Nevada Nuclear Waste Project Office activities related to the proposed high-level radioactive waste repository at Yucca Mountain. The research involved investigating the impact of sparse data on the estimation of correlation length and variance using geostatistical approaches and developing consistent information for use in a

Monte Carlo analysis. The research discussed in the first paper consisted of modifying and developing methods to estimate the semivariogram parameters. These methods were also used to investigate the estimation error of the semivariogram parameters when sparse data were available. The investigation required applying the methods to a synthetic data set and decreasing the number of data used in the semivariogram analysis. The methods presented in the paper yield an approach that can be used to help evaluate the level of uncertainty in the estimated semivariogram parameters.

The second paper presents research on the application of a geostatistical method called kriging to data that exhibit a trend. Kriging is an interpolation technique that considers the spatial correlation in the data and yields estimates at locations where no data exist and the corresponding estimation errors. The trended data that are used in the research are hydraulic heads from an aquifer in southern Arizona. A new method is developed that allows estimation of the trend in the data with the inclusion of "soft information" on hydraulic heads along the boundaries. The "soft information" consists of knowledge of no-flow boundaries along portions of the aquifer and is implemented in the method as constraints on the hydraulic head gradient along these boundaries. The appropriate weighting of these constraints is investigated by examining the tradeoff in fitting head measurements and no-flow boundary conditions. The results of the research showed that boundary constraints can improve the fit of the estimated heads to the no-flow boundaries with little deterioration of the fit to the head measurements. Thus, this new method allows inclusion of "soft information" in the geostatistical analysis of trended data, which yields more realistic estimates of interpolated data when kriging is used.

The hydraulic head estimates developed by the research discussed in the second paper were used as input data to an inverse model for groundwater flow. The results of the inverse modeling are consistent hydraulic properties (transmissivity) and their corresponding estimation errors, which can be used in a Monte Carlo analysis to investigate uncertainties in model output. The application of the inverse modeling based on the estimates of hydraulic heads with constraints on the no-flow boundaries is given in the third paper. In a previous inverse modeling study of the same aquifer conducted by Jacobson (1985), it was observed that when gradients in the prior hydraulic head distribution do not match the assumed no-flow boundary conditions, the inverse model can produce low transmissivity values along these no-flow boundaries. These low transmissivities are produced by the model in an attempt to reconcile inconsistencies in the head gradients and the boundary conditions. When estimates of hydraulic heads that include the constraints on the head gradient along the no-flow boundaries were used, the transmissivities along these boundaries were not unusually low. In addition, the estimation errors of the transmissivity along these boundaries were lower. The inclusion of the estimates of hydraulic heads with constraints on the no-flow boundaries in the inverse modeling led to more consistent estimates of transmissivity and corresponding estimation errors for use in a Monte Carlo analysis of uncertainty in model outputs. The next step would be to conduct a Monte Carlo analysis with Latin Hypercube sampling.

ABSTRACT

Techniques to estimate semivariogram parameters are investigated with respect to assessing the effects of sparse data and detecting the presence of a trend. These techniques are applied to the determination of semivariogram parameters used in the estimation of hydraulic head values at node locations from measured head data. The presence of no-flow boundaries is included in the estimation of hydraulic heads at node values by applying constraints to the head gradient across the no-flow boundaries. The resulting hydraulic head estimates are used in an inverse groundwater flow model to assess the impact of the no-flow boundary constraints on transmissivities determined from the inverse model. It is found in a case study that when gradients in the prior head distribution do not match assumed no-flow boundaries, the inverse model can produce low transmissivity values along these no-flow boundaries. Prior heads estimated with constraints on the head gradient across no-flow boundaries did not produce the low transmissivity values along no-flow boundaries.

CONTENTS

FIGURES

TABLE

INTRODUCTION

Although it is more traditional to describe a set of three papers starting with the first paper, the motivation for this work is a problem described in the third paper, Estimation of Aquifer Parameters Using Hydraulic Heads Estimated with Constraints on the Hydraulic Head Gradient Across No-Flow Boundaries. When using an inverse groundwater model with prior information, the degree of improvement in the transmissivities relies on the quality of the prior heads used in the model. If head estimates at nodes are to be used in the inverse model, then the method used to estimate the heads at nodes governs how effective the inverse model will be. Methods used to estimate the nodal heads from head measurements do not usually consider the gradient of the estimated heads. This can lead to inappropriate head gradients in regions where there are few head measurements, especially across no-flow boundaries where a non-zero head gradient will violate the boundary condition.

In the second paper, Incorporation of Constraints on Hydraulic Head Gradients Near No-Flow Boundary Conditions in the Determination of Spatial Drift, a method is developed to include constraints on the head gradient across no-flow boundaries when estimating head values at node points. This method assumes the head is composed of a polynomial drift component and a residual component. The constraints on the head gradient are included in the determination of the drift component. These constraints provide a way to include subjective or soft information concerning the presense of a no-flow boundary into the estimation of the nodal head values.

The weighting of the boundary constraints described in the second paper are evaluated by examining the tradeoff in fitting the head measurements and the boundary conditions, as well as examining the head residuals. The head residuals should have a zero-mean normal distribution and should exhibit a sample semivariogram with a distinct sill. The semivariogram parameters of the head residuals are also used in the generalized least squares regression used to determine the drift. During the development of the method presented in the second paper, it became evident that a technique to evaluate changes in the head residual semivariogram parameters and determine if the head residuals contain a trend was important to determine the correct order for the drift polynomial and the appropriate weighting of the boundary constraints.

The estimation and evaluation of semivariogram parameters is considered in the first paper, entitled Estimation of Semivariogram Parameters and Evaluation of the Effects of Data Sparcity. In this paper, a weighted least squares method and a jackknife kriging method are used to estimate semivariogram parameters. The weighted least squares method fits the sample semivariogram, while the jackknife kriging method minimizes the jackknifing error as a function of the semivariogram parameters. When the two methods yield different results, more data may be needed to reliably determine the semivariogram parameters, or a trend may be present in the data. One interesting feature of the jackknife kriging method of determining semivariogram parameters is that the jackknifing error that is minimized by the method can in turn be used to evaluate the effect of

other changes, such as the weighting of the boundary constraints considered in the second paper. This and the fact that the jackknife kriging method does not rely on the sample semivariogram make this method a powerful tool in optimization problems involving spatial data.

The semivariogram parameter estimation methods presented in the first paper can be used in applications other than those demonstrated in the second paper. The head residuals considered in the second and third papers are assumed to possess a zero nugget, the semivariogram parameter estimation methods in the first paper are generalized to include non-zero nuggets as well. The method has been developed for a spherical semivariogram model but can be adapted to other semivariogram models that exhibit distinct sills. The effects of data sparcity are investigated by varying the lag increment and maximum lag used in the weighted least squares method, and varying the number of kriging points used in the jackknife kriging method. Sparse data sets will produce poorly defined sample semivariograms that are difficult to fit with confidence using the weighted least squares method, whereas the jackknife kriging method does not rely on the sample semivariogram.

Determination of estimation errors is often just as important as the estimates themselves, especially in inverse problems where the estimation errors are carried through the model and used in the weighting of model parameters. In the second paper, a new method to determine the head estimation errors is presented that includes the drift component and the residual component of the error. The semivariogram parameters determined by methods described in the first paper should also help to improve the determination of the head estimation error.

The semivariogram parameter estimation methods of the first paper are applied to synthetic two-dimensional data sets containing 400, 200, and 100 points. These methods are also applied to estimation of hydraulic head values in a case study of the Avra Valley aquifer in southern Arizona considered in the second paper. The Avra Valley aquifer case study is further investigated in the third paper where an inverse model is used with prior heads estimated with and without the boundary constraints described in the second paper. Without the boundary constraints on the prior heads, the inverse model of the Avra Valley aquifer resulted in low transmissivity estimates along some no-flow boundaries where the model was attempting to reconcile the misfit between the head gradient and the boundary condition. The boundary constraints on the prior heads help to alleviate this problem.

Taken together, the three papers presented here provide an interesting example of how a very specific problem, inconsistencies between estimated head gradients and assumed boundary conditions in an inverse groundwater model, leads to the development of a method to include constraints on head gradients when estimating head values, which in turn lead to the development of very general methods to estimate semivariogram parameters. These papers demonstrate how parameter estimation problems, such as the inverse groundwater model, rely on solutions to

parameter estimation problems, such as estimating nodal head values and estimation errors, which in turn rely on solutions to parameter estimation problems, such as estimating semivariogram parameters. This hierarchy also implies that the most sophisticated inverse groundwater model is only as powerful as the methods used to derive the prior transmissivity and head estimates and their associated estimation errors.

ESTIMATION OF SEMIVARIOGRAM PARAMETERS AND EVALUATION OF THE EFFECTS OF DATA SPARSITY

ABSTRACT

Semivariogram parameters are estimated by a weighted least squares method and a jackknife kriging method. The weighted least squares method is investigated by varying the lag increment and maximum lag used in the fit. The jackknife kriging method minimizes the variance of the jackknifing error as a function of semivariogram parameters. The effects of data sparsity and the presence of a trend are investigated by using 400-, 200-, and 100-point synthetic data sets. When the two methods yield significantly different results, more data may be needed to reliably determine the semivariogram parameters, or a trend may be present in the data.

INTRODUCTION

Realistic modeling of natural processes often relies on an understanding of how model variables change from one location to another. The semivariogram is an important geostatistical tool in the determination of a variable's spatial characteristics. The fitting of a semivariogram to field data and the evaluation of this fit is usually done in a very subjective manner. More quantitative methods are needed to estimate and evaluate semivariogram parameters especially when assessing small changes in a variable's spatial characteristics or when limited field data are available.

Quantitative methods of estimating semivariogram parameters usually require the fitting of a sample semivariogram calculated from the data to a theoretical semivariogram model. Semivariogram parameters can be estimated using a variety of methods, one of the most common quantitative methods is a weighted least squares fit described by Cressie (1985). McBratney and Webster (1986) compare weighted least squares, generalized least squares, and maximum likelihood methods for fitting sample semivariograms and conclude that the weighted least squares method is often preferred because it gives good results and is not computationally demanding.

There are two values that are set, often arbitrarily, prior to the fitting of a sample semivariogram: the lag increment used to calculate the sample semivariogram, and the maximum lag considered in the fit. There are practical "rules of thumb" for these values that will yield reliable results given enough data (Journel and Huijbregts, 1978). In this investigation, the weighted least squares semivariogram fit is evaluated by examining the effects of changes in the lag increment and maximum lag values. In this study, the sensitivity of the semivariogram fit to small changes in the lag increment is used to evaluate if there are enough data to accurately define the sample semivariogram. The sensitivity of the semivariogram fit to the maximum lag distance is also used to evaluate data sparsity and to determine if the data have a trend.

Another method of estimating semivariogram model parameters using jackknife kriging is presented. Jackknife kriging is usually used for semivariogram model validation where a jackknifing error is calculated for specific semivariogram parameters determined from a sample semivariogram fit. The jackknife kriging method presented here estimates the semivariogram parameters by minimizing the jackknifing error as a function of the semivariogram parameters. This method estimates semivariogram parameters without calculation of the sample semivariogram.

The jackknife kriging method presented here is similar to a method described by Knudsen and Kim (1978). However, Knudsen and Kim (1978) identify the minimum jackknife error by trying various semivariogram parameters, whereas a search algorithm is described here. Solow (1990) and Kitanidis (1991) caution against using this type of cross validation technique to infer model covariance functions from raw covariance estimates. The jackknife kriging method is not advocated as a replacement to the calculation and analysis of sample semivariograms. Both types of methods should be applied and if results differ significantly, then the data need to be examined closer to determine why. Two possible reasons investigated here are insufficient data to define the sample semivariogram and the presence of a trend in the data.

The jackknife kriging and weighted least squares method provide two fundamentally different methods of estimating semivariogram parameters. The methods are demonstrated using two-dimensional, spatially correlated synthetic data. The effects of data sparsity on the determination of the spatial characteristics are investigated using different-sized data sets. With the most dense data set, it is expected that the jackknife kriging and weighted least squares methods will agree and the weighted least squares fit will not be sensitive to small changes in the lag increment and maximum lag used in the fit. As the size of the data set is decreased, the deterioration in the performance of the two methods will be examined. The assumption of a second order stationary process is investigated by analyzing the synthetic data with and without a trend.

The synthetic data is generated and semivariogram parameters are fit using a spherical semivariogram model. Other semivariogram models, such as Gaussian and exponential can be used in this type of analysis providing that the model displays a distinct sill. Nested models with several parameters are not considered here. Nested models should be used with care when analyzing sparse data to avoid fitting features that may be a product of data sparcity.

SEMIVARIOGRAM PARAMETER ESTIMATION

The semivariogram, $\gamma(x_1,x_2)$, is a function of the variance of the random function, Z, over the increment $[Z(x_1)-Z(x_2)]$ and is defined as:

$$\gamma(x_1,x_2) = \frac{1}{2} Var\left[Z(x_1) - Z(x_2)\right] \qquad (1)$$

If the semivariogram depends only on the distance between points, x_1 and x_2, then the sample semivariogram can be calculated by considering pairs of data points separated by a lag distance:

$$\hat{\gamma}(s) = \frac{1}{2N'} \sum_{i=1}^{N'} [Z(x_i + s) - Z(x_i)]^2 \qquad (2)$$

where N' is the number of data pairs at the lag distance s.

For the calculated sample semivariogram of equation (2) to be equivalent to the semivariogram of equation (1), the data must follow a type of second order stationarity commonly called the intrinsic hypothesis. The intrinsic hypothesis asserts that for a random function, $Z(x)$, the mean exists and does not depend on location; and for all vectors, s, the increment $[Z(x+s)-Z(x)]$ has a finite variance which does not depend on x. The presence of a drift results in a mean that is dependent on location, which violates the intrinsic hypothesis.

Semivariogram models are often characterized by three parameters: a sill, a range, and a nugget effect (Figure 1). The degree of correlation between values of a variable measured at two locations, $Z(x)$ and $Z(x+s)$, usually decreases as the lag distance increases. As the correlation decreases, the value of the sample semivariogram increases. The lag distance at which the correlation becomes zero is the range. At the lag value equal to the range, the sample semivariogram value will often stop increasing and level off at a value called the sill. If the sample semivariogram values continue to increase with increasing lags, a trend or drift may be present. As the lag distance goes to zero, the sample semivariogram may also approach zero, or it may approach a positive value called the nugget. The nugget effect is caused by measurement errors or small-scale variations in the measured values.

The semivariogram parameters can also be characterized as a range, total sill, and nugget ratio. The total sill is the sum of the sill and nugget (see Figure 1), while the nugget ratio is the ratio of the nugget to the total sill. This results in a semivariogram model that is scaled by one of the semivariogram parameters, the total sill. This is a condition that is necessary for the jackknife kriging method and convenient for the weighted least squares method.

Various theoretical semivariogram models have been developed, including spherical, exponential, and Gaussian models. For the analysis presented here, a spherical model is used, but the technique can be used with other semivariogram models as well. The semivariogram value, γ, for the spherical model can be expressed as:

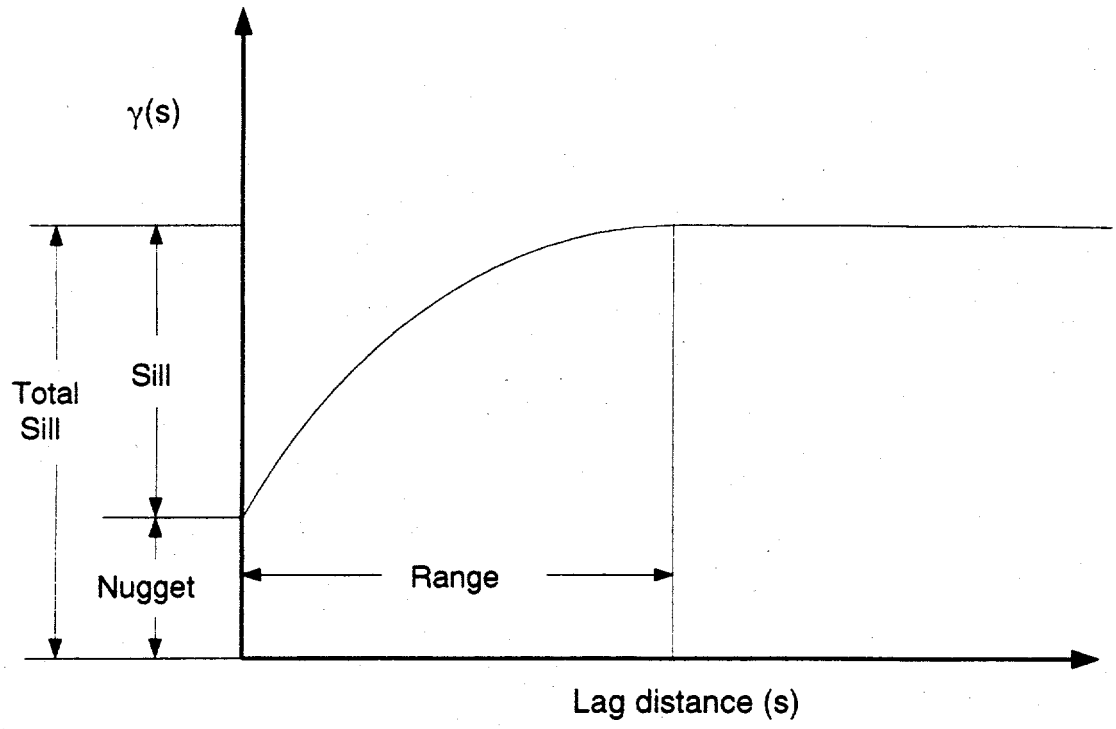

Figure 1. Characteristic features of a semivariogram.

$$\gamma(s;\lambda) = \begin{cases} c_t(c_r + (1 - c_r)[(3/2)(s/a) - (1/2)(s/a)^3]) & 0 < s \leq a \\ c_t & s \geq a \end{cases} \tag{3}$$

where s is the lag and λ represents the semivariogram parameters expressed as a nugget ratio, c_r, a total sill, c_t, and a range, a.

Weighted Least Squares

Once the theoretical semivariogram model has been selected, a weighted least squares fit described by Cressie (1985) can be used to estimate the semivariogram sill, range, and nugget. The following function is minimized with respect to λ:

$$\sum_{j=1}^{k} \frac{N_{s(j)}}{\gamma^2(s(j);\lambda)} \{\gamma^*(s(j)) - \gamma(s(j);\lambda)\}^2 \tag{4}$$

where each value of j represents an increment in the lag, $s(j)$ is the lag distance, $N_{s(j)}$ is the number of pairs used to calculate the semivariogram value, $\gamma^*(s(j))$ is the semivariogram value calculated from the measured data, and $\gamma(s(j); \lambda)$ is the semivariogram value calculated from the estimated parameters, λ. The least squares fit is weighted by $N_{s(j)}/\gamma^2(s(j); \lambda)$ so that more weight is given to semivariogram lags that are small compared to the range and to lags with a greater number of pairs.

The spherical semivariogram model fit requires the minimization of the following function obtained by combining equations (3) and (4):

$$f(s; c_r, c_t, a) = \sum_{j=1}^{(a)} N_{s(j)} \left\{ \frac{\gamma^*(s(j))}{c_t(c_r + (1 - c_r)[(3/2)(s(j)/a) - (1/2)(s(j)/a)^3])} - 1 \right\}^2 + \sum_{j=(a)+1}^{k} N_{s(j)} \left(\frac{\gamma^*(s(j))}{c_t} - 1 \right)^2 \quad (5)$$

where the brackets on the a in the summations indicate that the first summation considers lags out to the range and the second summation considers lags beyond the range.

The total sill, c_t, can be determined by setting $\partial f/\partial c_t$ equal to zero. To solve for a and c_r, the function of equation (5) must be minimized with respect to a and c_r. This is done using Powell's quadratically convergent method described by Press et al. (1986) in the two dimensions, a and c_r.

There are two parameters that can be varied in this fitting procedure: the lag increment used to calculate the sample semivariogram, and the maximum lag used to make the fit. A practical rule for the maximum lag suggested by Journel and Huijbregts (1978) is one half of the distance across the field of the data. A practical rule for the lag increment is not as straightforward. Journel and Huijbregts (1978) suggest that lags with less than 30 data pairs not be included in the sample semivariogram fit. To define the sample semivariogram at lags less than the range, the lag increment should be chosen so that there are at least three to five lags with more than 30 data pairs less than the range. This can be a problem when limited data are available and when the range is small compared to the field of the data.

Small changes in the lag increment result in a slightly different grouping of the pairs of data values when calculating the sample semivariogram. If a small change in this grouping results in a large change in the resulting semivariogram fit, then more data are needed to define a sample semivariogram that is not dependent on the grouping of the data. To minimize the effect of the choice of the lag increment in calculating the sample semivariogram, several lag increments are considered and their results are averaged. The variance of the semivariogram parameters calculated with

different lag increments can be used to evaluate the sensitivity of the semivariogram parameters to the lag increment.

Changes in the semivariogram fit due to changes in the maximum lag indicate how sensitive the fit is to the sample semivariogram values calculated at the maximum lag and if the data exhibit a trend. An unreliable sample semivariogram fit is indicated if a small increase in the number of sample semivariogram values included in the fit results in large changes in the estimated semivariogram parameters. If the value of the total sill increases with the number of lags included in the fit, then a trend in the data is indicated. The orientation of the trend can be identified by fitting sample semivariograms calculated along different directions called directional semivariograms.

Semivariogram Parameter Determination by Jackknife Kriging

The semivariogram parameters can be calculated using a kriging technique called jackknifing. Jackknife kriging systematically deletes one data point at a time and then calculates a value by kriging. The error of the kriged estimates should have a mean of zero and should be consistent with theoretical estimates of errors. A thorough discussion of kriging theory is presented by Journel and Huijbregts (1978).

The kriging estimator, Z'_m, is a linear combination of several of the observed data, expressed as:

$$Z'_m = \sum_{i=1}^{N_m} a_{mi} Z^*_{mi} \tag{6}$$

where there are N_m observations, Z^*_{mi}, to be used to estimate Z at location m. The kriging coefficients, α_{mi}, are calculated to ensure that the kriging estimator is unbiased, and that the variance of the estimation error is minimized.

The kriging coefficients are determined from the following kriging equations:

$$\begin{aligned} &\sum_{j=1}^{N_m} a_{mj}\gamma(\underline{x}_{mi}, \underline{x}_{mj}) - a_{mi}\sigma^2_{mi} + \beta_m = \gamma(\underline{x}_{mi}, \underline{x}_m), \quad i = 1, 2, \ldots, N_m \\ &\sum_{j=1}^{N_m} a_{mj} = 1 \end{aligned} \tag{7}$$

yielding N_m+1 equations and unknowns for each estimation location, m. β_m is a Lagrange multiplier, γ is calculated from the semivariogram, and $\sigma_{mi}{}^2$ is the variance of the measurement error for the i^{th} data.

The kriging variance, V_K, at location m is given by the diagonal terms of the covariance matrix of the kriging estimation error:

$$V_{K,mm} = -\gamma(\underline{x}_m, \underline{x}_m) + \sum_{i=1}^{N_m} \alpha_{mi}\gamma(\underline{x}_{mi}, \underline{x}_m) + \beta_m \tag{8}$$

The "kriging error" is the positive square root of the kriging variance and is the standard error of estimation.

The difference between the measured and kriged values at the measurement points yields an error called the "jackknifing error," that should have a mean of zero. This can be checked by summing the errors over all of the N measurement locations:

$$\frac{1}{N}\sum_{i=1}^{N}[Z_i' - Z_i^*] \approx 0 \tag{9}$$

The variance of the jackknifing errors, V_{JK}, can be calculated as:

$$V_{JK} = \frac{1}{N-1}\sum_{i=1}^{N}[Z_i' - Z_i^*]^2 \tag{10}$$

The variance of the jackknifing errors reflects the accuracy of the kriging procedure. The variance of the jackknifing errors should be as small as possible and certainly less than the variance of the original data.

The kriging error gives a theoretical estimate of the error expected from kriging. It depends only on the location of the data and the semivariogram parameters and is independent of the actual data values. The jackknifing error is based on the data values and the kriged estimates. If the jackknifing errors are consistent with the kriging errors, then the following equation should hold:

$$\left\{\frac{1}{N}\sum_{i=1}^{N}\frac{[Z_i' - Z_i^*]^2}{V_{K,ii}}\right\}^{1/2} \approx 1 \tag{11}$$

Jackknifing is usually used to check an estimate of the semivariogram parameters. However, if the variance of the jackknifing errors of equation (10) is minimized with respect to the semivariogram parameters, then the optimum semivariogram parameters for kriging can be identified without relying on the sample semivariogram. The minimization depends on an understanding of the relationship between jackknifing errors, kriging errors, and the semivariogram parameters.

The semivariogram parameters are used in kriging to determine the relative weighting of data points based on the distance between points. The kriging estimator, $Z_i^{'}$, is independent of the total sill because the weights are all scaled by this value. Because of this, the variance of the jackknifing errors can be minimized with a search in the two dimensions, the range and nugget ratio. As with the weighted least squares semivariogram fit, Powell's quadratically convergent method (Press et al., 1986) is used for this minimization. The minimization can be computationally intensive if there are many data values since a matrix must be inverted for each data point when jackknifing. The size of this matrix is equal to the number of points used in the kriging procedure.

The number of data points used to calculate the kriging estimator must be set prior to jackknifing. These values are often determined subjectively. The best choice for the number of data points can be determined by varying the number of points used when minimizing the jackknifing error with respect to the range and nugget ratio. If small changes in the number of data points used in jackknifing result in large changes in the calculated semivariogram parameters, then more data may be required to achieve a reliable result.

The total sill can be estimated from the variance of the data. The variance of the data should be slightly smaller than the total sill since spatially correlated values are included in the calculation of the variance but not in the total sill. The total sill can also be estimated by setting the kriging variance equal to the variance of the jackknifing errors, a relationship expressed in equation (11). The kriging variance is a function of the total sill, nugget ratio, and range, while the jackknifing errors rely only on the range and nugget ratio. These two methods of determining the total sill provide a means to check the estimated semivariogram parameters.

The method to estimate semivariogram parameters from jackknifing is similar in many ways to the weighted least squares fit of the sample semivariogram. Both methods search for a minimum over the two parameters, the range and nugget ratio, and then derive a value for the total sill. If the two methods yield very different results, then either more data are required or the variable may be non-intrinsic.

SYNTHETIC DATA CASE STUDY

Synthetic Data Generation

A spatially correlated data set is generated using a technique described by Clifton and Neuman (1982). To generate a two-dimensional realization of spatially correlated data points, a random scatter of N points over a range of x and y values is first generated. The values of the spatially correlated random variable, Z, are determined by the following equation:

$$Z = M\varphi \tag{12}$$

where φ is a zero mean, unit variance, N-dimensional random vector with a normal distribution. M is a lower triangular matrix defined as:

$$MM^T = V \tag{13}$$

where V is the covariance matrix for the N values of Z. The values of V are determined from the x, y position of the data points and the desired semivariogram parameters. Values of M are then determined by a Cholesky decomposition of V.

This method has been used to create a two-dimensional, 400-point data set randomly scattered over a 10-by-10-square region that has a range of 1.25, a nugget of 0.5, and a sill of 0.5, or a nugget ratio of 0.5 and a total sill of 1 (Figure 2). The weighted least squares semivariogram fit and the jackknifing methods are used to determine the semivariogram parameters in terms of the range, nugget ratio, and total sill. To examine the effects of sparse data, calculations are made using all 400 data points, only the first 200 data points, and only the first 100 data points. When evaluating these fits, it is important to be aware that the true semivariogram parameters are not exactly equal to the expected values since only one realization of a stochastic process is being considered.

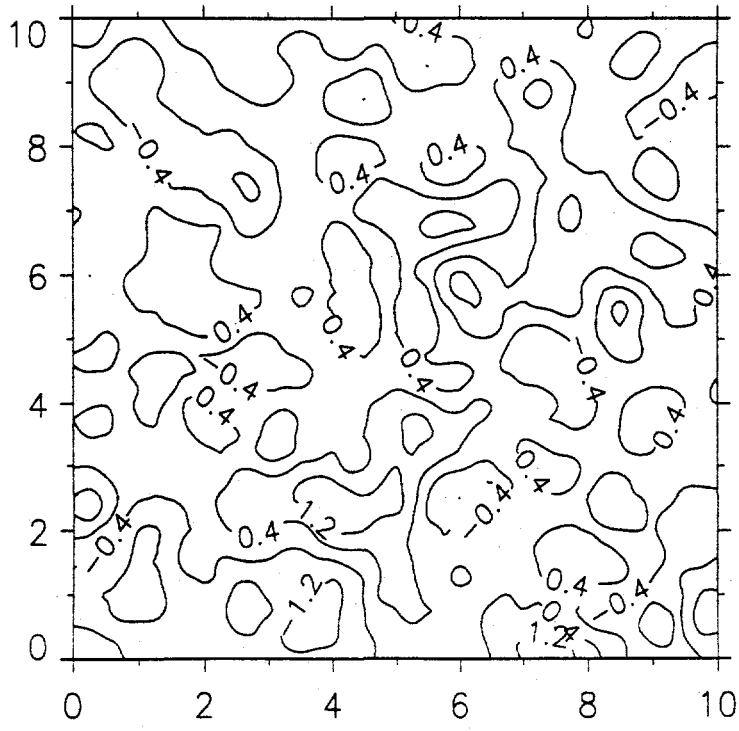

Figure 2. Contour plot of 400-point synthetic data set with range of 1.25, nugget ratio of 0.5, and total sill of 1.

Weighted Least Squares Semivariogram Analysis

Sample semivariograms for the 400-, 200-, and 100-point data synthetic sets are presented in Figure 3. For each data set, sample semivariograms with lag increments of 0.25 and 0.30 are shown. The 400-point data set has a well-formed sample semivariogram with little difference between the two lag increments. The 200-point data set sample semivariogram is less distinct, but a reasonable range, nugget, and sill can still be recognized. The 100-point data set sample semivariogram almost appears to be a pure nugget effect with little similarity between the two lag increments.

The sample semivariograms have been fit to spherical semivariogram models with the weighted least squares method using several lag increments. Figure 4 shows the range, nugget ratio, and total sill calculated for the 400-, 200-, and 100-point data sets using 76 lag increment values between 0.20 and 0.35 at 0.002 intervals. The maximum lag used is 5, one half of the distance across the data field. The semivariogram fit with 400 points changes little with changes in the lag increment and is close to the expected values. The fit with 200 points is stable over the lag increments of 0.24 to 0.30 and are also close to the expected values. Outside this interval of lag increments, the nugget ratio and range vary significantly, but the total sill is stable. With only 100 points, the semivariogram fit for the range and nugget ratio is unstable over the interval of lag increments used, but again the total sill is stable.

Generalizing from the 400-, 200-, and 100-point data set results, as the number of data points used in the weighted least squares fit is decreased, the semivariogram fit becomes unstable with respect to the lag increment value and small changes in the lag increment can result in large changes in the calculated semivariogram parameters. The range is the most sensitive semivariogram parameter to this effect. The nugget ratio changes along with the range but with much less variation. The total sill value is relatively unaffected by changes in the lag increment.

For each lag increment used, the range and nugget ratio are determined by a two-dimensional search for the minimum of the error of the semivariogram fit given by equation (5). To investigate how the error of the semivariogram fit changes with the range and nugget ratio and if there are any potential problems with local minimums, the error of the semivariogram fit can be calculated for various values of range and nugget ratio. For the 400-, 200- and 100-point data sets, the semivariogram fit error has been calculated for range values between 0.5 and 2.5 and nugget ratio values between 0 and 1. Contour plots of the resulting errors are presented in Figure 5 for lag increments of 0.25 and 0.30.

The Figure 5 error contour plots for the 400-point data set show a distinct minimum and little difference for the two lag increments. The error contour plots for the 200-point data set show a less distinct minimum and the shape of the contour plot changes somewhat with the different lags. Low values for the error can be calculated using low range and low nugget ratio values or high range and

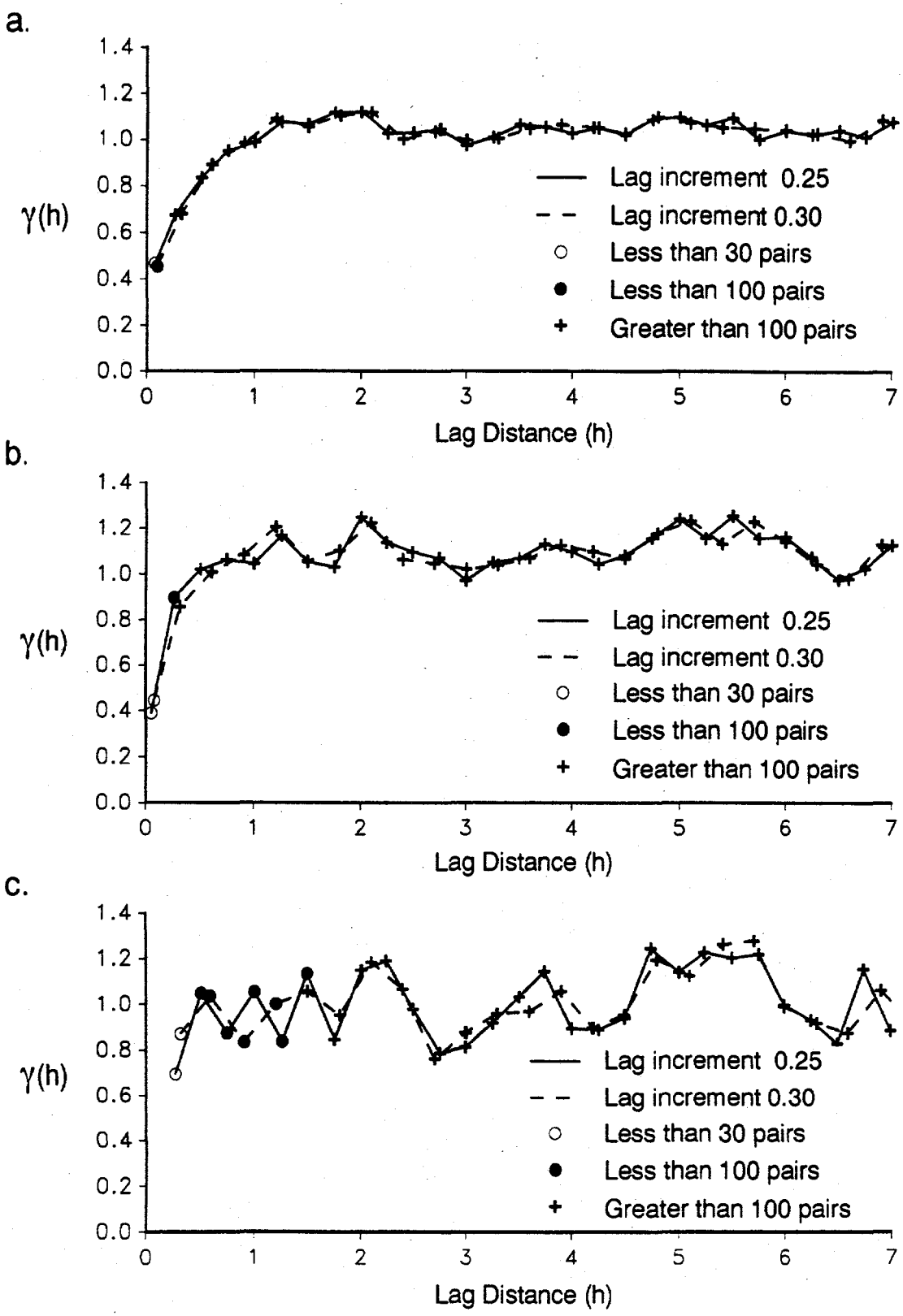

Figure 3. Sample semivariograms with lag increments of 0.25 and 0.30 for (a) 400-point data set, (b) 200-point data set, and (c) 100-point data set.

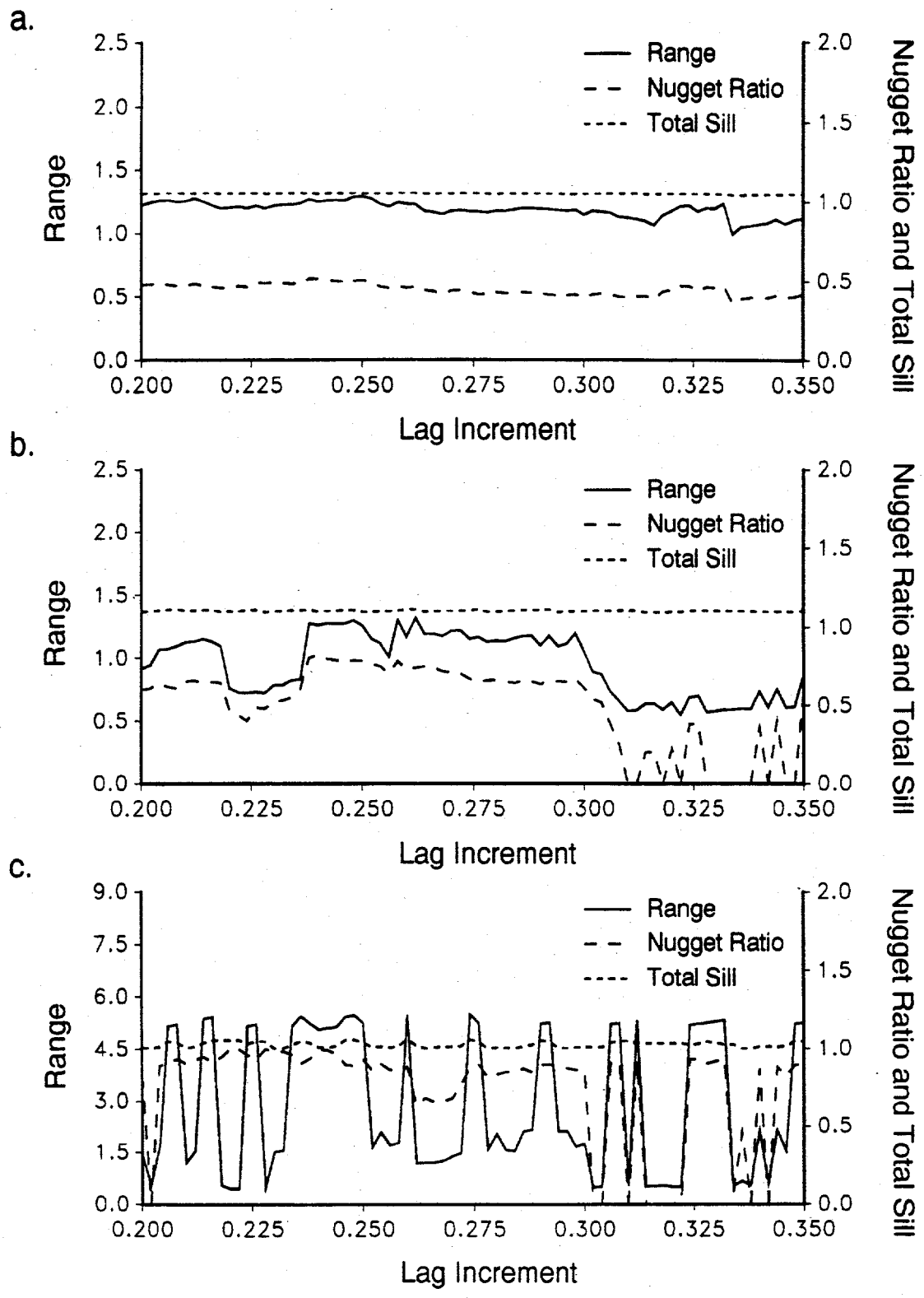

Figure 4. Semivariogram parameters determined with weighted least squares method and various lag increments for (a) 400-point data set, (b) 200-point data set, and (c) 100-point data set.

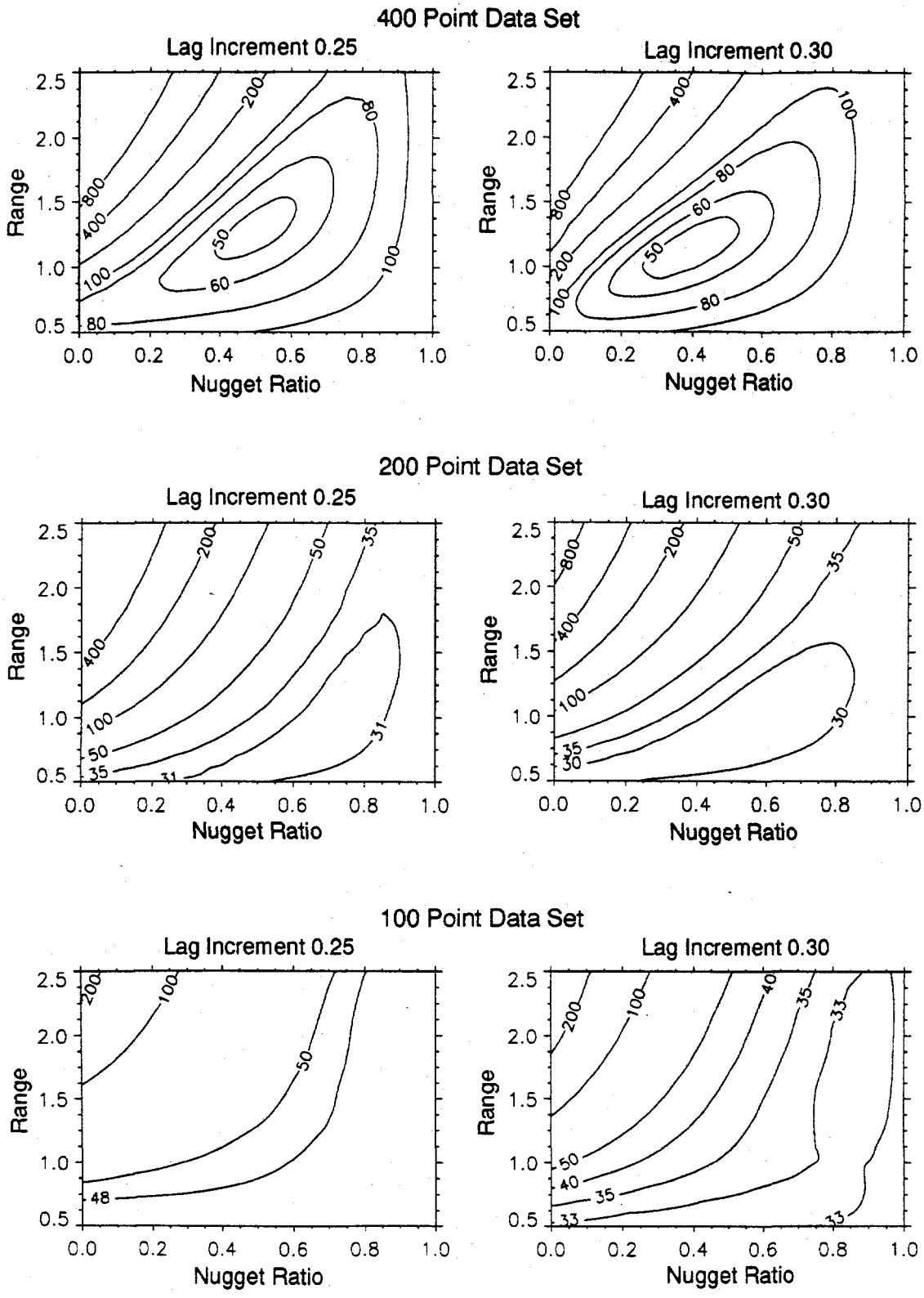

Figure 5. Error contour plots for 400-, 200-, and 100-point data sets using weighted least squares method and lag increments of 0.25 and 0.30.

high nugget ratio values. This can increase the problem of local minimum error values. The 100-point data set error contour plot shows no distinct minimum and again low errors can be obtained from low range and low nugget ratio or high range and high nugget ratio values.

Semivariogram parameters calculated at the lag increments used in the Figure 5 plots are summarized in Table 1. Also presented in Table 1 are the average, standard deviation, and coefficient of variation of the semivariogram parameters calculated for 26 lag increments between 0.25 and 0.30 using lag increment intervals of 0.002. The standard deviation and coefficient of variation values indicate the sensitivity of the calculated semivariogram parameters to changes in the lag increment. These values should not be interpreted as a statistical deviation from a true value but instead as indicators of data sparsity. The semivariogram parameters calculated for the 400- and 200-point data sets are stable with respect to the lag increment with coefficients of variation of 7 percent or less for the range and nugget ratio and virtually no variation in the total sill value. For the 100-point data set, the range is unstable with respect to the lag increment as indicated by the coefficient of variation of 76 percent, the nugget ratio varies with a coefficient of variation of 10 percent, while the total sill remains stable with a coefficient of variation of only 2 percent.

Another semivariogram fitting parameter that can be examined is the maximum lag used in the fit. For a variable that is not trended, the calculated semivariogram parameters should not be very sensitive to changes in the maximum lag except, possibly, at very short maximum lags. In Figure 6, the semivariogram parameters calculated for 400, 200, and 100 data points are plotted against the

Table 1. Results from Weighted Least Squares Method for 400–, 200–, and 100–point Data Sets with Lag Increments of 0.25, 0.30, and Averaged Over 26 Values Between 0.25 and 0.30 with 0.002 Intervals.

Number of Data Points	Lag Increment	Range	Nugget Ratio	Total Sill
400	0.25	1.29	0.50	1.05
	0.30	1.15	0.39	1.05
	Average	1.20	0.43	1.05
	St. Dev.	0.035	0.026	0.00
	Co. of Var.	3%	6%	0%
200	0.25	1.26	0.78	1.09
	0.30	1.05	0.61	1.10
	Average	1.16	0.69	1.10
	St. Dev.	0.069	0.050	0.005
	Co. of Var.	6%	7%	0%
100	0.25	2.27	0.91	1.03
	0.30	1.72	0.86	1.01
	Average	2.51	0.83	1.01
	St. Dev.	1.59	0.086	0.017
	Co. of Var.	76%	10%	2%

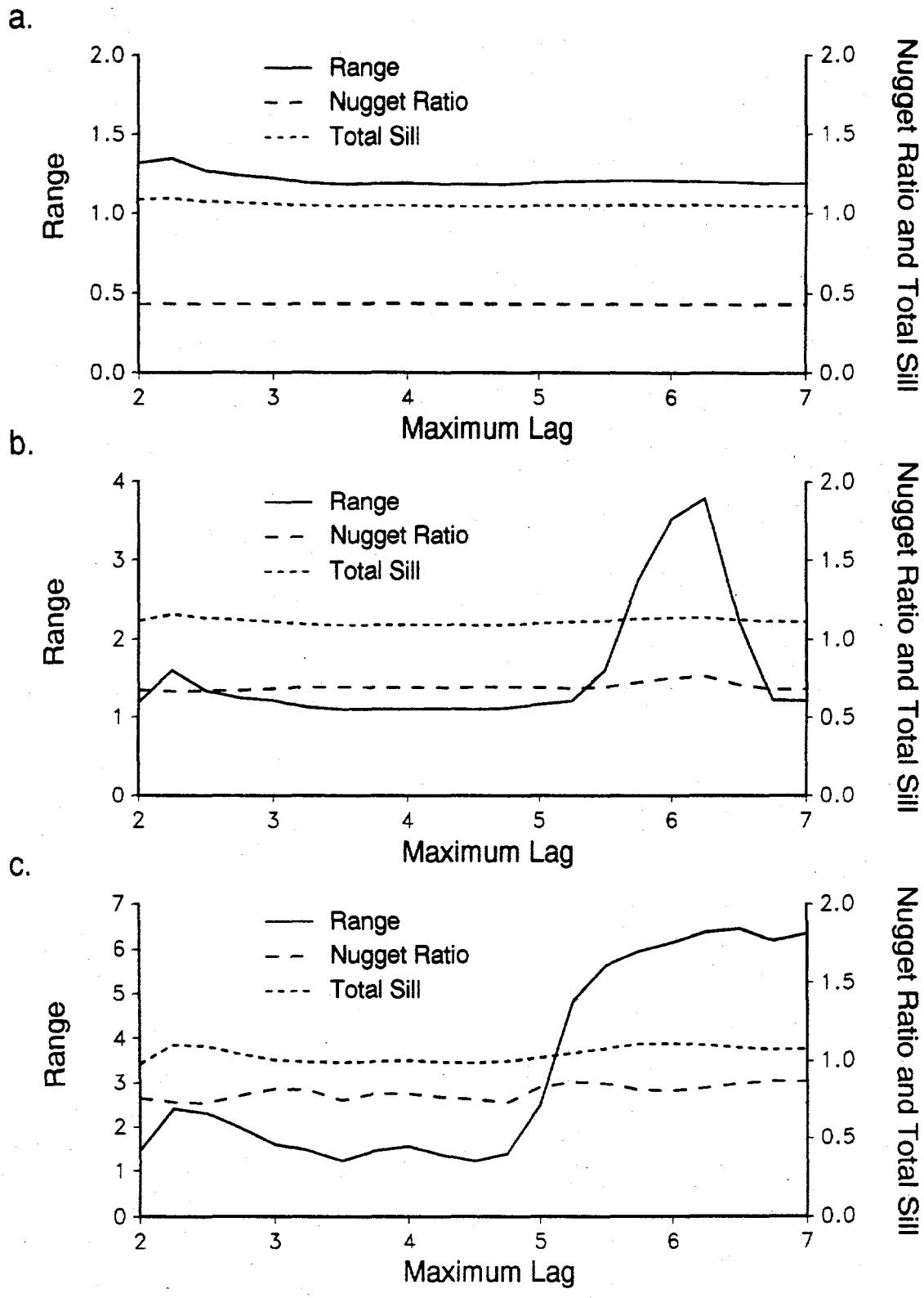

Figure 6. Semivariogram parameters determined with weighted least squares method and various maximum lags for (a) 400-point data set, (b) 200-point data set, and (c) 100-point data set.

maximum lag used in the semivariogram fit. Maximum lags between 2 and 7 with increments of 0.25 are considered. The semivariogram parameters calculated at each maximum lag are obtained by averaging the results from 26 lag increments values between 0.25 and 0.30 to reduce the effect of the particular lag increment used.

The effects of the lag increment and maximum lag on the range, nugget ratio, and total sill calculated from the weighted least squares fit are shown in the contour plots of Figure 7 for the 400-, 200-, and 100-point data sets. In these contour plots, the x axis represented the lag increment values from 0.25 to 0.30, the y axis represented the maximum lag values from 2 to 7, and the contoured variables are the calculated semivariogram parameters. The plots of Figure 4 are represented by horizontal lines through the contour plots of Figure 7, since the Figure 4 plots are calculated for a maximum lag set to 5. The plots of Figure 6 can be obtained by averaging the lag increment represented by the x axis in Figure 7 for each maximum lag value along the y axis.

The 400-point data set in Figure 7 shows little variation in any of the semivariogram parameters. For the 200-point data set, the range is stable except for lag increment values less than 0.27 and maximum lag values between 5.5 and 6.5 where the calculated range is greater than 6. The corresponding nugget ratio for the 200-point data set also increases for these values of lag increment and maximum lag. For the 100-point data set, the variation in the range and nugget ratio is greater still. The range for the 100-point data set is over 6 for all maximum lags greater than 6. The nugget ratio for the 100-point data set varies from less than 0.1 to greater than 0.9. For all three data sets, the total sill value is relatively unaffected by changes in the lag increment or maximum lag.

Jackknife Kriging Analysis

The semivariogram parameters were also calculated for the synthetic data sets using the jackknife kriging method. The variance of the jackknifing errors from equation (10) is minimized with respect to the range and nugget ratio. In Figure 8, the minimum variance of the jackknifing errors and the corresponding range and nugget ratio are plotted as a function of the number of points used in the kriging procedure for the 400-, 200-, and 100-point data sets. The lowest jackknife errors for all three data sets were obtained using over 40 kriging points.

Figure 8 shows that the jackknife kriging results for the 400-point data set are stable with respect to the number of kriging points used. There is a slight decrease in the range and increase in the nugget ratio with an increase in the number of kriging points. The results for the 200-point data set are stable when more than 12 kriging points are used. With only 100 data points, the range and nugget ratio are less stable especially with less than 25 kriging points, but the variation is less than results obtained from the weighted least squares method. The results from the jackknife kriging method using 18, 24, 30, 36, and 48 points for kriging are summarized in Table 2. The values of the total sill obtained by

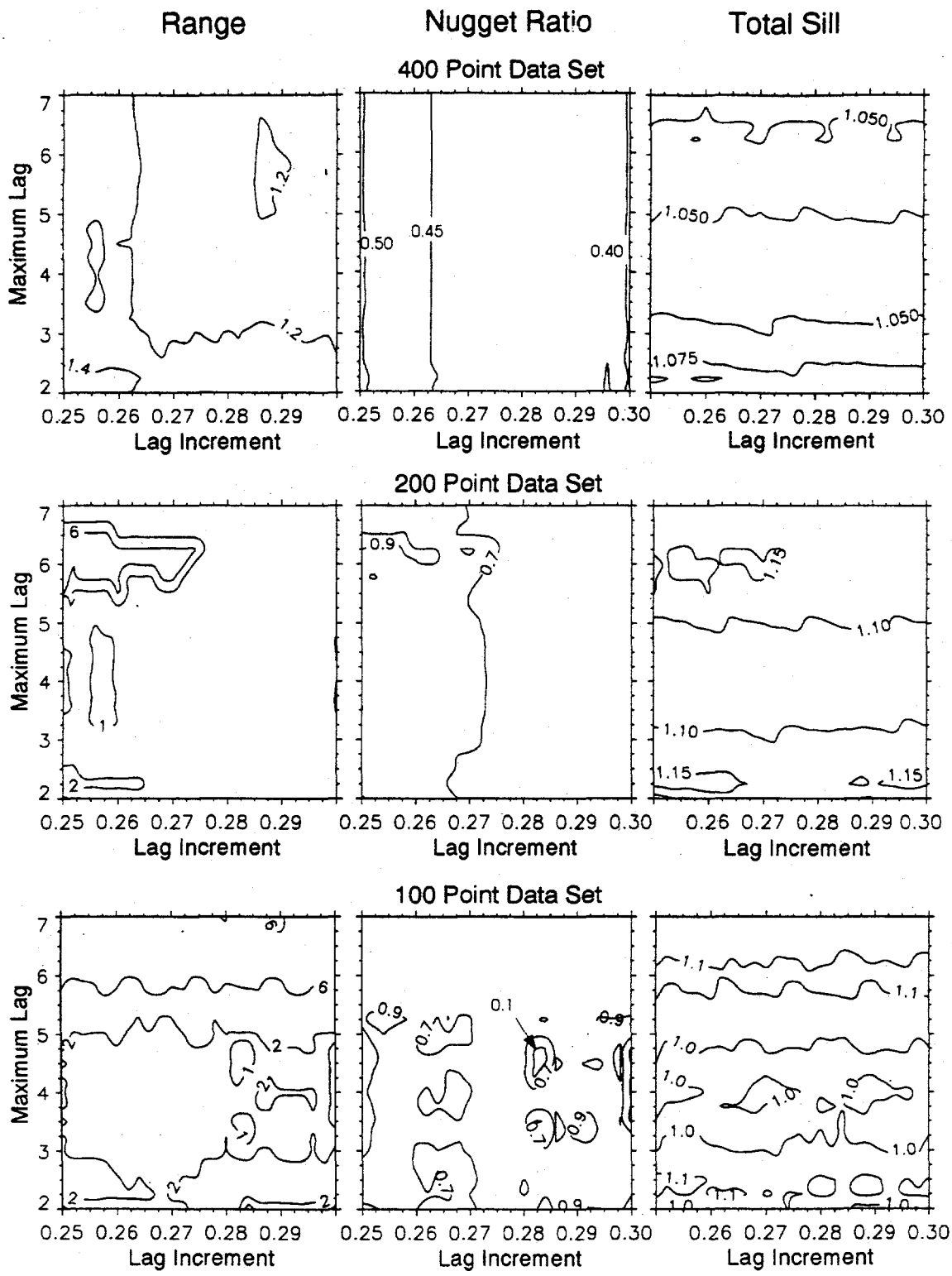

Figure 7. Semivariogram parameters for 400-, 200-, and 100-point data sets determined with weighted least squares method using various lag increments and maximum lags.

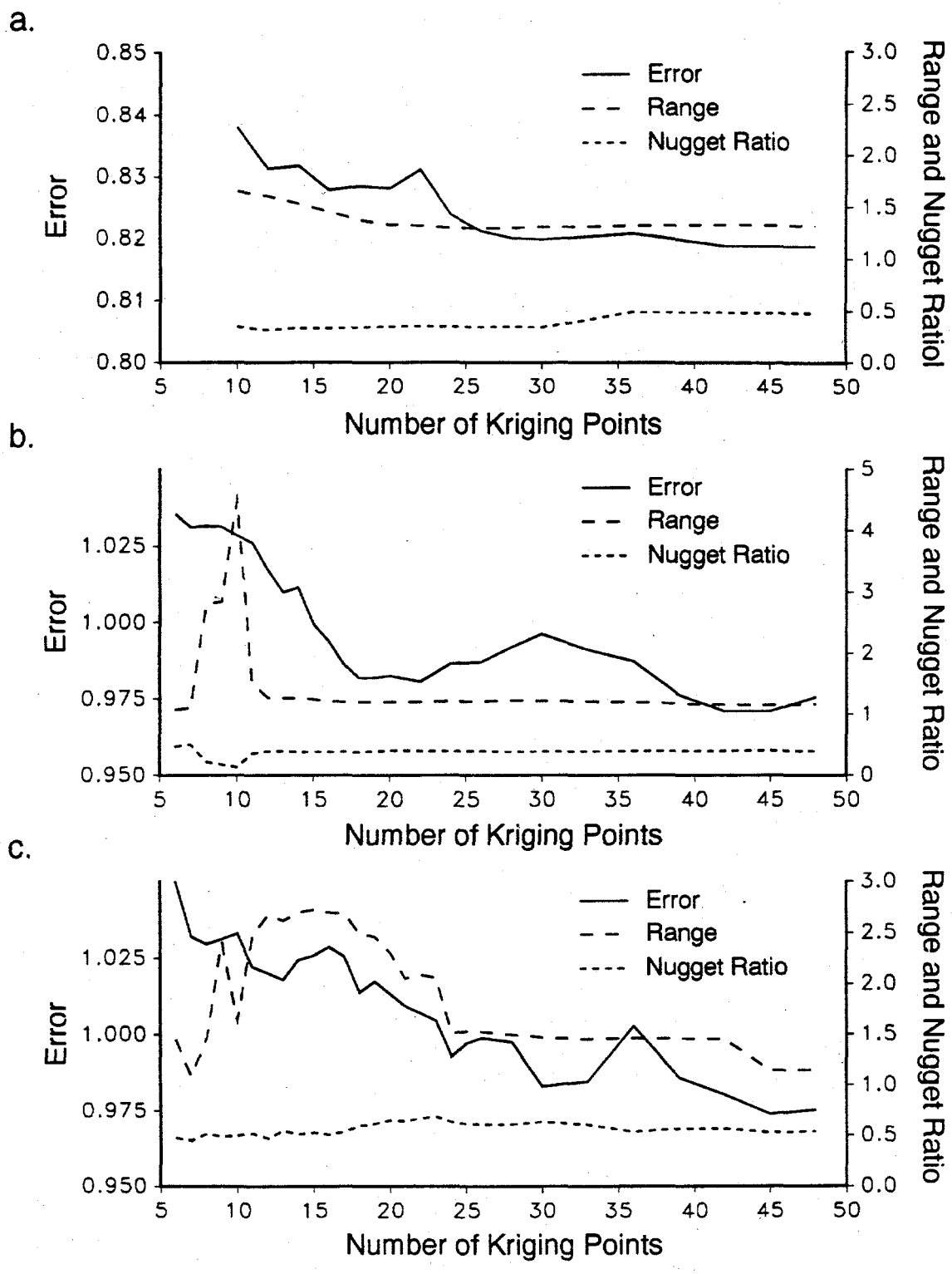

Figure 8. Semivariogram parameters determined with jackknife kriging method and various number of kriging points for (a) 400-point data set, (b) 200-point data set, and (c) 100-point data set.

Table 2. Results from Jackknife Kriging for 400–, 200–, and 100–point Data Sets with 12, 18, 24, 36, and 48 Kriging Points.

Number of Data Points	Number of Kriging Points	Range	Nugget Ratio	Total Sill	Error Variance (Variance of Data)
400	12	1.61	0.31	1.14	0.831
	18	1.38	0.34	1.25	0.828
	24	1.30	0.35	1.20	0.824
	36	1.33	0.49	1.13	0.821
	48	1.33	0.48	1.24	0.919
					(1.05)
200	12	1.27	0.38	1.24	1.017
	18	1.20	0.37	1.23	0.982
	24	1.21	0.38	1.22	0.986
	36	1.19	0.39	1.23	0.996
	48	1.17	0.38	1.21	0.056
					(1.10)
100	12	2.67	0.47	1.05	1.020
	18	2.48	0.60	1.15	1.014
	24	1.51	0.64	1.02	0.993
	36	1.46	0.54	1.04	1.003
	48	1.14	0.54	1.02	0.975

calculating the variance of the original data and by setting the kriging errors equal to the jackknifing errors are also presented in Table 2. The total sill is estimated better by the variance of the data than by setting the kriging errors equal to the jackknifing errors. One reason for this is that the total sill value calculated by equating the kriging and jackknifing errors is sensitive to errors in the calculated range and nugget ratio values.

In Figure 9, the variance of the jackknifing errors are plotted for the 400-, 200-, and 100-point data sets as a function of the range and nugget ratio over the same intervals as in Figure 5 using 18 and 24 points in the kriging procedure. For the 400-point data set, there is a distinct minimum when using 24 and 18 kriging points, but the variance increases much less at large ranges for the 18 kriging points plot. This is because with 18 kriging points, most of the data points used are within the range and there are few data points to establish at what lag the semivariogram levels off. The plots for the 200-point data set show distinct and similar minimums using 18 and 24 kriging points. For the 100-point data set, the shape of the contour plot and the location of the minimum error change considerably with 18 and 24 kriging points.

The weighted least squares and jackknife kriging methods can be compared by considering the error contour plots of Figures 5 and 9. For the less dense 200- and 100-point data sets, the weighted least squares method can have problems with local minimums where small range and nugget ratio

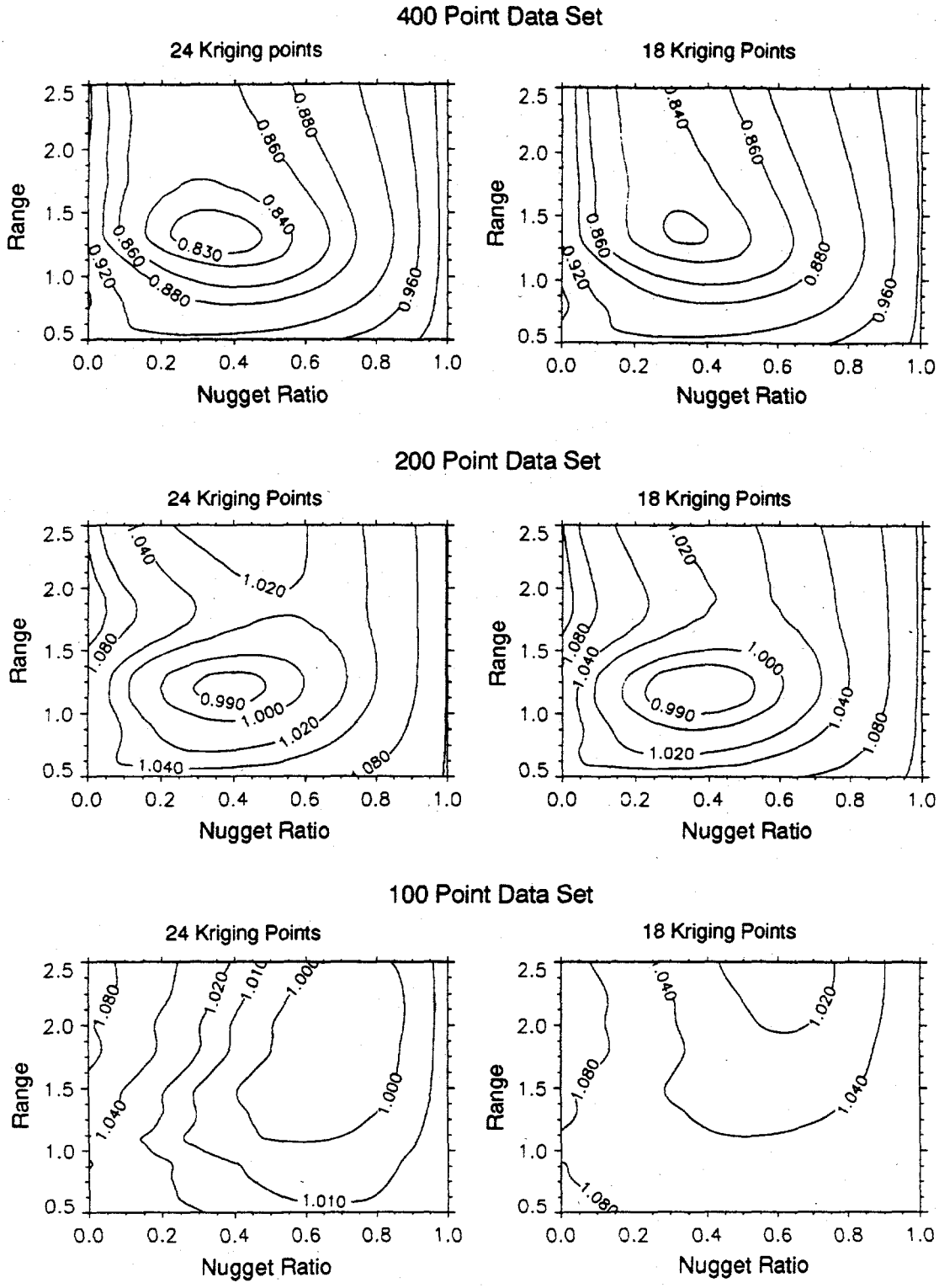

Figure 9. Error contour plots for 400-, 200-, and 100-point data sets using jackknife kriging with 24 and 18 kriging points.

values and large range and nugget ratio values result in similar error values. The jackknife kriging method performed well with sparse data sets since it does not rely on the sample semivariogram. The jackknife kriging method can be especially convenient if the calculated semivariogram parameters are to be used for kriging since the model validation analysis for the kriging has already been done.

Trended Synthetic Data

A trended synthetic data set was generated by adding a linear trend to the original synthetic data set along the y axis with a 15 percent slope. A linear trend is the simplest type of trend to analyze and will be used to investigate how the weighted least squares and jackknife kriging methods are affected by trended data. Semivariograms of the trended data using 400-, 200-, and 100-point data sets for lag increments of 0.25 and 0.30 are presented in Figure 10. The semivariograms for the 400-, 200-, and 100-point data sets all increase with increasing lags indicating the presence of a trend.

The results of fitting semivariograms to the trended data sets with the weighted least squares method using maximum lag values between 2 and 7 are shown in Figure 11 and summarized in Table 3 for maximum lags of 2 and 5. As with the untrended data, the semivariogram parameters are averaged over 26 lag increments values between 0.25 and 0.30 to minimize the effects of small changes in the lag increment. The range and total sill for the 400-, 200-, and 100-point trended data sets increase with increasing the maximum lag value, making accurate estimation of these parameters difficult. Using the "rule of thumb" maximum lag distance of one half of the distance across the field of the data, which is equal to 5, the range is over 5 and the total sill is over 1.5 for all three sized trended data sets.

The semivariogram parameters of the trended data sets were also determined using the jackknife kriging method. These results are also summarized in Table 3, using 24 points in the kriging procedure. The corresponding error contour plots are presented in Figure 12 along with the plots calculated with no trend. There is little difference in the shape of the contour plots or the location of the minimum for the data with and without the trend. This is because the jackknife kriging method only considers a local neighborhood of points in the kriging procedure. The jackknife kriging method provides an estimate of the range and nugget ratio that is much less sensitive to the presence of a linear trend than the weighted least squares method. It may be possible to use differences in the semivariogram parameters determined from the weighted least squares and jackknife kriging methods to help to identify trends in actual data. However, care must be exercised when extending results from a linear trend to other types of trends.

Included in Table 3 are the total sill values determined from two methods: the variance of the data, and by equating the jackknifing error and the kriging error. The total sill determined from equating the kriging and jackknifing errors is much less sensitive to the trend than the variance of the

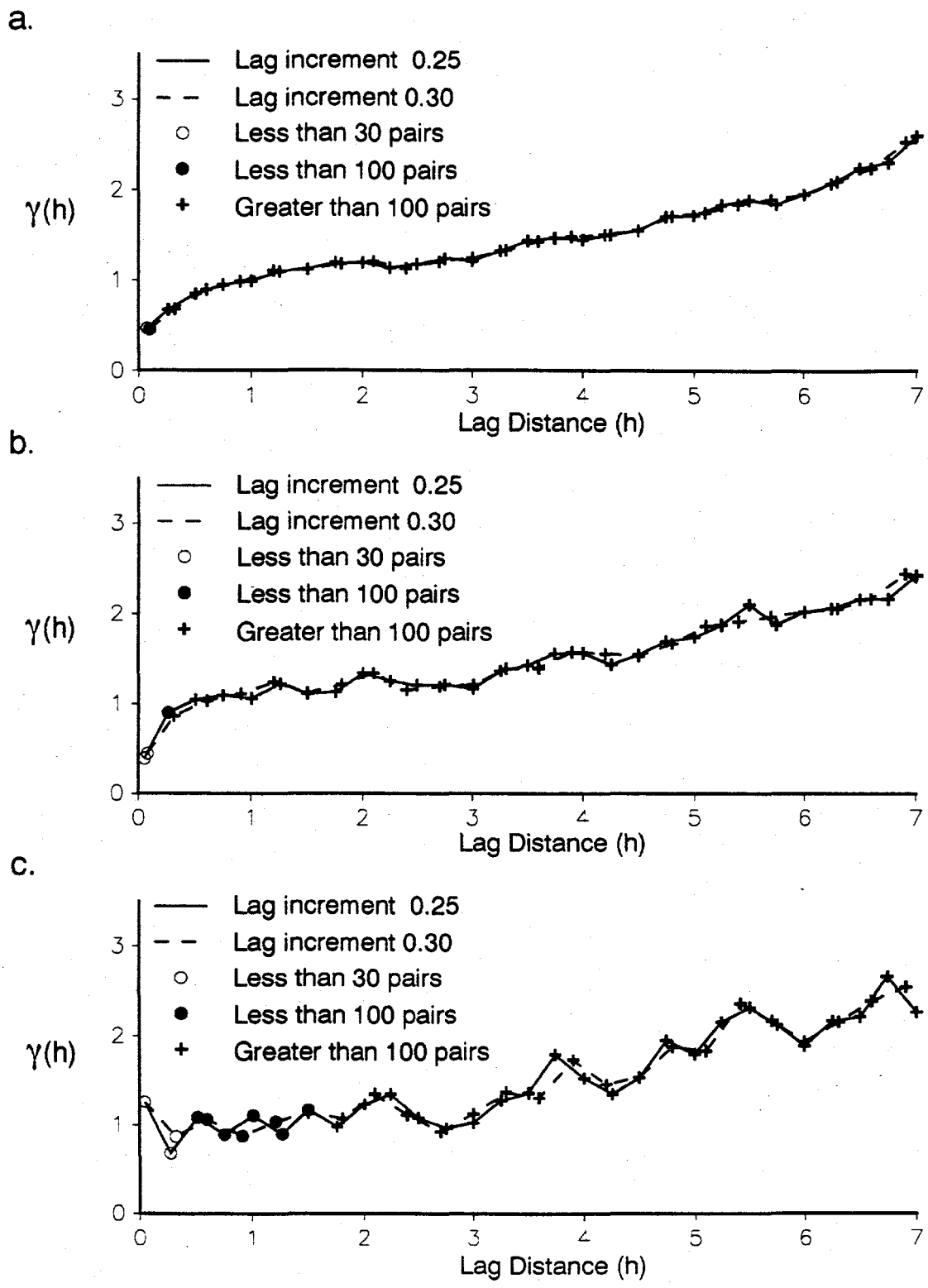

Figure 10. Sample semivariograms with lag increments of 0.25 and 0.30 for (a) 400-point trended data set, (b) 200-point trended data set, and (c) 100-point trended data set.

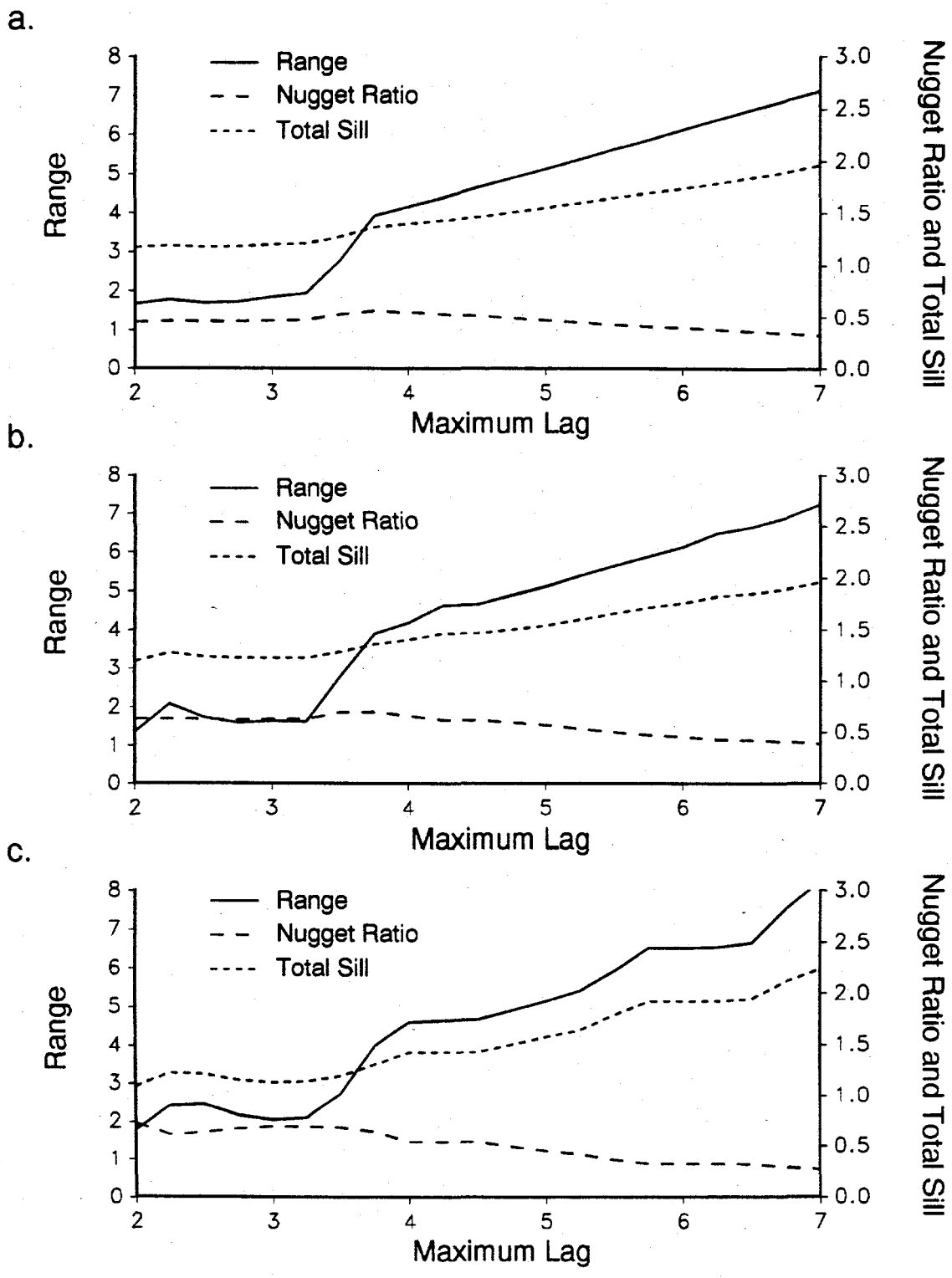

Figure 11. Semivariogram parameters determined with weighted least squares method and various maximum lags for (a) 400-point trended data set, (b) 200-point trended data set, and (c) 100-point trended data set.

Table 3. Results from Weighted Least Squares and Jackknife Kriging Methods for 400–, 200–, and 100–point Trended Data Sets.

Number of Points (Variance of Data)	Type of Fit	Range	Nugget Ratio	Total Sill
400 (1.96)	weighted least squares with max. lag of 2	1.66	0.45	1.16
	weighted least squares with max. lag of 5 (untrended results)	5.13 (1.20)	0.47 (0.43)	1.55 (1.05)
	jackknife kriging (untrended results)	1.32 (1.30)	0.34 (0.35)	1.21 (1.20)
200 (1.88)	weighted least squares with max. lag of 2	1.34	0.63	1.19
	weighted least squares with max. lag of 5 (untrended results)	5.11 (1.16)	0.57 (0.69)	1.54 (1.10)
	jackknife kriging (untrended results)	1.21 (1.21)	0.36 (0.38)	1.26 (1.22)
100 (1.93)	weighted least squares with max. lag of 2	1.77	0.73	1.09
	weighted least squares with max. lag of 5 (untrended results)	5.13 (2.51)	0.45 (0.83)	1.57 (1.01)
	jackknife kriging (untrended results)	1.49 (1.51)	0.66 (0.64)	1.02 (1.02)

data. Again, this is because the kriging error and jackknifing error consider a local neighborhood of points, while the variance is calculated from all of the data. However, errors in the estimated range and nugget ratio affect the calculation of the kriging error.

Directional Semivariogram Analysis

The weighted least squares method has also been applied to directional sample semivariograms. The untrended synthetic data are considered first to determine how well the weighted least squares fit performs with the directional sample semivariograms of the different-sized data sets. Directional sample semivariograms for the 400-, 200-, and 100-point data sets with no trend are presented in Figure 13. The directional sample semivariograms shown are calculated along the x axis, or 0 degrees, and the y axis, or 90 degrees, with a window angle of 45 degrees and a lag increment of 0.275. The 45 degree window angle results in sample semivariograms calculated from only about one fourth of the number of pairs of points that were used for the isotropic semivariogram analysis. The range and nugget ratio is fairly distinct in the directional sample semivariograms for the 400-point data set but not for the 200- and 100-point data sets.

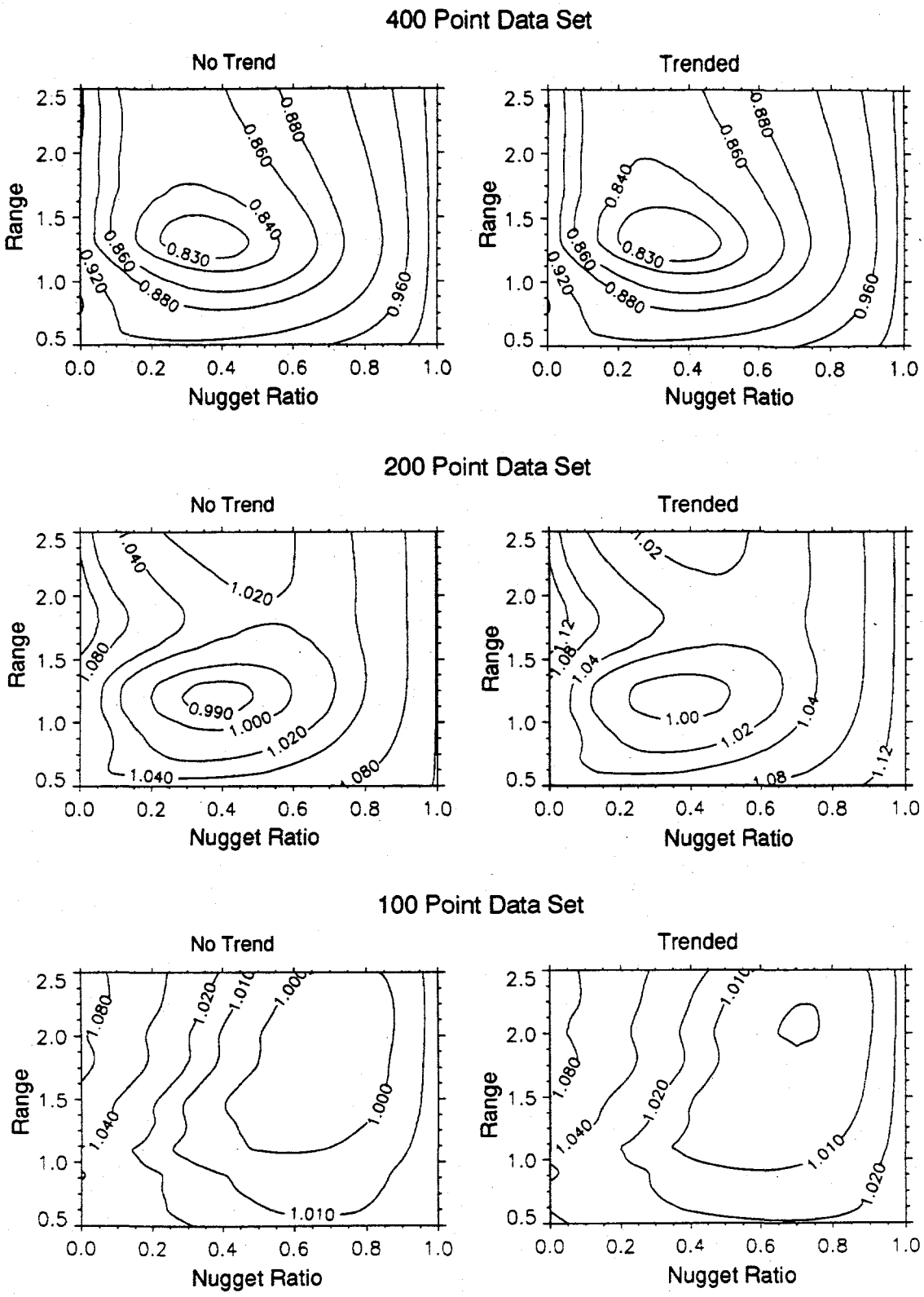

Figure 12. Error contour plots for 400-, 200-, and 100-point trended and untrended data sets using jackknife kriging with 24 kriging points.

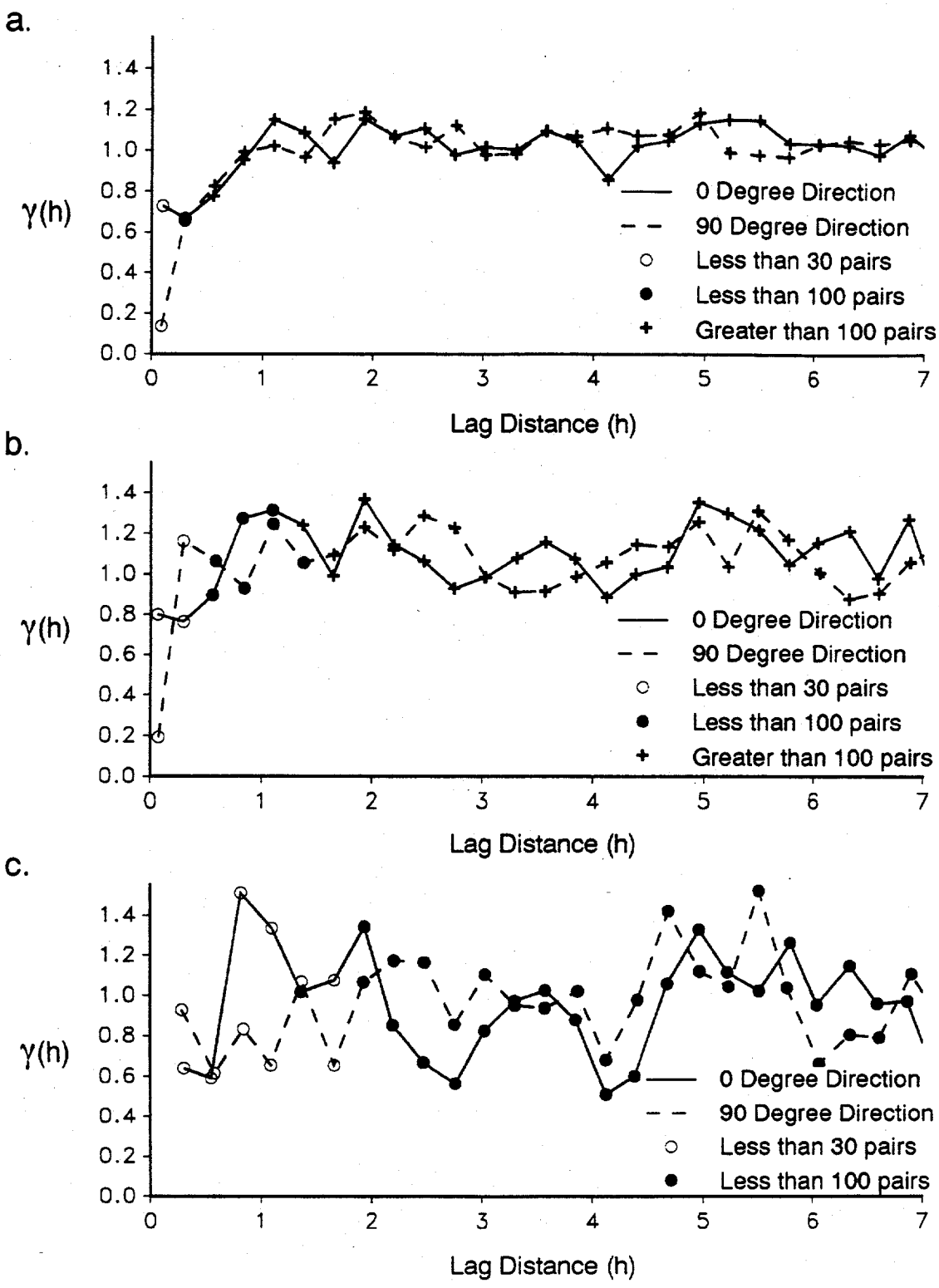

Figure 13. Anisotropic sample semivariograms with lag increment of 0.275 and 45 degree window angle for (a) 400-point data set, (b) 200-point data set, and (c) 100-point data set.

Weighted least squares semivariogram fits have been made using directional sample semivariograms calculated along several directions and for several maximum lag values. The results for the untrended synthetic data are presented as contour plots of the semivariogram parameters with x and y axes represented by the direction and the maximum lag, as shown in Figure 14 for the 400- and 200-point data sets. Fits of directional sample semivariograms with window angles of 45 degrees are calculated along 12 directions with increments of 15 degrees and for 21 maximum lag values between 2 and 7 with increments of 0.25. For each direction and maximum lag value, the semivariogram parameters have been averaged over 26 lag increments between 0.25 and 0.30, as with the isotropic semivariograms. For the 200-point data set, the range and nugget ratio values shown in Figure 14 change dramatically as a function of the direction and maximum lag. The 400-point data set shows range and nugget ratio values that are much less sensitive to the maximum lag and direction used in the fit. For both data sets, the total sill values change very little with changes in the maximum lag and direction.

The weighted least squares method has also been performed on directional sample semivariograms for the data sets with a trend. Directional sample semivariograms for the 400-, 200-, and 100-point trended data sets are shown in Figure 15. All three data sets show an increasing total sill in the 90 degree, or y axis, direction and a relatively well-defined total sill in the x axis direction. Contour plots of the total sill as a function of direction and maximum lag for the 400-, 200-, and 100-point trended data sets with window angles of 45 degrees are presented in Figure 16. The direction of the trend, which is along 90 degrees or the y axis, is easy to identify from these plots as the direction along which the total sill increases with increasing maximum lag.

CONCLUSIONS

Two fundamentally different methods of estimating semivariogram parameters have been applied to two-dimensional, spatially correlated, synthetic data sets of various data densities. The weighted least squares method fits the sample semivariogram, while the jackknife kriging method optimizes a kriging procedure with respect to the semivariogram parameters. These methods are used together to evaluate data sparsity and the presence of a trend.

The effect of data sparsity on the weighted least squares fit method to determine semivariogram parameters was examined by varying the lag increment used to calculate the sample semivariogram and the maximum lag used in the fit. The coefficient of variation of the estimated semivariogram parameters calculated over a range of lag increment values reflects how sensitive the fit is to slight changes in the grouping of data pairs when calculating the sample semivariogram. Small changes in the maximum lag used in a fit reflect how sensitive the fit is to adding an additional sample

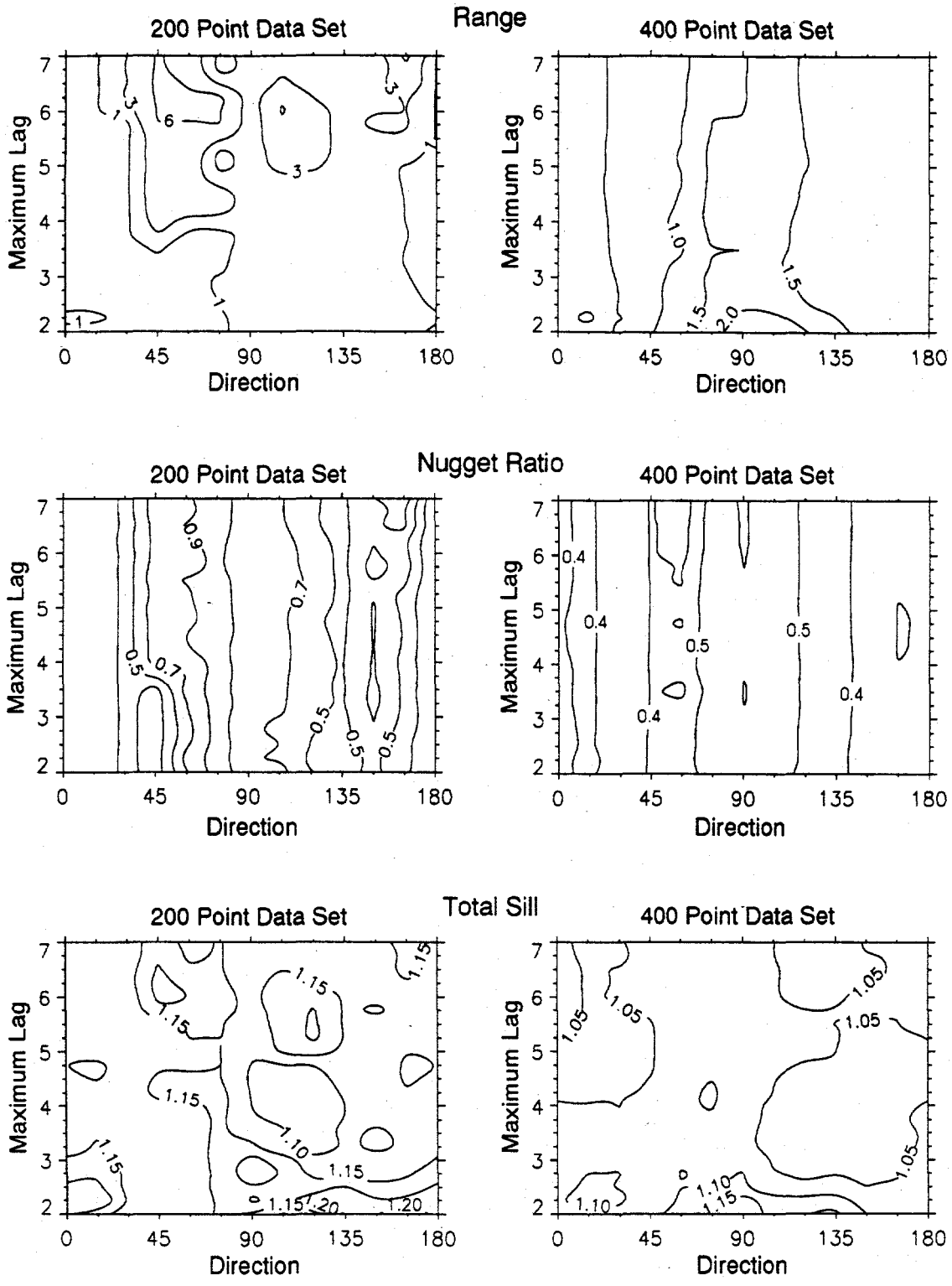

Figure 14. Semivariogram parameters for 400- and 200-point data sets determined with weighted least squares method of anisotropic semivariograms.

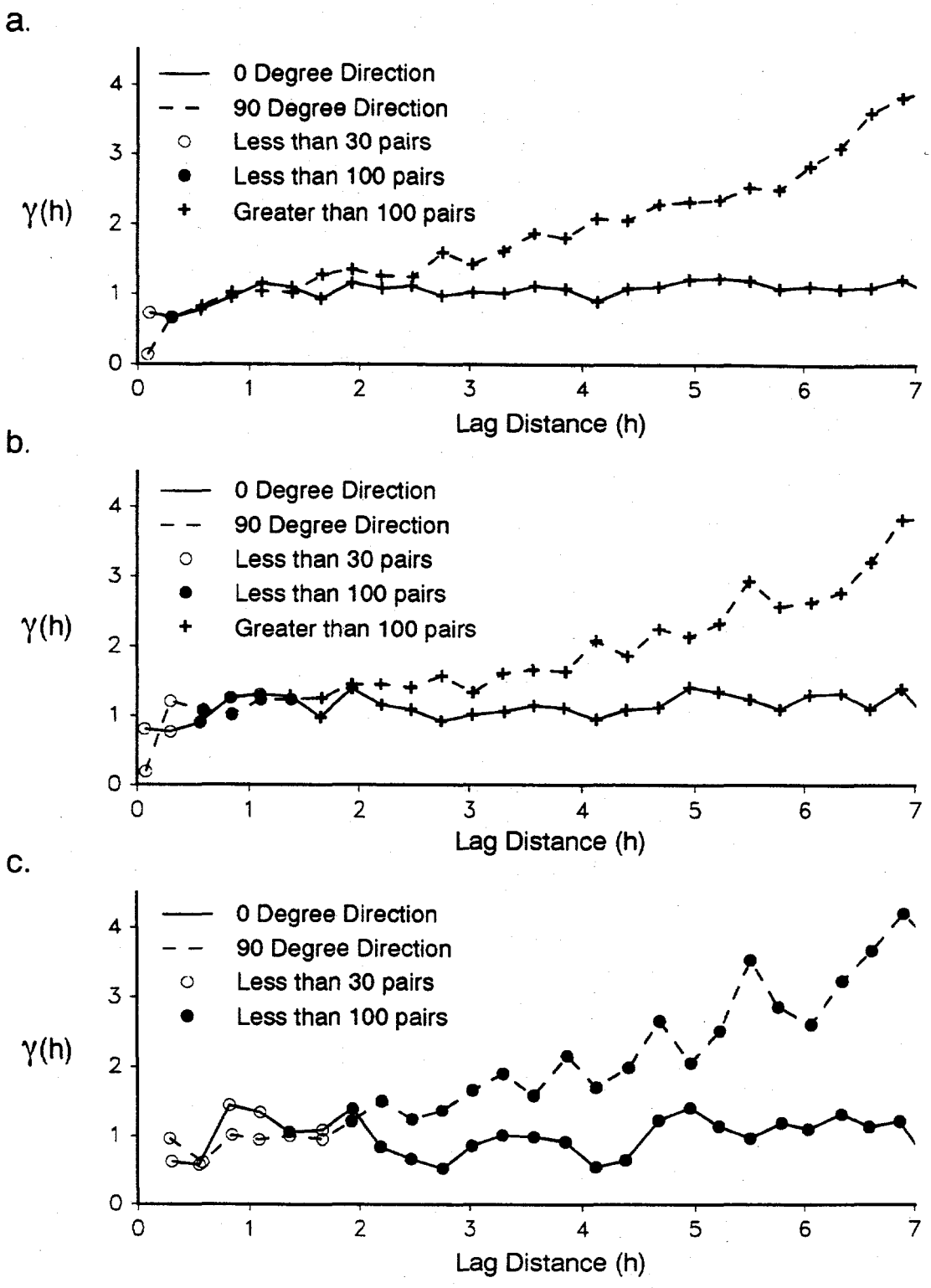

Figure 15. Anisotropic sample semivariogram with lag increment of 0.275 and 45 degree window angle for (a) 400-point trended data set, (b) 200-point trended data set, and (c) 100-point trended data set.

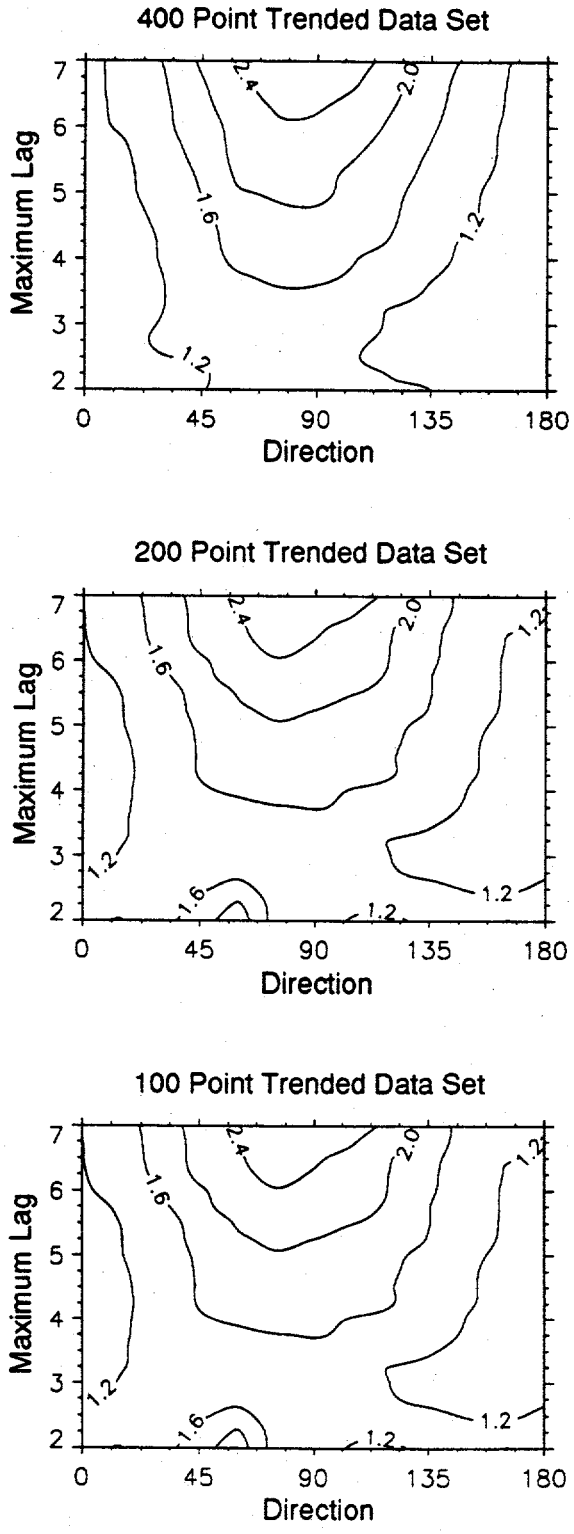

Figure 16. Total sill for 400-, 200-, and 100-point trended data sets determined with weighted least squares method of anisotropic semivariograms.

semivariogram value. Larger changes in the maximum lag can be used to identify the presence of a trend.

The maximum lag used in fitting semivariograms is typically one half of the data field. Care must be exercised in applying this general rule, especially with sparse data. The decision of what maximum lag to use should also take into account the size of the range to avoid placing too much weight on lags that are long with respect to the range. It is useful to calculate the semivariogram parameters for a range of lag increment and maximum lag values to identify values of lag increment and maximum lag values that result in stable semivariogram parameters.

A method to determine the semivariogram parameters that uses jackknife kriging was presented. The variance of the jackknife kriging errors is minimized with respect to the range and nugget ratio. The total sill can be determined by equating the kriging variance and the jackknife error or by calculating the variance of the original data. The jackknife kriging method does not rely on the sample semivariogram but estimates the range and nugget ratio from the performance of a kriging procedure. This can be useful with sparse data where the sample semivariogram is not well defined. The number of points used in the kriging procedure can be varied when calculating the jackknife kriging error. The optimum number of points to use when kriging can be identified by minimizing the jackknife kriging error with respect to the number of kriging points used. The total sill was estimated as the variance of the data and by equating kriging and jackknifing errors.

The weighted least squares and jackknife kriging methods were also applied to synthetic data with a linear trend. The weighted least squares method calculated increasing range and total sill values with increasing maximum lag values. The jackknife kriging method was found to be much less sensitive to the presence of a linear trend than the weighted least squares method. The variance of the data was a better estimator of the total sill with no trend, while equating the kriging and jackknifing errors gave a better estimate of the total sill when a linear trend was present. If the weighted least squares fit and the jackknife kriging methods do not agree, the presence of a trend can be investigated by applying the weighted least squares fit to directional sample semivariograms. By examining directional sample semivariograms of the trended and untrended data, it was found that the total sill is the most stable semivariogram parameter, especially with smaller data sets, and can be used to identify the orientation of a trend.

The weighted least squares and jackknife kriging methods can be used together to check the estimated semivariogram parameters, especially when problems with sparse data are suspected. Initially, the weighted least squares method should be applied using a wide range of lag increment and maximum lag values. From these results, lag increment and maximum lag values that give stable results can be identified. The semivariogram parameters from this method can be used as the initial

point in a search to identify the semivariogram parameters that yield the minimum jackknife kriging error. If the two methods yield similar results, then it will not make too much difference what method is used. If different results are obtained, then the data should be examined more closely to determine why. This analysis can be computationally demanding especially when applying the jackknife kriging method to data sets with over 200 points. However, sample semivariograms are usually well defined when over 200 points are available and the weighted least squares fit of the sample semivariogram will provide good semivariogram parameter estimates.

There are several potential areas for future work with the weighted least squares and jackknife kriging methods for estimating semivariogram parameters. Synthetic data with various range and nugget ratio values can be generated to investigate the effect of the range and nugget ratio on the uncertainty of the calculated semivariogram parameters. Several realizations of the synthetic data can be considered to examine the accuracy and bias of the two methods. Actual data sets should also be used to verify conclusions from the synthetic data sets.

REFERENCES

Clifton, P.M. and S.P. Neuman, 1982. Effects of kriging and inverse modeling on conditional simulation of the Avra Valley aquifer in southern Arizona, *Water Resources Research,* 18(4):1215-1234.

Cressie, N., 1985. Fitting variogram models by weighted least square, *Mathematical Geology,* 17(5):563-586.

Journel, A.G. and C.J. Huijbregts, 1978. Mining Geostatistics, Academic Press, New York, NY.

Kitanidis, P.K., 1991. Orthonormal residuals in geostatistics: model criticism and parameter estimation. *Mathematical Geology,* 23(5):741–758.

Knudsen, H.P. and Y.C. Kim, 1978. Application of geostatistics of roll front type uranium deposits. AIME Preprint no. 78–AR–94, unpaginated.

McBratney, A.B. and R. Webster, 1986. Choosing functions for semivariograms of soil properties and fitting them to sampling estimates, *Journal of Soil Science,* 37(4):617-639.

Press, W.H., B.P. Flannery, S.A. Taukolsky and W.T. Vetterling, 1986. Numerical Recipes, Cambridge University Press, Cambridge, MA.

Solow, A.R., 1990. Geostatistical cross validation: a cautionary note, *Mathematical Geology,* 22(6):637–639.

INCORPORATION OF CONSTRAINTS ON HYDRAULIC HEAD GRADIENTS NEAR NO-FLOW BOUNDARY CONDITIONS IN THE DETERMINATION OF SPATIAL DRIFT

ABSTRACT

A method is presented that includes constraints on hydraulic head gradients across no-flow boundaries when estimating hydraulic head values at node points from hydraulic head data at measurement locations. As the weighting on these constraints is increased, the hydraulic head gradient across the no-flow boundaries is decreased at the expense of fitting the head measurements. The method is applied to a case study of the Avra Valley aquifer in southern Arizona. The appropriate weighting of these constraints is investigated by examining the tradeoff in fitting head measurements and no-flow boundary conditions. Changes in the semivariogram of the head residuals and the estimation error of the heads are also considered. It is found that boundary constraints can improve the fit of the estimated heads to the no-flow boundaries with little deterioration of the fit to the head measurements.

INTRODUCTION

Analysis of groundwater flow often requires estimation of hydraulic head values at selected locations from head measurements at wellbores. Estimation of hydraulic head values at nodes within a finite element or finite difference mesh is particularly important in inverse groundwater flow models where hydraulic conductivities or transmissivities are estimated based, in part, on gradients in nodal head values (Neuman and Yakowitz, 1979). Current methods to estimate hydraulic head values at selected locations typically rely only on measured head data and do not consider boundary conditions (Jacobson, 1994). A method is presented here to incorporate no-flow boundaries into the estimation of hydraulic head.

There are several reasons why it is important to consider the presence of no-flow boundary conditions in the estimation of hydraulic head. First, if the estimated heads are used in a groundwater flow model where no-flow boundaries are employed and the estimated head gradient does not match the boundary conditions, then the no-flow boundary condition will be violated. Second, no-flow boundaries are often known with a relative high degree of certainty based on topographical or geological evidence. This subjective knowledge can be important if there are sparse well data to define the hydraulic head near no-flow boundaries. Finally, if the head measurements and the hypothesized no-flow boundary conditions are found to conflict, then the presence and extent of the no-flow boundary should be re-evaluated.

Neuman and Jacobson (1984) present a method to estimate hydraulic head values based on a stepwise iterative regression procedure to determine a trend and simple kriging of residuals. Kriging

is an interpolation technique described by Journel and Huijbregts (1978) that is based on a linear combination of nearest neighboring points with the weights determined from the range and sill of the semivariogram of the data. A polynomial is used to describe the trend where the order of the polynomial is determined by examining the semivariogram of the residuals. The estimate of the hydraulic head is the sum of the kriged and polynomial components. This method was used by Jacobson (1985) to estimate hydraulic head values at node points for use in an inverse model to estimate transmissivities of the Avra Valley aquifer in southern Arizona. The highest estimation errors for the transmissivities from the inverse model were found in the vicinity of no-flow boundaries. It is possible that these errors could be reduced if the procedure to estimate the hydraulic heads included consideration of the no-flow boundaries.

A modification of the Neuman and Jacobson approach is presented here that includes constraints on the hydraulic head gradient perpendicular to no-flow boundaries in the determination of estimated head values. The hydraulic head data from the Avra Valley aquifer are considered as a case study. A semivariogram analysis and fitting procedure described by Lamorey and Jacobson (1994) that includes a weighted least squares fit of the sample semivariogram and a procedure to minimize the error from jackknife kriging is used in determining semivariogram parameters of the residuals.

Neuman and Jacobson (1984) also present a method to evaluate the variance and covariance of the error of estimation for the estimated hydraulic heads that is based on the kriging variance of the head residuals. Cressie (1993) discusses problems with this method and how these problems can lead to underestimating the variance of the estimated heads. A modification of Neuman and Jacobson's method is presented here that includes the error from the drift component of the head estimate in the calculation of the variance of the estimate. To examine the impact of the new method, both methods are considered and compared in the Avra Valley case study.

STEPWISE ITERATIVE REGRESSION

The stepwise iterative regression method developed by Neuman and Jacobson (1984) yields simultaneous estimates of the drift and the spatial characteristics of the residuals. The hydraulic head is assumed to be composed of a non-intrinsic polynomial drift component and a zero-mean intrinsic residual component. The hydraulic head at a point is estimated by kriging the residual component and adding it to the drift component. The drift is determined with a generalized least squares procedure.

The measured hydraulic heads, drift, and residuals are related by the following matrix equation:

$$Z = Fa + R \qquad (1)$$

where Z is an N by 1 matrix of N hydraulic head measurements. F is an N by M matrix of the basis functions of the drift, a represents the M coefficients for the basis functions (an M by 1 matrix), and R contains the residuals (an N by 1 matrix). The basis functions for the spatial drift combine to form a polynomial function:

$$a_1 + a_2X_i + a_3Y_i + a_4X_i^2 + a_5X_iY_i + a_6Y_i^2... \quad (2)$$

for a point located at X_i, Y_i.

The residuals are initially assumed to be independent and an ordinary least squares solution for increasing orders of drift is calculated from the following equation:

$$a^* = (F^TF)^{-1}F^TZ \quad (3)$$

where a^* is the matrix that contains the estimated coefficients for the basis functions.

The ordinary least squares solution from equation (3) can be refined by including the spatial correlation of the residuals in a generalized least squares solution of the form:

$$a^* = (F^TV^{-1}F)^{-1}F^TV^{-1}Z \quad (4)$$

where the solution is weighted by V, the covariance matrix for the residuals.

The ordinary and generalized least squares solutions require matrix inversions involving F. For high order polynomial basis functions, such as fourth order and higher, numerical problems can be encountered during these inversions due to the nearly linear behavior of the basis function. These problems are alleviated by expressing the basis functions as Chebyshev polynomials. Chebyshev polynomials produce the same solution as the more traditional polynomial forms but with a greatly reduced condition number during the matrix inversions. The use of Chebyshev polynomials is discussed in Appendix A.

The components of V in equation (4) are determined from the semivariogram of the residuals. The semivariogram, $\gamma(x_1,x_2)$, is a function of the variance of the random function Z over the increment $[Z(x_1)-Z(x_2)]$ and is defined as:

$$\gamma(x_1,x_2) = \frac{1}{2}Var\{Z(x_1) - Z(x_2)\} \quad (5)$$

If the semivariogram depends only on the distance between points, x_1 and x_2, then the sample semivariogram can be calculated by considering pairs of data points separated by a lag distance:

$$\hat{\gamma}(s) = \frac{1}{2N'}\sum_{i=1}^{N'}[Z(x_i + s) - Z(x_i)]^2 \quad (6)$$

where N' is the number of data pairs at the lag distance s.

For the calculated sample semivariogram of equation (6) to be equivalent to the semivariogram of equation (5), the data must follow a type of second order stationarity commonly called the

intrinsic hypothesis. The intrinsic hypothesis asserts that for a random function Z(x), the expectation, or mean, exists and does not depend on location; and for all vectors s, the increment [Z(x+s)-Z(x)] has a finite variance which does not depend on x. The presence of a drift results in a mean that is not independent of location, which violates the intrinsic hypothesis.

Theoretical semivariogram models are often characterized by three parameters: a sill, a range, and a nugget effect (Figure 1). The degree of correlation between values of a variable measured at two locations, Z(x) and Z(x+s), usually decreases as the lag distance increases. As the correlation decreases the value of the sample semivariogram increases. The lag distance at which the correlation becomes zero is the range. At lag values greater than the range, the sample semivariogram value will often stop increasing and level off at a value called the sill. The sill represents the variance of uncorrelated values of the variable. If the sample semivariogram does not level out at a sill but continues to increase with increasing lags, a trend or drift may be present. As the lag distance goes to zero, the sample semivariogram may also approach zero, or it may approach a positive value called the nugget. The nugget effect is caused by measurement errors or small-scale variations in the measured values.

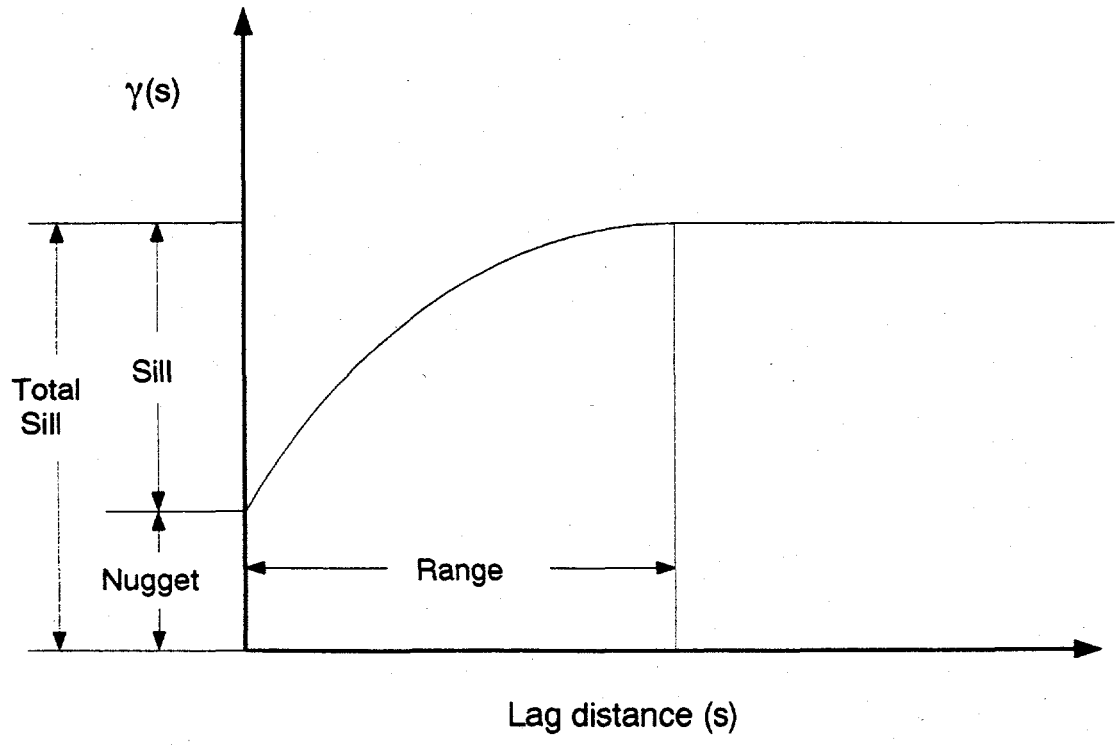

Figure 1. Characteristic features of a semivariogram.

After determining the semivariogram parameters of the residuals, the (i,j)th term of V in equation (4) can be determined from the following equation:

$$V_{i,j} = \varrho_R(s_{i,j}) = \varrho_R(0) - \gamma_R(s_{i,j}) \quad (7)$$

where $s_{i,j}$ is the distance between points i and j, ϱ_R is the covariance function of the residual as a function of $s_{i,j}$, and γ_R is the value of the residual semivariogram for a lag of $s_{i,j}$. The covariance function for zero lag, $\varrho_R(0)$, is the sill of the residual semivariogram.

The stepwise iterative regression procedure to determine the spatial drift first determines the appropriate order for the drift using the ordinary least squares solution. The appropriate order for the drift is the lowest order that produces intrinsic residuals. This can be checked by examining the semivariogram of the residuals. If a trend is present in the residuals, the semivariogram will continue to increase with increasing lag. The direction of the trend can be identified by examining sample semivariograms calculated along different directions called directional semivariograms. The order of the drift is increased until the semivariogram of the residuals exhibits a distinct sill in all directions.

After the appropriate order for the drift has been determined, the estimated drift is refined using a generalized least squares solution. The semivariogram of the residuals from the ordinary least squares fit for a selected order of drift is initially used to calculate V of equation (4) for the generalized least squares solution. The generalized least squares solution yields a new set of residuals. The sample semivariogram from these residuals is used to determine the range and sill that are used in the next iteration of the generalized least squares solution. The solution is only sensitive to changes in the range since all the values in V are scaled by the sill. This iterative process is continued until the change in the range of the residuals is below a specified tolerance. Residuals at each node point are estimated by kriging the residuals determined at the measurement points. Nodal head estimates are obtained by adding these residuals and the drift calculated at each node point.

BOUNDARY CONDITION CONSTRAINTS

The Neuman and Jacobson stepwise iterative regression approach has been modified to include constraints on the gradient of the hydraulic head drift along no-flow boundaries into the determination of the drift. The slope of the drift for the hydraulic head can be approximated as the difference between head drift values at two points divided by the distance between the points. The slope of the hydraulic head drift surface perpendicular to a no-flow boundary can be constrained to be zero by choosing points on opposite sides of the no-flow boundary and constraining their difference to equal zero as shown in Figure 2. These constraints on the hydraulic head gradient can be incorporated into the least squares solution by making the following substitution:

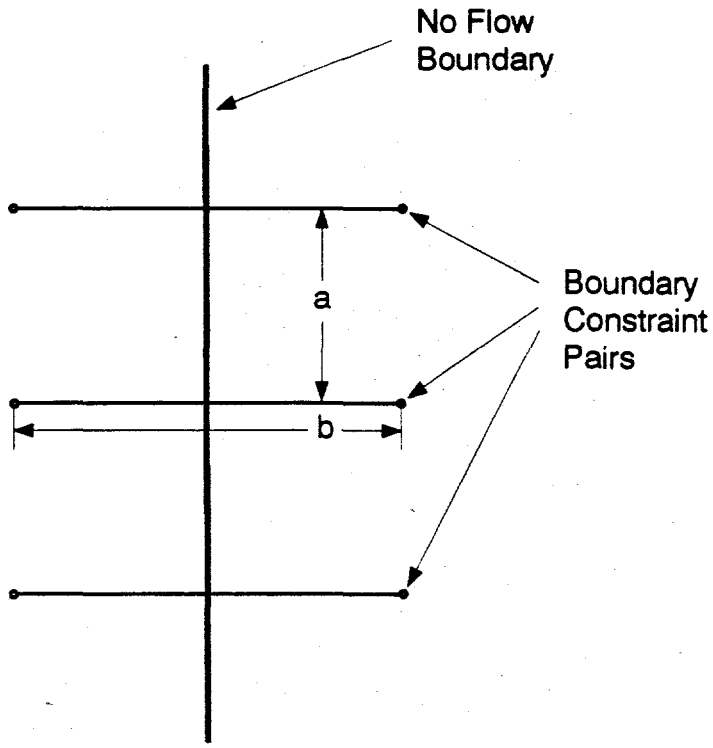

Figure 2. Configuration of no-flow boundary constraints.

$$
\begin{aligned}
H_1 &= a_1 + a_2x_1 + a_3y_1 + a_4x_1^2 + a_5x_1y_1 + a_6y_1^2... \\
H_2 &= a_1 + a_2x_2 + a_3y_2 + a_4x_2^2 + a_5x_2y_2 + a_6y_2^2 \\
0 &= H_1 - H_2 \\
&= a_2(x_1 - x_2) + a_3(y_1 - y_2) + a_4(x_1^2 - x_2^2) + a_5(x_1y_1 - x_2y_2) + a_6(y_1^2 - y_2^2)...
\end{aligned}
\tag{8}
$$

where H_i is the hydraulic head drift estimate at point i.

The equation for the drift and residuals becomes:

$$Z' = F'a + R' \tag{9}$$

where Z' contains measured hydraulic head values and zeros for the hydraulic head gradient perpendicular to no-flow boundaries; F' contains the values of the basis functions at the points of the hydraulic head measurements and of points used to constrain the hydraulic head gradient along no-flow boundaries; and R' contains hydraulic head residuals and residuals from the boundary condition constraints.

The number of boundary constraints imposed and the spacing between the pairs of points need to be chosen with care. The number of boundary constraints must be large enough to describe the

shape of the boundary. In a finite element mesh, the boundary constraints should be at least as close together as the nodes that define the boundary. This distance is shown as distance "a" in Figure 2. The distance between pairs of points used to calculate the gradient of the hydraulic head drift is shown in Figure 2 as distance "b". When using a finite element mesh, the average distance between nearby finite element nodes is a reasonable choice for distance "b" since this is the distance over which flow is calculated. Distances "a" and "b" determine the coordinates of the points used in equation (8). Different values for distances "a" and "b" can be considered and their results compared to ensure that the results are not dependent on the choice of the number and spacing of the boundary constraints.

The covariance matrix of the residuals used in the generalized least squares solution is complicated by the addition of the boundary constraints. The covariance function can be expressed as a partitioned matrix:

$$V = \begin{matrix} cov(R_{mh},\ R_{mh}) & cov(R_{mh},\ R_{bc}) \\ cov(R_{bc},\ R_{mh}) & cov(R_{bc},\ R_{bc}) \end{matrix} \qquad (10)$$

where $cov(R_{mh},R_{mh})$ is the covariance of measured head residuals with other measured head residuals, $cov(R_{mh},R_{bc})$ is the covariance of measured head residuals with the residuals of the individual boundary constraints, and $cov(R_{bc},R_{bc})$ is the covariance of the boundary constraints with other boundary constraints. $Cov(R_{mh},R_{mh})$ is determined using the range and sill of the semivariogram of the measured head residuals and is equal to V of equation (4).

Each diagonal term of $cov(R_{bc},R_{bc})$ represents the weighting of individual boundary constraints expressed in equation (8). Large values along the diagonal of $cov(R_{bc},R_{bc})$ result in little weighting of the boundary constraints, since this implies a large variance in the expected residuals. In the case study presented below, the boundary constraint weighting is expressed as the value of the diagonal of $cov(R_{bc},R_{bc})$ divided by the sill of the head residuals. In this way, a boundary constraint weighting of 0 corresponds to no boundary constraint weighting and a weighting of 1 corresponds to weighting each boundary constraint as much as each head measurement. Non-uniform weighting of the boundary constraints can be achieved by using different values along the diagonal of $cov(R_{bc},R_{bc})$. Non uniform boundary constraint weighting could be useful if the presence of various no-flow boundaries is known with different degrees of certainty. Only uniform weightings are considered in the case study below.

The off-diagonal terms of $cov(R_{bc},R_{bc})$ and all of the terms of $cov(R_{mh},R_{bc})$ and $cov(R_{bc},R_{mh})$ are difficult to evaluate. A value of zero for these terms implies that the boundary constraint residuals are independent of each other and of the measured head residuals. This assumption is made in the case study. It may be possible to refine this solution if these terms can be better evaluated. This

approach is analogous to treating these parts of the covariance matrix as an ordinary least squares solution while treating the $cov(R_{mh},R_{mh})$ part as a generalized least squares solution.

The order of the polynomial used to express the drift is determined initially with no boundary constraints. To allow the drift flexibility to fit boundary constraints as well as the measured head data, it may be necessary to increase the order of the drift when applying the boundary constraints. The measured head residuals should remain intrinsic and the semivariogram of the head residuals should continue to exhibit a distinct sill after the boundary constraints are applied.

As the weights on the boundary constraints are increased, the range and sill of the measured head residuals may change. For a given boundary constraint weighting, the change in the range and sill of the measured head residuals is used to calculate new values of $cov(R_{mh},R_{mh})$ and the generalized least square solution is iterated until the change in the range is below a specified tolerance. The nodal head estimates are obtained by kriging the residuals from the last iteration and adding this to the drift calculated at each node point. The degree of change in the range and sill when the boundary constraints are applied may indicate the degree to which the assumption of independence between boundary constraint residuals and measured head residuals is violated.

The appropriate weighting of the boundary constraints can be examined by considering the error in fitting the measured heads and the error in fitting the boundary constraints. The fit of the estimated heads to the head measurements can be checked by jackknifing head estimates and calculating the jackknifing error. Jackknife kriging is discussed in more detail below with regard to semivariogram parameter estimation. The boundary constraint error can be calculated by subtracting the estimated head values at the pairs of boundary constraint points and calculating the average of this error over all of the boundary constraints. Head estimates at boundary constraint points are calculated by adding the drift from the least squares solution and the kriged residual at each of the boundary constraint points, just as was done for each node point. These checks of the head measurement fit and boundary constraint fit are different from their counterparts in the least squares solution of equation (9) because the kriging component of the estimates are also included. The optimum tradeoff in fitting the measured heads and boundary constraints may be identified by plotting the percent change in the boundary constraint error against the percent change in the jackknifing error.

In addition to examining changes in the range and sill of the head residuals and the tradeoff in fitting the measured heads and boundary constraints, other statistics can be examined to determine the appropriate boundary constraint weighting. The mean of the head residuals should be zero since the residuals are assumed to be non-biased for kriging. Kriging of the head residuals also requires

that the head residuals be normally distributed. This can be checked by performing a χ^2 test on the head residuals.

ESTIMATION OF SEMIVARIOGRAM PARAMETERS

Estimation of the sill and range of the measured head residuals is an important aspect of the boundary constraint weighting. Not only are these parameters used in the calculation of the covariance matrix of the residuals, they are used to evaluate the independence of the measured head and boundary constraint residuals. This estimation method needs to be sensitive to small changes in the semivariogram as well as provide an accurate estimate of the range and sill. It is also important to determine if the measured head residuals exhibit a trend or are otherwise non-intrinsic.

The methods to estimate semivariogram parameters used here are discussed in Lamorey and Jacobson (1994) and include a weighted least squares fit of the sample semivariogram and a jackknife kriging optimization technique. The weighted least squares method is examined by varying the lag increment used in calculating the sample semivariogram and the maximum lag used in the fit. The jackknife kriging method does not rely on the calculation of the sample semivariogram and was found by Lamorey and Jacobson (1994) to be less sensitive to the presence of a trend than the weighted least squares method. Comparison of the results from the two methods can help to determine if the head residuals are intrinsic.

A modified form of a weighted least squares fit described by Cressie (1985) is used to estimate the semivariogram model parameters for the measured head residuals. The following function is minimized with respect to λ:

$$\sum_{j=1}^{k} N_{s(j)} \left\{ \frac{\gamma^*(s(j))}{\gamma(s(j);\lambda)} - 1 \right\}^2 \qquad (11)$$

where λ is the estimated parameters, each value of j represents an increment in the lag, s(j) is the lag distance, $N_{s(j)}$ is the number of pairs used to calculate the semivariogram value, $\gamma^*(s(j))$ is the semivariogram value calculated from the measured data, and $\gamma(s(j);\lambda)$ is the semivariogram value calculated from the estimated parameters, λ.

The measured head residuals are fit to a spherical semivariogram model with a zero nugget in the case study considered here. A zero nugget is used because the residuals are assumed to be known at the measurement locations. A zero nugget spherical semivariogram model is chosen because it seems to fit the sample semivariogram well. The semivariogram value for this model can be expressed as:

$$\gamma(s;\lambda) = \begin{cases} c_s\left[(3/2)(s/a_s) - (1/2)(s/a_s)^3\right] & 0 < s \le a_s \\ c_s & s \ge a_s \end{cases} \qquad (12)$$

where c_s is the sill and a_s is the range of the semivariogram model.

To minimize the effect of the choice of the lag increment used to calculate the semivariogram, several lag increments are considered and their results are averaged. In this way, small changes in the spatial characteristics of the measured head residuals can be detected that are not just a product of the particular choice of a single lag increment value. If small changes in the lag increment result in large changes in the calculated semivariogram parameters, then there may not be enough data to accurately define the sample semivariogram.

The semivariogram parameters are also calculated using a kriging technique called jackknifing. Jackknife kriging systematically deletes one data point at a time and then calculates a value by kriging. A thorough discussion of kriging theory is presented by Journel and Huijbregts (1978). The difference between the original measured value and the kriged estimate is called the "jackknifing error." The sum of the jackknifing errors over all of the measurement points should be unbiased and the variance of the jackknifing errors should be as small as possible. Optimum semivariogram parameters can be selected by minimizing the variance of the jackknifing errors.

The kriging estimator, Z'_m, is a linear combination of several of the observed data expressed as:

$$Z'_m = \sum_{i=1}^{N_m} a_{mi} Z^*_{mi} \qquad (13)$$

where there are N_m observations, Z^*_{mi}, to be used to estimate Z at location m. The kriging coefficients, a_{mi}, are calculated to ensure that the kriging estimator is unbiased, and that the variance of the estimation error is minimized. The value of N_m must be chosen with care when minimizing the variance of the jackknifing errors. N_m is often determined as a specified maximum number of pairs and/or maximum specified separation distance.

The kriging coefficients are determined from the following kriging equations:

$$\sum_{j=1}^{N_m} a_{mj}\gamma(\underline{x}_{mi}, \underline{x}_{mj})a_{mi}\ \sigma^2_{mi} + \beta_m = \gamma(\underline{x}_{mi}, \underline{x}_m), \qquad i = 1, 2, \ldots, N_m \qquad (14)$$

$$\sum_{j=1}^{N_m} a_{mj} = 1$$

yielding N_m+1 equations and unknowns for each estimation location, m. β_m is a Lagrange multiplier, γ is calculated from the semivariogram, and σ_{mi}^2 is the variance of the measurement error for the i^{th} data.

Only the range and ratio of the nugget to the sill can be estimated with the jackknife approach since the N_m kriging equations of equation (14) are all scaled by the sill. Since the nugget is set to

zero for the measured head residuals, the jackknife kriging method is used only to estimate the range. The sill can be estimated from the variance of the data. The variance of the data should be slightly smaller than the sill from a sample semivariogram since spatially correlated values are included in the calculation of the variance but not in the sill. If a trend is present in the data, the variance will often be greater than the sill from a sample semivariogram.

ESTIMATION ERROR FOR HYDRAULIC HEADS

Determination of the variance and covariance of the error of estimation for the hydraulic heads can be an important consideration especially when these values are used in subsequent inverse modeling. Neuman and Jacobson (1984) describe a method to calculate the error of estimation based on the kriging variance of the head residuals. According to this method, referred to here as the kriging variance method, the variance of the estimation error is given by:

$$Var[e_{Km}] = 2\sum_{i=1}^{N_m} \alpha_{mi}\gamma(x_{mi},x_m) - \sum_{i=1}^{N_m}\sum_{j=1}^{N_m} \alpha_{mi} \propto_{mj} \gamma(x_{mi},x_{mj}) + \sum_{i=1}^{N_m} \alpha_{mi}^2\sigma_{mi}^2 \quad (15)$$

The kriging variance method is developed by defining the estimation error as the difference in the true residuals and the estimated residuals. It does not include error in the estimation of the drift component of the head. The estimation error of the drift can be very large in regions with sparse data, as is often the case near no-flow boundaries.

A method to calculate the error of estimation for the hydraulic head is presented in Appendix B that includes contributions from the drift component of the head as well as the residual component. This method is called the drift plus kriging variance method, and defines the variance of the estimation error as:

$$
\begin{aligned}
Var[e_{Dmn}] = & \sum_{p=1}^{J_p}\sum_{q=1}^{J_p} f_p(x_m)V_{apq}\,f_q(x_n) + E[R_m\,R_n] \\
& - \sum_{j=1}^{N_n}\alpha_{nj}\left\{\sum_{p=1}^{J_p}\sum_{q=1}^{J_p} f_p(x_m)V_{apq}\,f_q(x_{nj}) + E[R_m\,R'_{nj}]\right\} \\
& - \sum_{i=1}^{N_m}\alpha_{mi}\left\{\sum_{p=1}^{J_p}\sum_{q=1}^{J_p} f_p(x_n)V_{apq}\,f_q(x_{mi}) + E[R_n\,R'_{mi}]\right\} \\
& + \sum_{i=1}^{N_m}\sum_{j=1}^{N_n}\alpha_{mi}\,\alpha_{nj}\left\{\sum_{p=1}^{J_p}\sum_{q=1}^{J_p} f_p(x_{mi})V_{apq}\,f_q(x_{nj})\right\} \\
& + E[R'_{mi}\,R'_{nj}] + \delta_{mi,nj}\,\sigma_{mi}\,\sigma_{nj}
\end{aligned}
\tag{16}
$$

where there are J_p coefficients of the drift polynomial.

The drift plus kriging variance method defines the estimation error as the sum of the difference between the true drift and the estimated drift and the difference between the true residual and the estimated residual. Since the no-flow boundary constraints are included in the drift determination, the weighting of the no-flow boundary constraints should be reflected in the error of estimation determined from this method.

Assumptions made in both the kriging variance method of Neuman and Jacobson (1984) and the drift plus kriging variance method developed in Appendix B include no correlation between measurement errors at different locations and no correlation between measurement errors and true residuals. The drift plus kriging variance method also assumes that the error in the drift estimate is not correlated to true residuals or measurement errors. This assumption is reasonable since the drift estimation error increases in areas where the head data are less abundant, while the measurement errors and residuals are not expected to be related to the abundance or sparsity of the head data.

AVRA VALLEY CASE STUDY

Description of the Avra Valley Aquifer

Avra Valley is located in southern Arizona and contains an extensive alluvial aquifer (Figure 3). The valley is oriented north and south and is about 50 km long and 10 to 20 km wide. Avra Valley is bounded by the Roskruge, Waterman, and Silverbell mountains on the west and the Tucson and Tortolita mountains on the east. The southern end of the valley is about 750 m above mean sea level, dropping off to about 550 m in the north. Two major intermittent watercourses cross the valley, the Santa Cruz River and Brawley Wash, which becomes the Los Robles Wash in the north. The valley is arid with a mean annual rainfall of 24 cm.

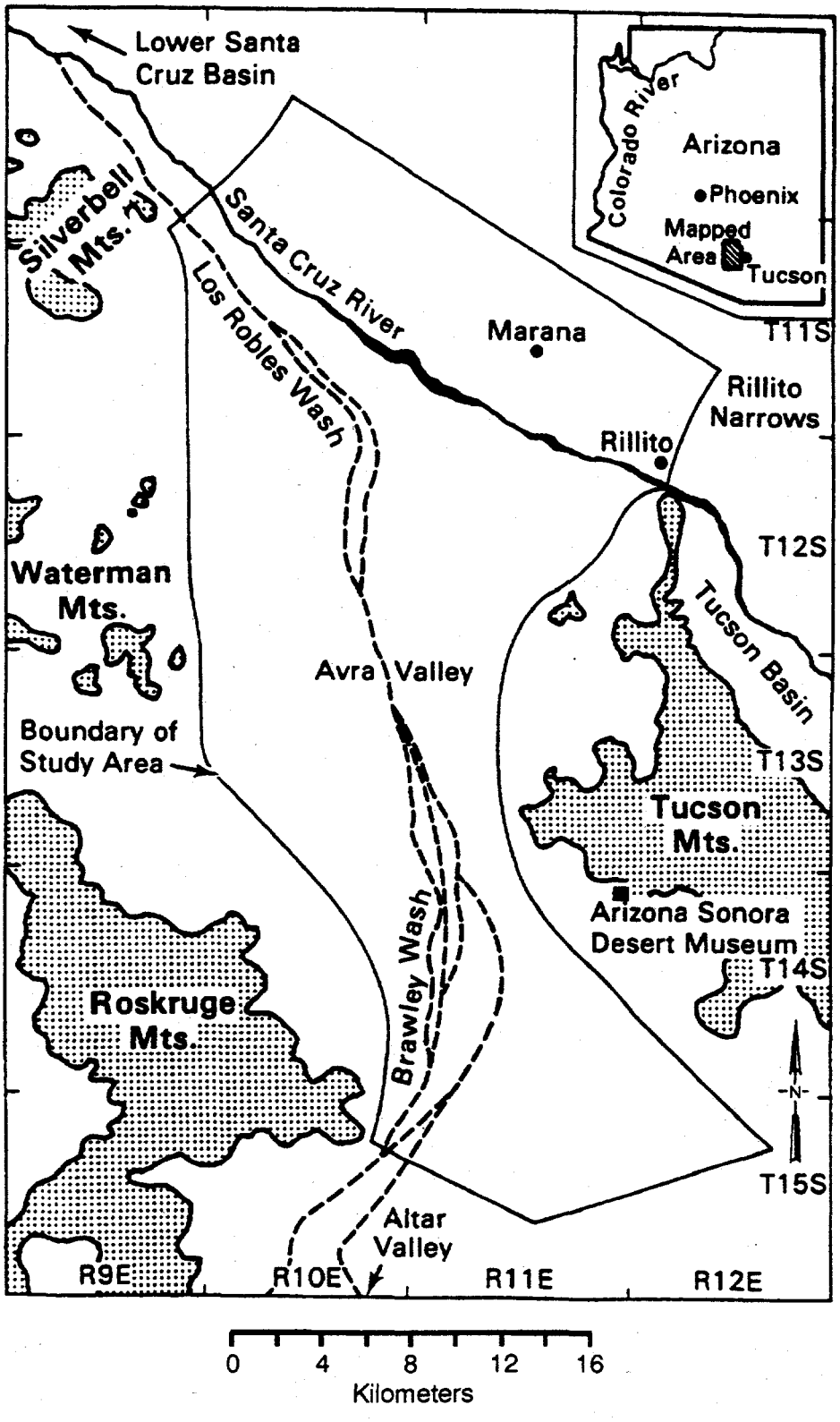

Figure 3. Location of Avra Valley aquifer.

The Avra Valley basin is a graben filled with Cenozoic alluvium and surrounded by Mesozoic and Tertiary volcanic rocks, Paleozoic sedimentary rocks, and Precambrian granites. The basin can be subdivided into a 2900-m-deep northern subbasin and a 760-m-deep southern basin. The fill consists of sandy gravel, gravely sand, silt and clay. The upper 180 to 210 m of the alluvium appear to be hydraulically connected and form a single unconfined aquifer with groundwater flowing to the north and northwest. A more detailed description of the valley and aquifer is presented in Clifton (1981).

Figure 4 shows the 99 locations where wellbore water level data are available and the finite element mesh where hydraulic head values are to be estimated. No-flow boundaries, shown with a bold line in Figure 4, are assumed along sections of the north, east and west boundaries. These no-flow boundaries correspond to those proposed by Clifton (1981). Neuman and Jacobson (1984) determined that a fourth order polynomial was necessary to describe the drift in the hydraulic head as indicated by the sample semivariogram of the hydraulic head residuals.

At high orders of polynomial drift, such as fourth order, the gradient of the drift can change dramatically in areas where no data are available. As seen in Figure 4, some sections of the no-flow boundaries have several nearby head measurements, such as the west end of the north no-flow boundary and the north end of the west no-flow boundary. Other sections of the no-flow boundaries have few nearby head measurements, such as the east end of the north no-flow boundary and the south end of the east no-flow boundary. The no-flow boundary constraints should help to define the drift of the hydraulic head in the vicinity of the no-flow boundaries where few head measurements are available.

Order of the Drift for the Hydraulic Heads

The choice of the order of the drift is examined first by considering third, fourth, and fifth order drifts without the no-flow boundary constraints. The range values of the semivariogram used in the stepwise iterative regression are estimated by the weighted squares and jackknife kriging methods. The iterations are terminated when the change in the range estimate is less than 0.01 percent the range estimate.

The results of the weighted least squares and jackknife kriging methods for determining the range and sill of the Avra Valley head residuals are summarized in Table 1. In the weighted least squares method, the maximum lag used is 12 kilometers (km) with the range and sill estimates averaged over 26 lag increment values between 1.2 and 1.6 km. In the jackknife kriging method, the maximum number of kriging points used to estimate each head value is 30 points and the maximum separation distance is 16 km. The variance of the head residuals and the jackknifing error for the head estimates are also presented in Table 1.

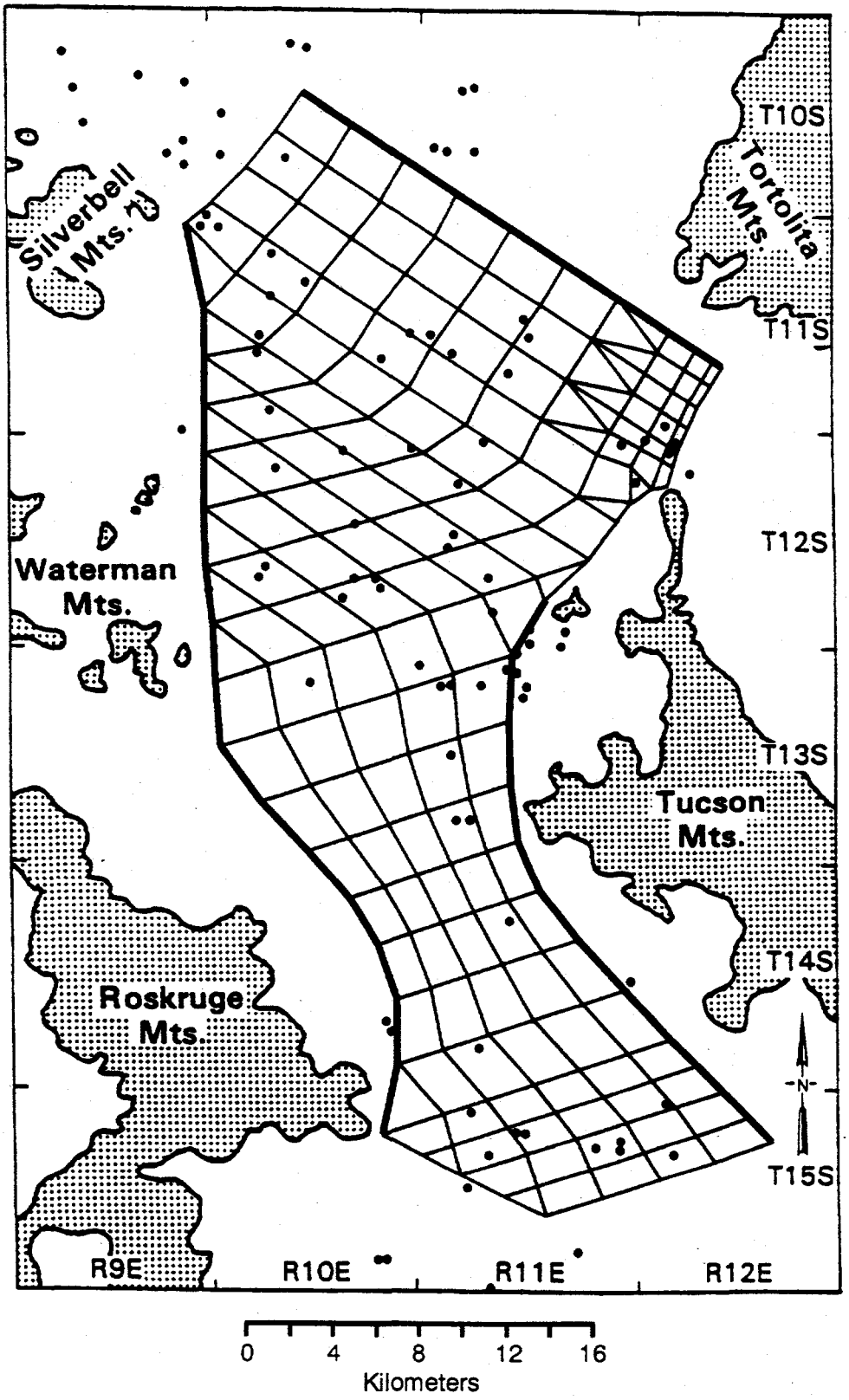

Figure 4. Location of wellbore water level data and finite element grid for estimation of hydraulic heads in the Avra Valley. No-flow boundaries are indicated by bold lines.

Table 1. Semivariogram Parameters and Head Residual Statistics for the Third, Fourth, and Fifth Order Drift Solutions Obtained from the Weighted Least Squares and Jackknife Kriging Methods.

Weighted Least Squares Method

Order of Drift	Range (km)	Sill (m^2)	Mean (m)	Variance (m^2)	χ^2 Test
3	8.03	16.26	–0.0195	18.09	0.470
4	6.34	9.47	0.0817	8.86	0.968
5	4.36	5.44	0.0448	4.96	0.115

Jackknife Kriging Method

Order of Drift	Range (km)	Mean (m)	Variance (m^2)	χ^2 Test
3	5.94	0.0329	17.53	0.433
4	4.46	0.0111	8.58	0.888
5	4.28	0.0427	4.94	0.057

Isotropic and directional sample semivariograms of the head residuals produced by the stepwise iterative regression for third, fourth, and fifth order drift solutions using the jackknife kriging method are presented in Figure 5. A lag increment of 1.4 km is used to calculate all the sample semivariograms shown in Figure 5 and the directional semivariograms are calculated using a 45-degree-angle window.

The isotropic sample semivariogram of the head residuals for the third order drift solution shown in Figure 5a increases with increasing lag, indicating a drift in the residuals. The range determined from the weighted least squares method for an increasing semivariogram is very sensitive to the maximum lag used, increasing as the apparent sill increases. From Table 1, the range for the third order drift solution determined by the jackknife kriging method is 5.94 km, while the weighted least squares method range is 8.04 km. The range calculated from the jackknife kriging method seems to be much less sensitive to the presence of a trend than the weighted least squares method. The variance of the head residuals from the weighted least squares method is greater than the estimated sill, another indication of a drift in the head residuals for the third order solution.

The isotropic sample semivariogram for the fourth order drift solution, shown in Figure 5b, exhibits a distinct sill at about 9 m^2. However, the northeast-southwest and north-south directional sample semivariograms reach a sill of about 11 m^2, while the northwest-southeast and east-west directions exhibit a sill of only about 7 m^2. The different sills of the directional sample semivariograms indicate that the head residuals could be non-intrinsic. The range for the fourth order drift solution determined with the jackknife kriging method, 4.46 km, is much less than the range determined with the weighted least squares method, 6.34 km, as shown in Table 1. This is

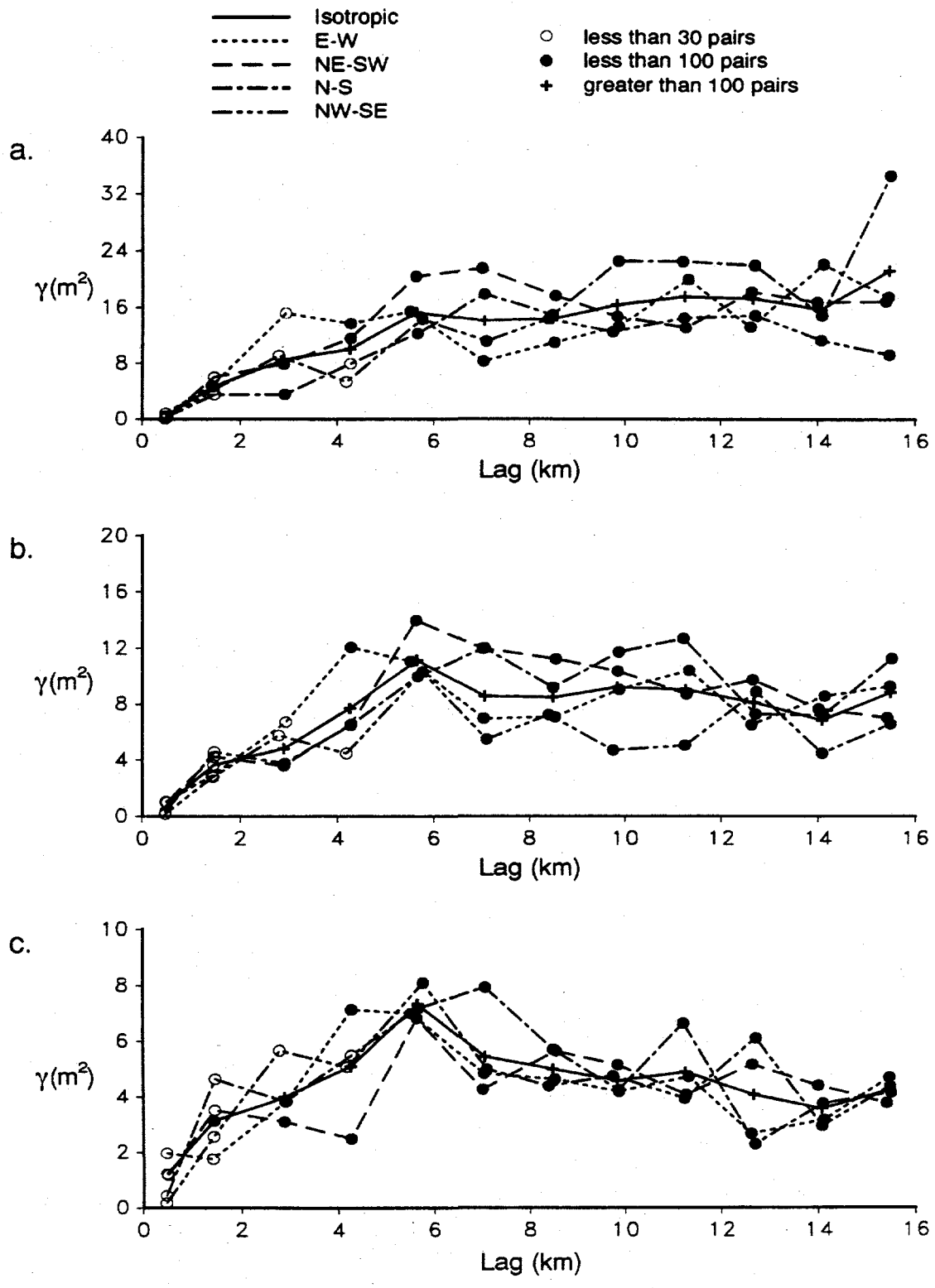

Figure 5. Sample semivariograms of head residuals for (a) third, (b) fourth, and (c) fifth order drift solutions.

another indication that the residuals from the fourth order drift solution could be non-intrinsic. It is more conservative to use the shorter range of the jackknife kriging method since overestimating the range will result in underestimating the estimation error. Both methods yield head residuals that approximate a zero mean normal distribution with a mean less than 0.1 m and a χ^2 goodness of fit statistic for a normal distribution greater than 0.85.

Contour plots of the residuals and estimated heads for a fourth order drift solution using the weighted least squares and jackknife kriging methods of estimating the semivariogram parameters are presented in Figure 6. There appears to be little difference in the residual or head values due to the two methods. The contour plot of the residuals from the weighted least squares method, shown in Figure 6a, and from the jackknife kriging method, shown in Figure 6b, both show certain areas where the residual values change dramatically over short distances, such as in the northeast and east central regions. These areas could be the cause of the variation in the sill for the directional sample semivariograms and the difference in the range calculated from the weighted least squares and jackknife kriging methods.

The isotropic sample semivariogram for the fifth order drift solution, shown in Figure 5c, peaks at about 7 m^2 with a lag of about 5.5 km and then levels out to about 4.5 m^2 at longer lags. All of the directional sample semivariograms for the fifth order drift solution follow similar patterns. Well-behaved sample semivariograms should increase or level out with increasing lags. A decrease in the sample semivariogram with increasing lag indicates that values are more correlated at larger lags. In this instance, the fifth order drift could be overfitting the data resulting in lower sample semivariogram values at longer lags. If this is the case, then the true range and sill should be indicated by the peak at about 5.5-km lag. As shown in Table 1, there is little difference in the range calculated for the fifth order drift solution from weighted least squares or jackknife methods, 4.36 and 4.28 km, respectively. Both methods produce head residuals with non-bias mean values, less than 0.05 m. However, the χ^2 statistic for both methods is very low, less than 0.12, indicating that the head residuals are not normally distributed. This is another indication that the fifth order drift solution could be overfitting the data.

Contour plots of the residuals and estimated heads for the fifth order drift solution using the jackknife kriging method to estimate the semivariogram parameters are presented in Figures 7a and 7b, respectively. The head estimates from the fourth order drift solution are also shown in Figure 7b for comparison. The estimated heads from the fourth and fifth order drift solutions are very similar except in the north and southeast corners. The pattern of the residuals are also similar except the fifth order residuals are smaller as expected. Both solutions show a large step in the head residuals across the east central part of the aquifer. This step in the residuals indicates a step in the hydraulic head

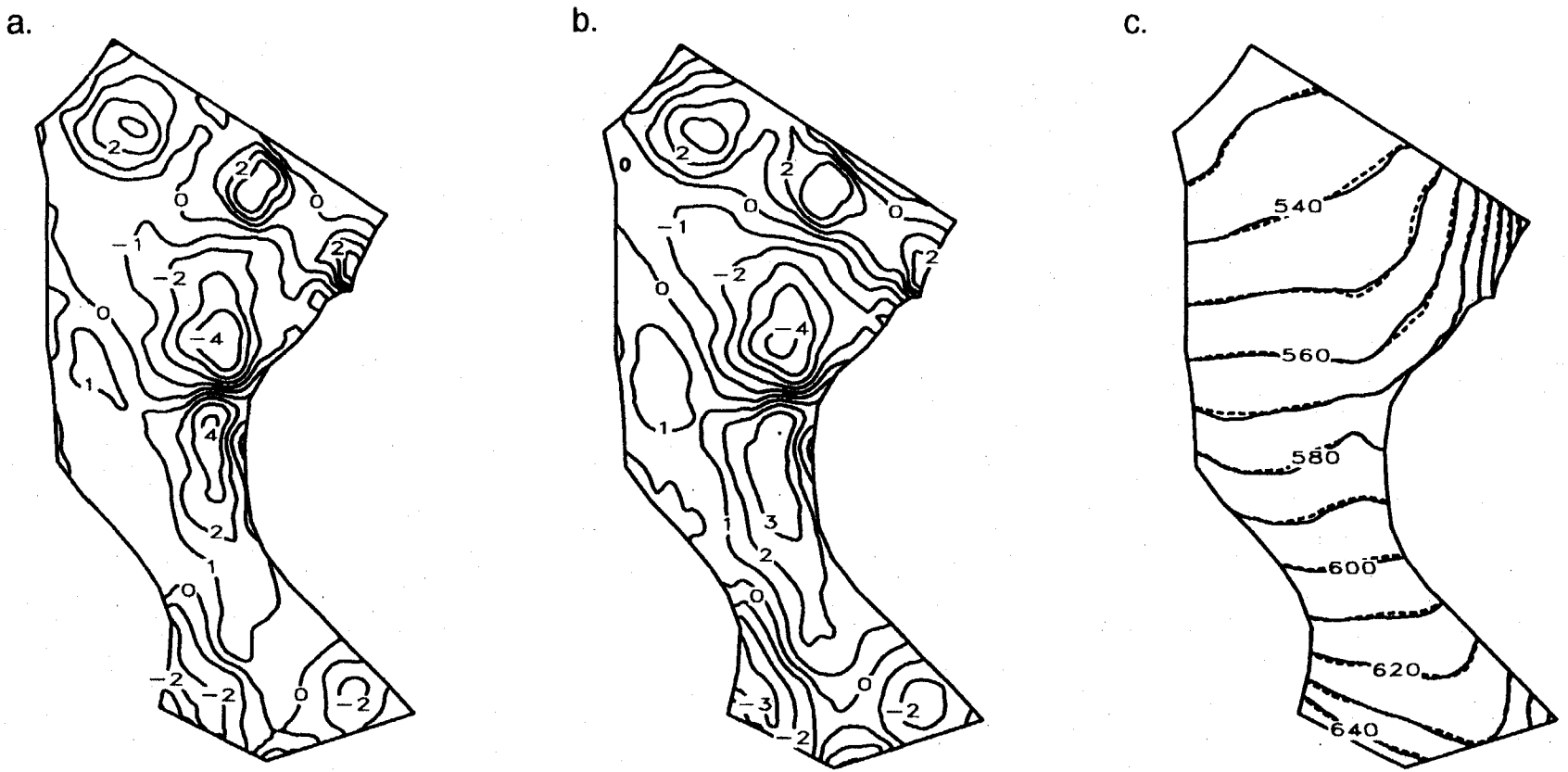

Figure 6. Head residuals in meters for fourth order drift solution using (a) weighted least squares and (b) jackknife kriging methods of estimating semivariogram parameters, and (c) head estimates in meters A.M.S.L. for both methods with solid line for jackknife kriging method and dashed line for weighted least squares method.

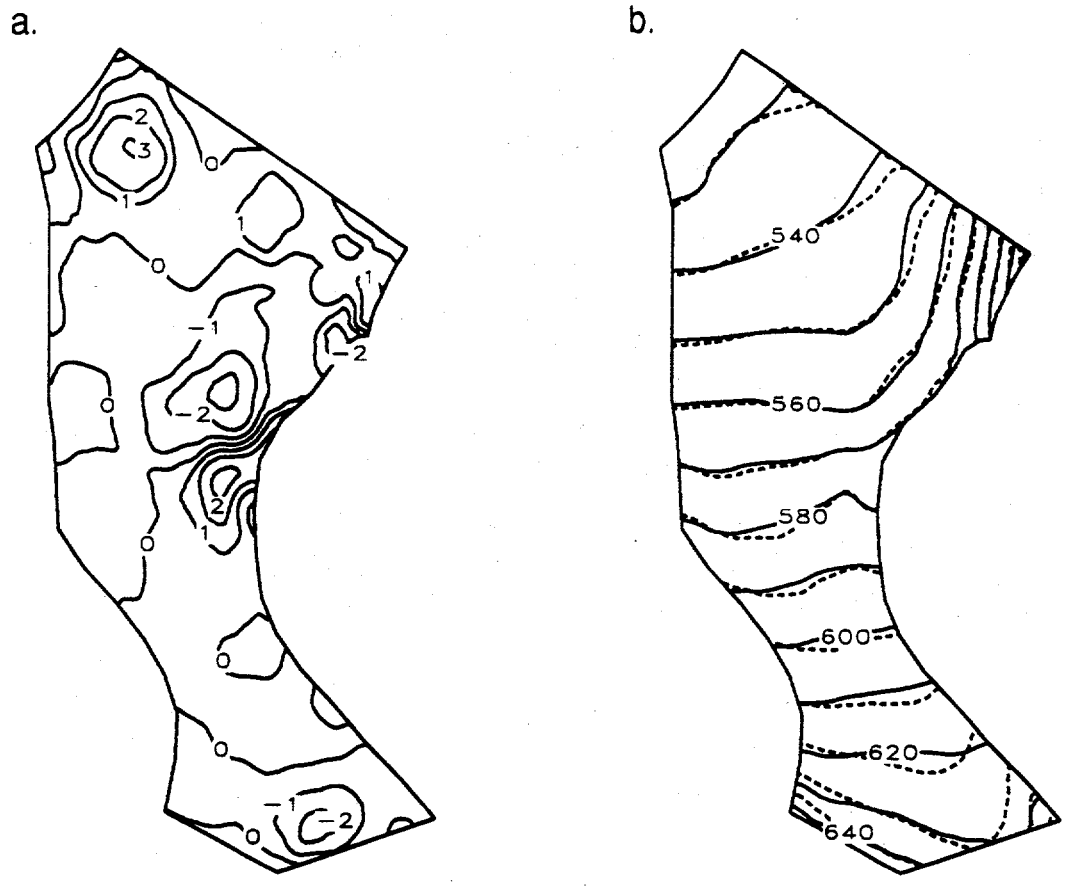

Figure 7. (a) Head residuals in meters and (b) estimated heads in meters A.M.S.L. for fifth order drift solutions using jackknife kriging method of estimating semivariogram parameters shown with solid line and estimated heads for fourth order drift solution shown with dashed line for comparison.

surface since the polynomial drift component generally varies smoothly. A step in the hydraulic head surface could indicate a step in transmissivities in this region.

The appropriate order of the drift in the Avra Valley heads seems to be either fourth or fifth order. The fourth order solution produces residuals that are somewhat non-intrinsic as indicated by the anisotropic sill. The fifth order solution appears to overfit the data with reduced variances at longer lags. Both of these problems result in sample semivariograms that are not well suited for the weighted least squares method of estimating semivariogram parameters. The jackknife kriging method of estimating the semivariogram parameters does not rely on the sample semivariogram and seems to be less sensitive to these problems. Both fourth and fifth order drift solutions will be considered when applying the no-flow boundary constraints. If there is little difference between

results of fourth and fifth order drift solutions, then the fourth order drift solution is preferred since it is a simpler model representation.

Calculation of the estimation error requires an estimate of the sill and range of the head residuals. The weighted least squares method of fitting the sample semivariogram yields an estimate of the sill. However, the jackknife kriging method can only be used to estimate the range. A reasonable estimate of the sill that does not rely on the sample semivariogram is the variance of the head residuals. Figures 8a and 8b show contour plots of the head estimation errors for the fourth and fifth order drift solutions using the jackknife kriging method to estimate the range and sill of the head residuals. The highest estimation errors for both solutions are in the southeast and the northeast corners. The estimation errors are high in these areas because few head measurements are present to define the drift component. Except where the drift component of the estimation error dominates, the

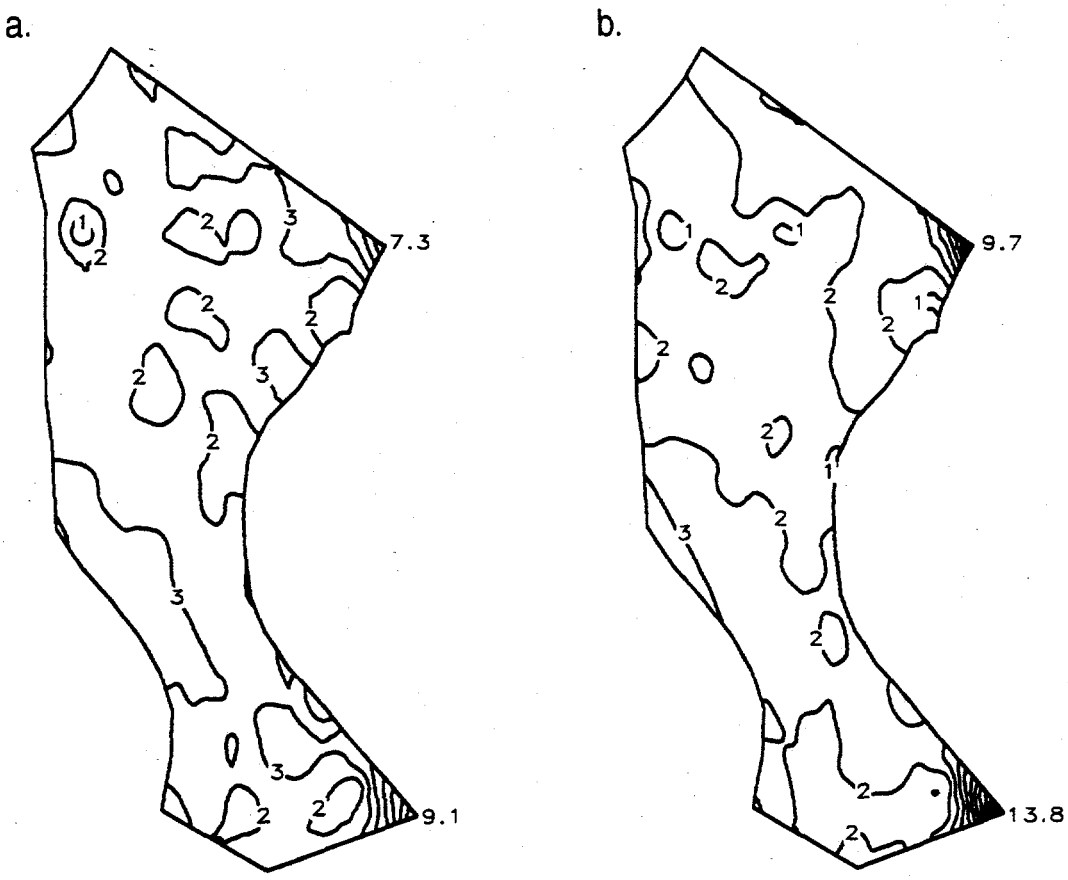

Figure 8. Estimation error for heads in meters estimated with (a) fourth order drift solution and (b) fifth order drift solution.

estimation errors for the fifth order fit are less than those for the fourth order fit because the sill of the head residuals is smaller for the fifth order fit. Where the drift component dominates, in the northeast and southeast corner, the estimation error peaks at 9.7 and 13.8 m, respectively, for the fifth order drift compared to values of 7.3 and 9.1 m for the fourth order drift.

No-Flow Boundary Constraints Applied to the Fourth Order Drift Solution

Three different no-flow boundary constraint configurations have been used to check the effects of the choice of distances "a" and "b" of Figure 2. These configurations, shown in Figure 9, are: a) 75 boundary constraints with distance "a" equal to 1.34 km and distance "b" equal to 1.61 km; b) 75 boundary constraints with "a" equal to 1.34 km and distance "b" equal to 2.42 km; and c) 58 boundary constraints with 1.74 km for distance "a" and distance "b" equal to 1.61 km. These values were chosen to be similar to the average distance between adjacent nodes and different enough from each other to reveal if the resulting heads are very sensitive to the different boundary constraint spacing.

As the weighting of the boundary constraints is increased, there is a tradeoff in the fit of the head measurements and the fit of the boundary constraints. The range and sill of the semivariogram of the head residuals may also change as the weighting of the boundary constraints is increased. How much the head residuals deviate from a zero mean normal distribution is checked by calculating the mean of the head residuals and a χ^2 test. These factors will be examined to determine the appropriate boundary constraint weighting. A uniform weighting among all the boundary constraints is considered here.

Plots of the jackknifing error, boundary constraint error, and head residual range, sill, mean, and χ^2 test are presented in Figure 10 for a fourth order drift solution with various boundary constraint weightings using the boundary constraint configuration of Figure 9a. The boundary constraint weighting is expressed as a relative value where a weighting of one indicates that each boundary constraint is weighted by the same amount as each head measurement. Plots are shown for both the weighted least squares method and jackknife kriging methods of estimating semivariogram parameters.

Figure 10a shows that the range and sill estimated by the weighted least squares method increase dramatically at the higher boundary constraint weightings while the jackknife kriging method shows a much smaller increase in the estimated range and sill. The jackknife kriging method of determining the range and sill is less sensitive to changes in the sample semivariogram. However, the weighted least squares method is useful in determining how severely the sample semivariogram is affected by the boundary constraints.

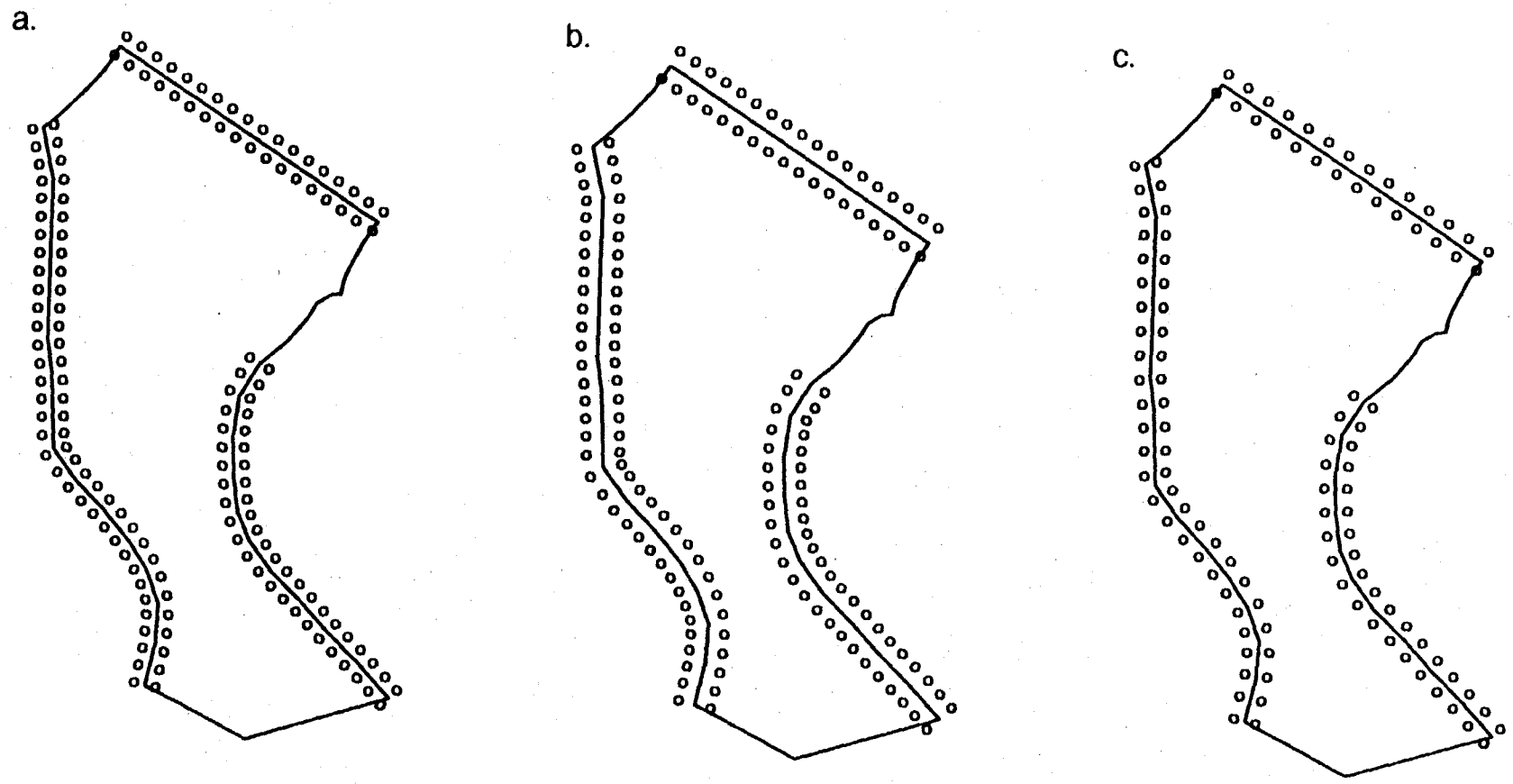

Figure 9. No–flow boundary constraint configurations: (a) 75 boundary constraints with distance "a" equal to 1.34 km and distance "b" equal to 1.61 km, (b) 75 boundary constraints with "a" still equal to 1.34 km and distance "b" equal to 2.42 km, and (c) 58 boundary constraints with 1.74 km for distance "a" and distance "b" equal to 1.61 km (distance "a" and "b" shown in Figure 2).

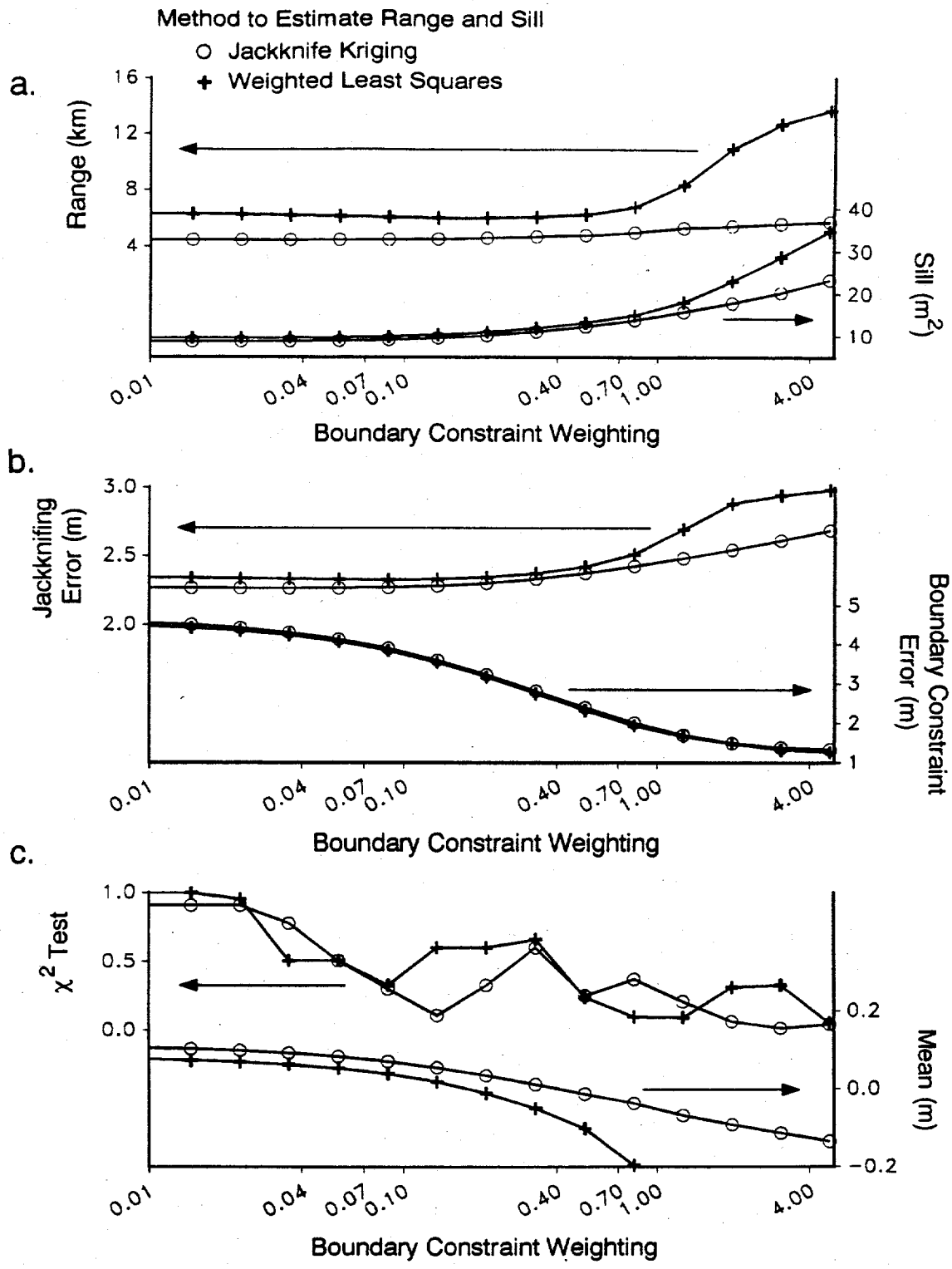

Figure 10. (a) Estimated range and sill for head residuals, (b) jackknifing error and boundary constraint error, and (c) χ^2 test and mean of head residuals for various boundary constraint weightings and a fourth order drift.

The boundary constraint error decreases similarly for both weighted least squares and jackknife kriging methods as shown in Figure 10b. However, the jackknifing error for the weighted least squares method is much higher than the jackknife kriging method at high boundary constraint weightings due to the large range produced by the weighted least squares method. From Figure 10c, the mean of the head residuals deviates far from zero for the weighted least squares method at high boundary constraint weighting. For both weighted least squares and jackknife kriging methods, the χ^2 test statistic decreases with increasing boundary constraint weightings, indicating that the head residuals are not normally distributed at the higher boundary constraint weightings.

The tradeoff in the jackknifing error and the boundary constraint error of the plots in Figure 10b can be evaluated by plotting the percent increase in the jackknifing error against the percent decrease in the boundary constraint error, as shown in Figure 11a. Figures 11b and 11c show how the range and variance of the head residuals changes with the percent decrease in the boundary constraint error. These plots indicate that the boundary constraint error can be reduced by about 50 percent with minor increases in the range, variance, and jackknifing error. The range, variance, and jackknifing error increase more rapidly as the decrease in the boundary constraint error approaches its maximum of about 70 percent of the no-boundary-constraint value. All of the plots in Figure 11 contain results from using the three different boundary constraint configurations shown in Figure 9. Although the different configurations are sensitive to different levels of boundary constraint weightings, the range variance and jackknife error all change similarly as the boundary constraint error is reduced. Because of these similarities, only one boundary constraint configuration, consisting of 75 boundary constraints with distance "a" equal to 1.34 km and distance "b" equal to 1.61 km shown in Figure 9a, is used for the remainder of this analysis.

Contour plots of the head residuals produced from the fourth order drift solution using boundary constraint weightings of 0.125, 0.5, and 2.0 are presented in Figures 12a, 12b, and 12c, respectively. The problem with large changes in the residuals over short distances in the northeast corner of the aquifer discussed previously is increased with the increasing boundary constraint weighting. This could be a cause for the deterioration of the sample semivariogram and low χ^2 values at high boundary constraint weightings.

Figures 13a, 13b, and 13c show isotropic and directional sample semivariograms of head residuals from the fourth order drift solution with boundary constraint weightings of 0.125, 0.5, and 2.0, respectively, using the boundary constraint configuration of Figure 9a. The sample semivariograms for the 0.125 weighting are very similar to the sample semivariograms with no boundary constraints shown in Figure 4b. With boundary constraint weightings of 0.5 and 2.0, the isotropic sample semivariogram starts to increase with increasing lags and the directional sample semivariograms start to diverge indicating a possible trend along the northeast-southwest direction.

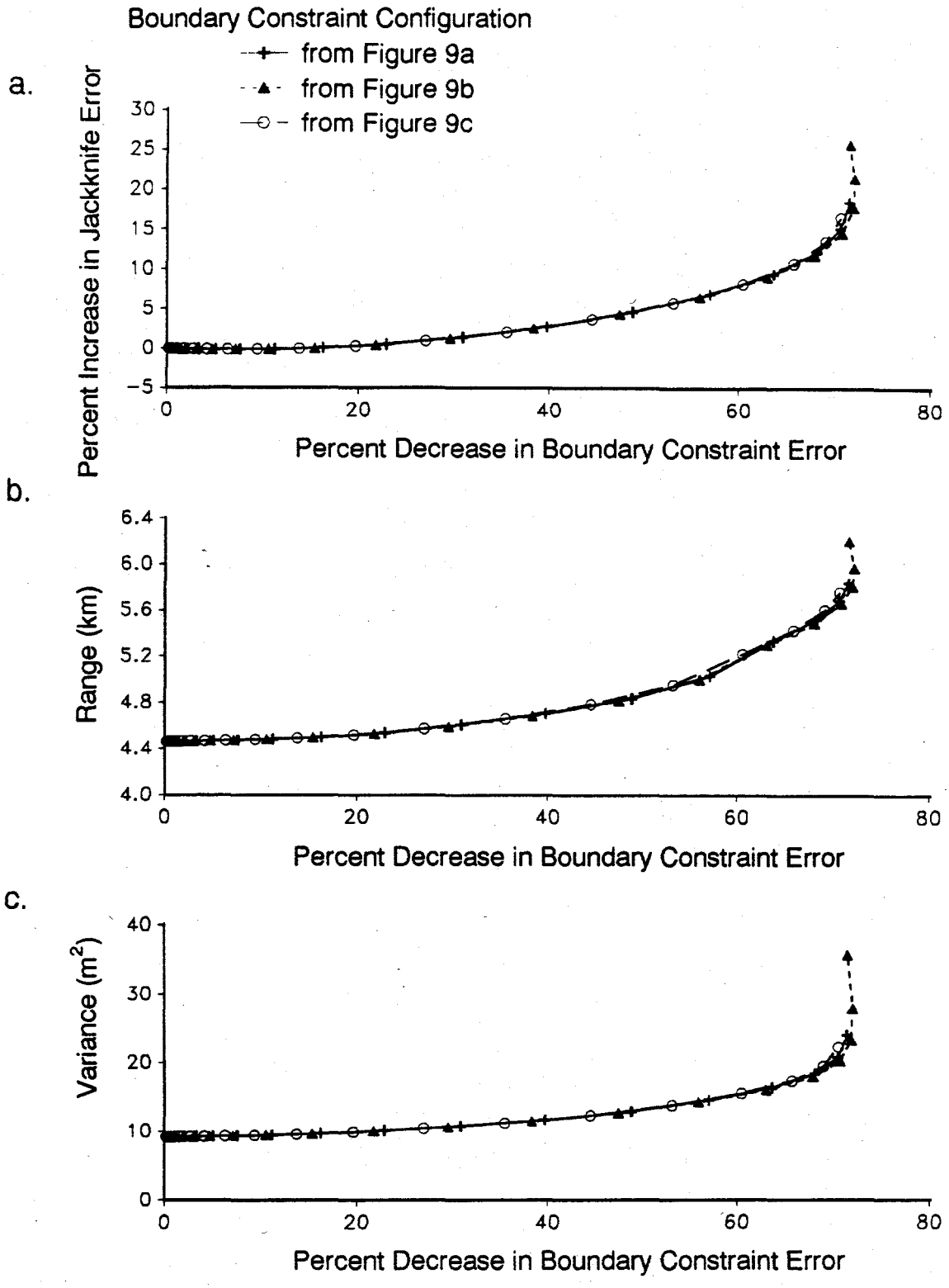

Figure 11. (a) Percent change in jackknifing error, (b) head residual range estimate, and (c) head residual variance verses the percent change in the boundary constraint error for fourth order drift solution.

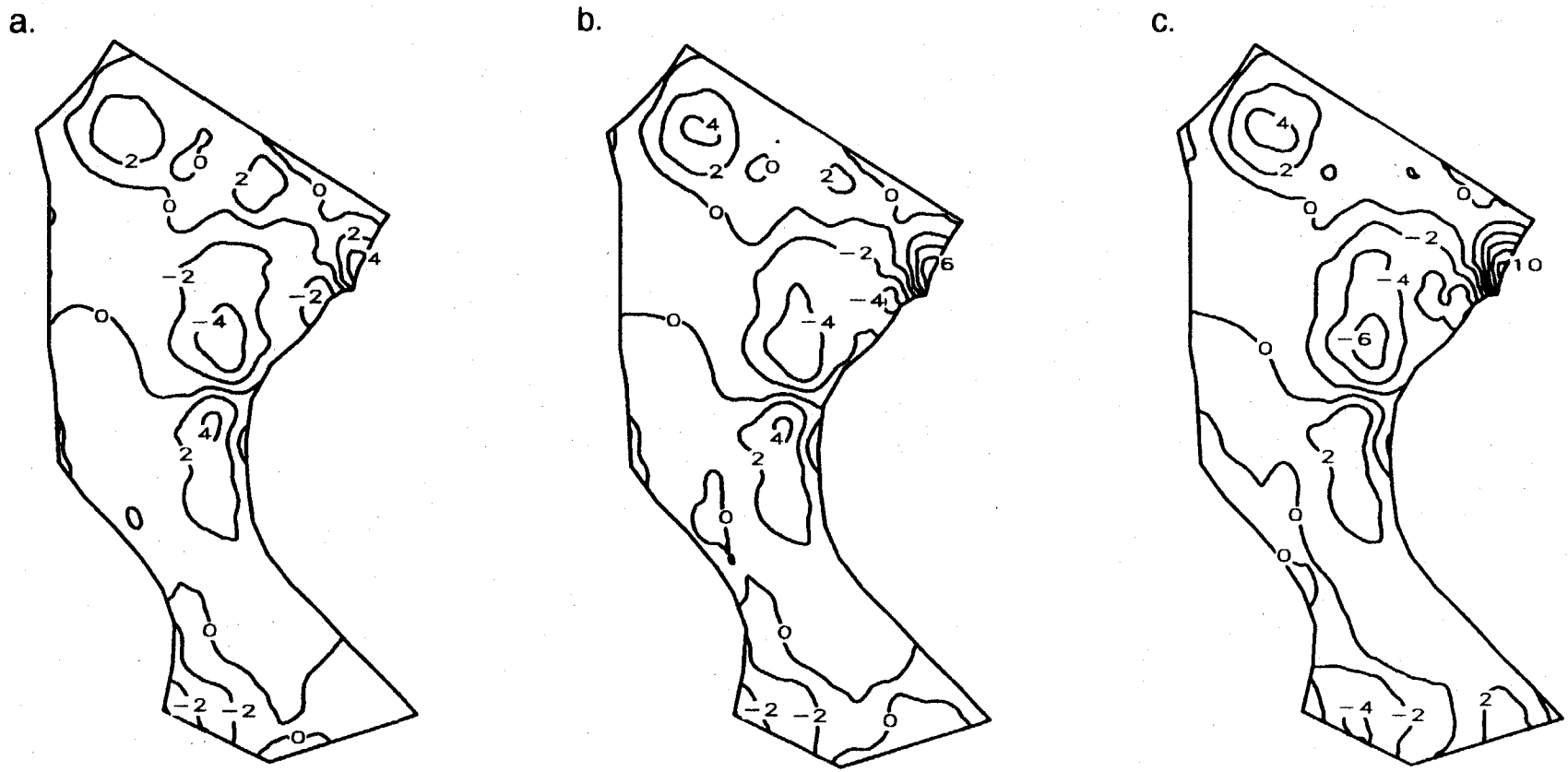

Figure 12. Head residuals in meters for fourth order drift solution using boundary constraint weightings of (a) 0.125, (b) 0.5, and (c) 2.0.

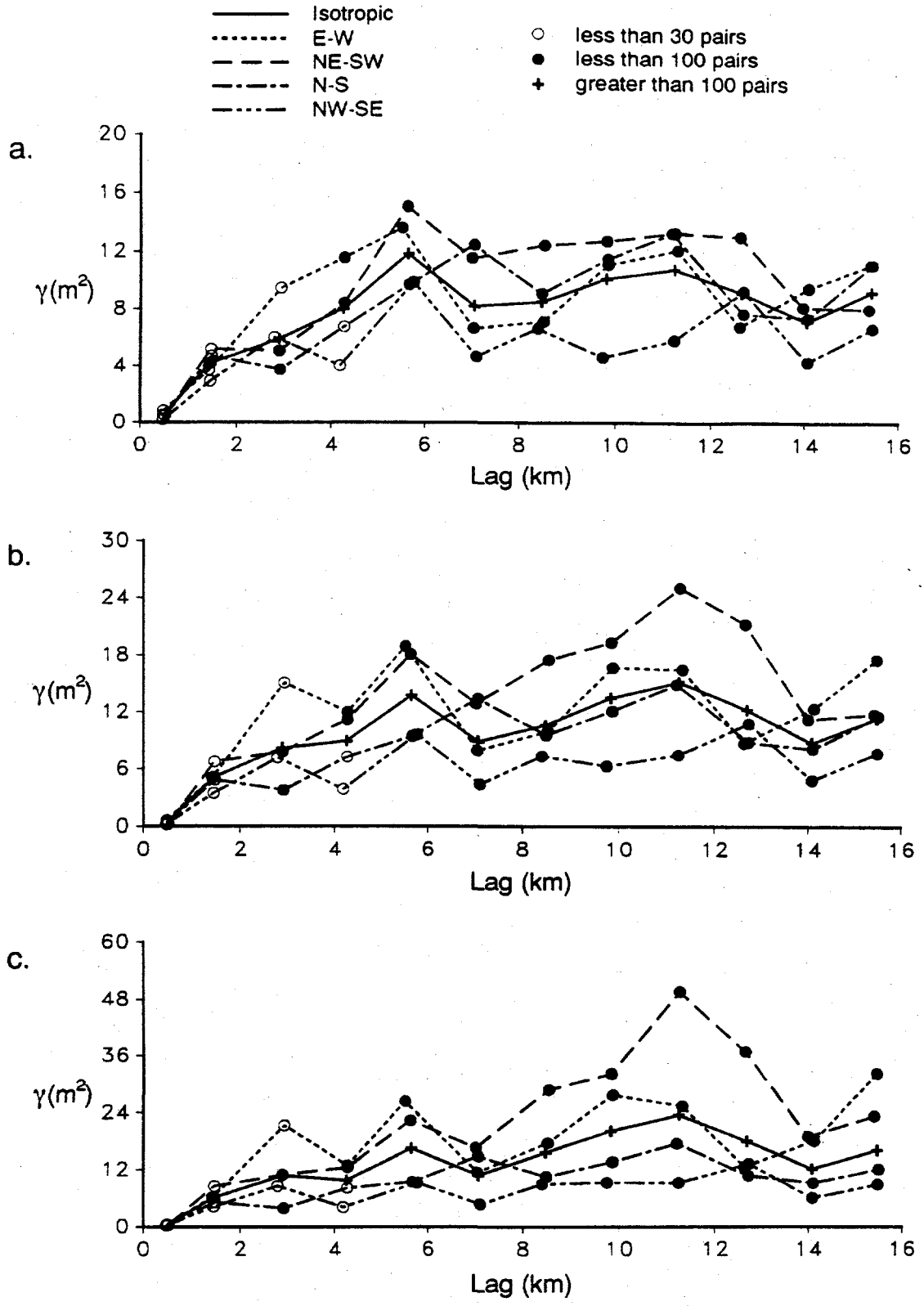

Figure 13. Sample semivariograms of head residuals for fourth order drift solution using boundary constraint weightings of (a) 0.125, (b) 0.5, and (c) 2.0.

Contour plots of heads estimated using a fourth order drift solution with a boundary constraint weighting of 0.5 and with no boundary constraints are shown in Figure 14. Also shown in Figure 14 are graphs of the boundary constraint residuals along the no-flow boundaries. These graphs indicate the slope of the estimated head surface perpendicular to the no-flow boundary. There are three regions where the boundary constraints have the most influence: 1) along the eastern 3 km of the north no-flow boundary; 2) along the southern 5 km of the east no-flow boundary; and 3) 5 km along the central part of the western no-flow boundary.

Differences between the heads estimated with and without boundary constraints of Figure 14 can be examined by contouring the difference of the head values estimated at each node point, as shown in Figure 15a. By far the biggest differences are in the northeast and southeast corners where the head estimates are 22.1 and 18.5 m less, respectively, with the boundary constraints applied. The estimation errors are also reduced in these regions when the boundary constraints are applied, as shown in Figure 15b. The estimation errors without the boundary constraints from Figure 8a are reduced by about 13 percent in the northeast and southeast corners with the boundary constraint weightings of 0.5.

No Flow Boundary Constraints Applied to the Fifth Order Drift Solution

The boundary constraints have also been applied to the fifth order drift solution. The three boundary constraints configurations have been used on the fifth order solution and, as with the fourth order drift solution, the different configurations do not affect the tradeoff in the jackknifing and boundary constraint errors. Only results using the boundary constraint configuration of Figure 9a consisting of 75 constraints with distance "a" equal to 1.34 km and distance "b" equal to 1.61 km are presented for the fifth order drift.

Figure 16 shows the head residual range, sill, mean and χ^2 test, as well as jackknifing and boundary constraint errors, for the fifth order drift solution as the boundary constraint weighting is varied using both the weighted least squares and jackknife kriging methods of estimating the range and sill. The range and sill from both methods vary much less than those of the fourth order drift solution. The jackknifing error increases little while the boundary constraint error drops significantly as the boundary constraint weighting is increased. The mean of the head residuals increases with increasing boundary constraint weighting while the χ^2 statistic is low for boundary constraint weightings between about 0.2 and 2.

The percent increase in the jackknifing error and the increase in the range and variance of the head residuals are plotted against the percent decrease in the boundary constraint error for the fifth order drift solution in Figure 17. These plots indicate that the boundary constraint error can be reduced by about 50 percent without much affect on the jackknifing error or the range of the head

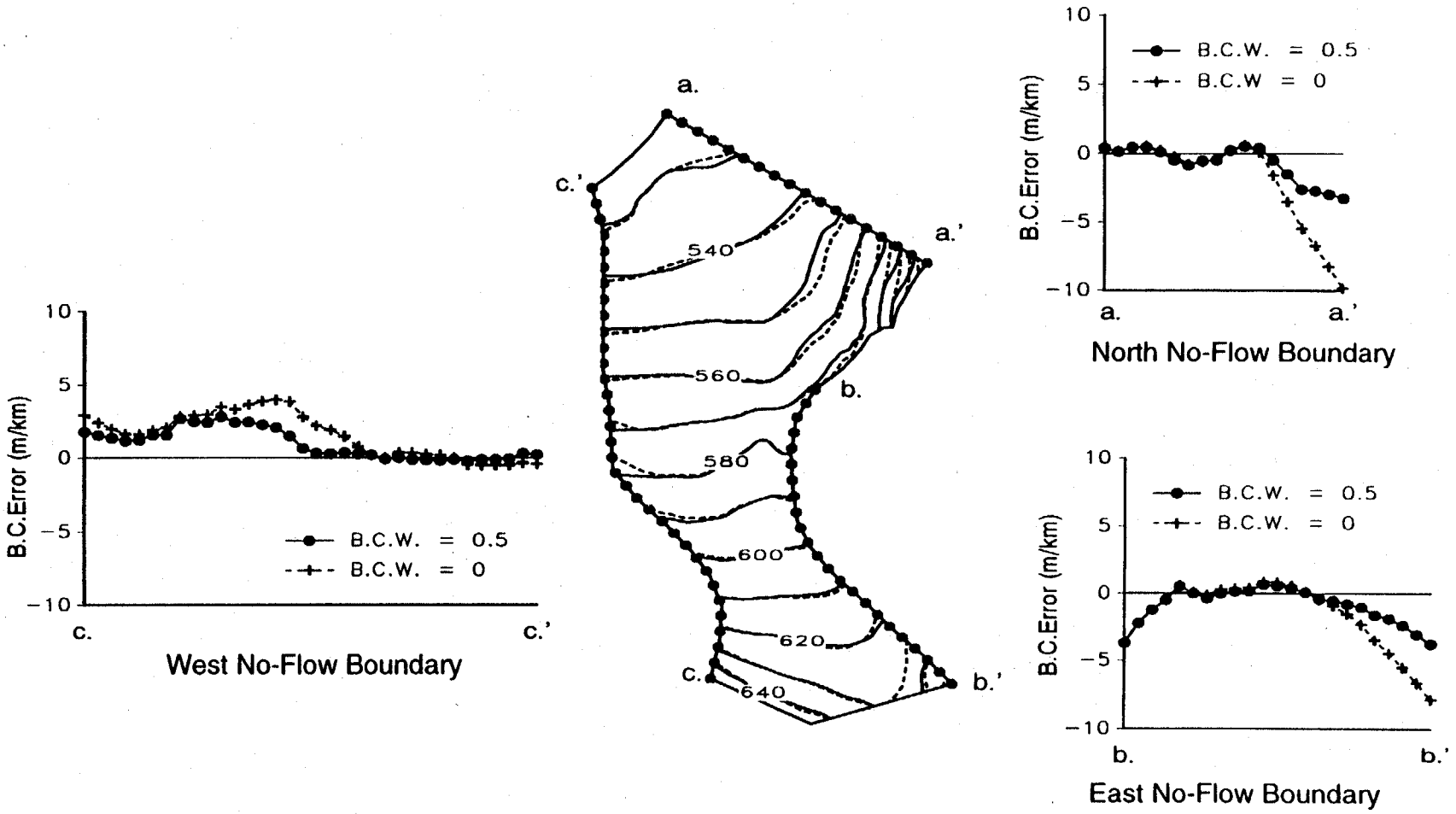

Figure 14. Estimated heads in meters A.M.S.L. and boundary constraint residuals with boundary constraint weightings of 0 and 0.5 for the fourth order drift solution. Heads estimated with boundary constraint weighting of 0.5 shown with solid line and heads estimated with no boundary constraint weighting shown with dashed line (B.C. Error is the boundary constraint error).

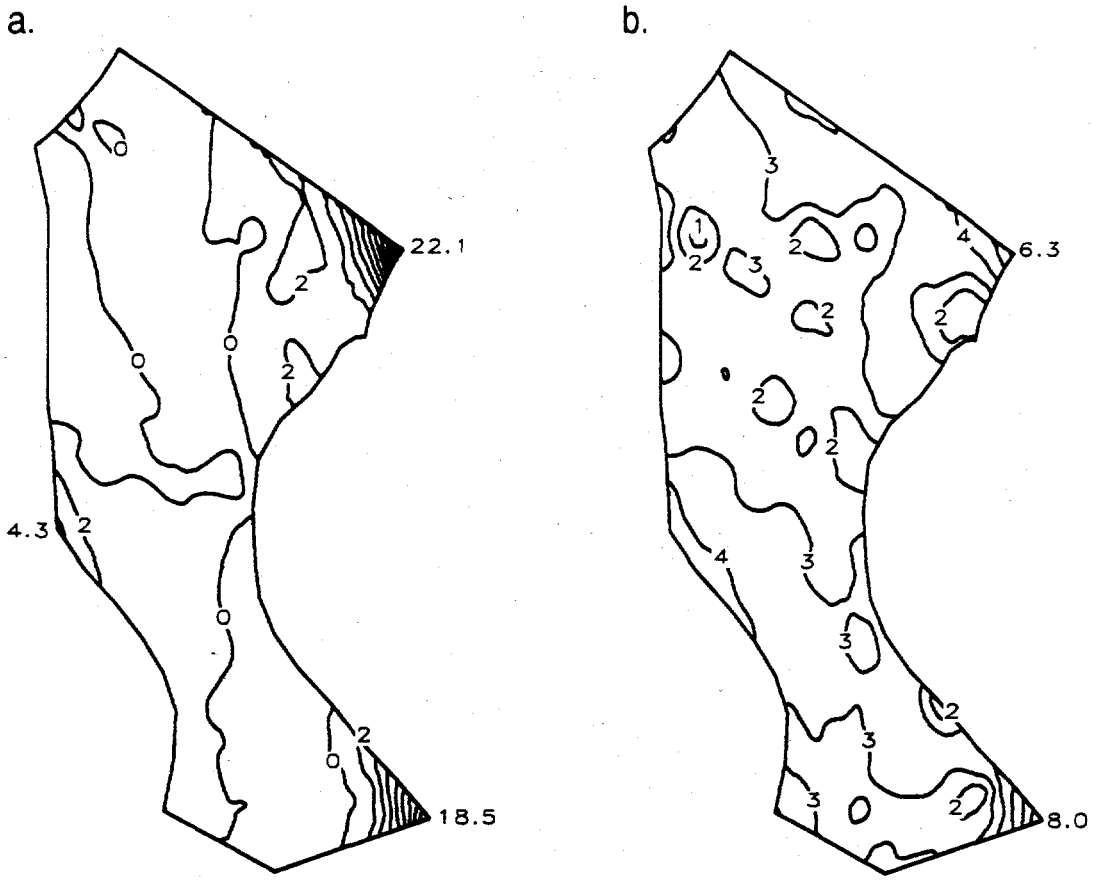

Figure 15. (a) Difference in meters of heads estimated with no boundary constraints and with boundary constraint weighting of 0.5 and (b) estimation error of heads estimated with boundary constraint weighting of 0.5 for fourth order drift solution.

residuals. This corresponds to a boundary constraint weighting of about 0.5. At higher boundary constraint weightings, the range decreases slightly and the jackknifing error increases dramatically, especially when the decrease in the boundary constraint error is greater than 60 percent.

Contour plots of the head residuals for the fifth order drift solution are presented in Figures 18a, 18b, and 18c for boundary constraint weights of 0.125, 0.5, and 2.0, respectively. As with the fourth order solution, the biggest change is in the northeast corner where the head residuals change considerably over a short distance at higher boundary constraint weightings. Isotropic and directional sample semivariograms of the head residuals for the fifth order drift solution and boundary constraint weights of 0.125, 0.5, and 2 are shown in Figures 19a, 19b, and 19c, respectively. These sample semivariograms show little change as the boundary constraint weighting is increased. This indicates that the assumption of independence between the head residuals and

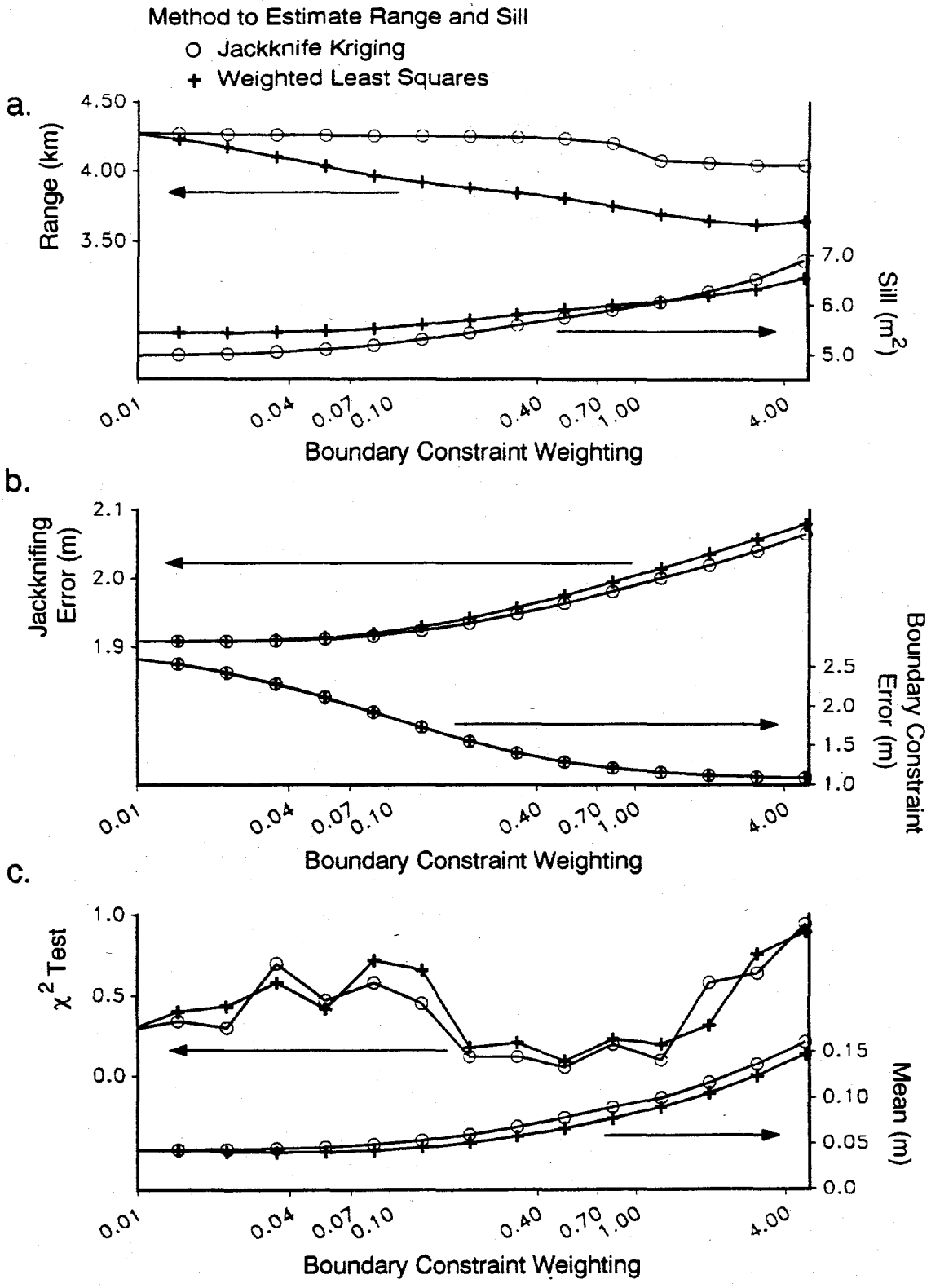

Figure 16. (a) Estimated range and sill for head residuals, (b) jackknifing error and boundary constraint error, and (c) χ^2 test and mean of head residuals for various boundary constraint weightings and a fifth order drift.

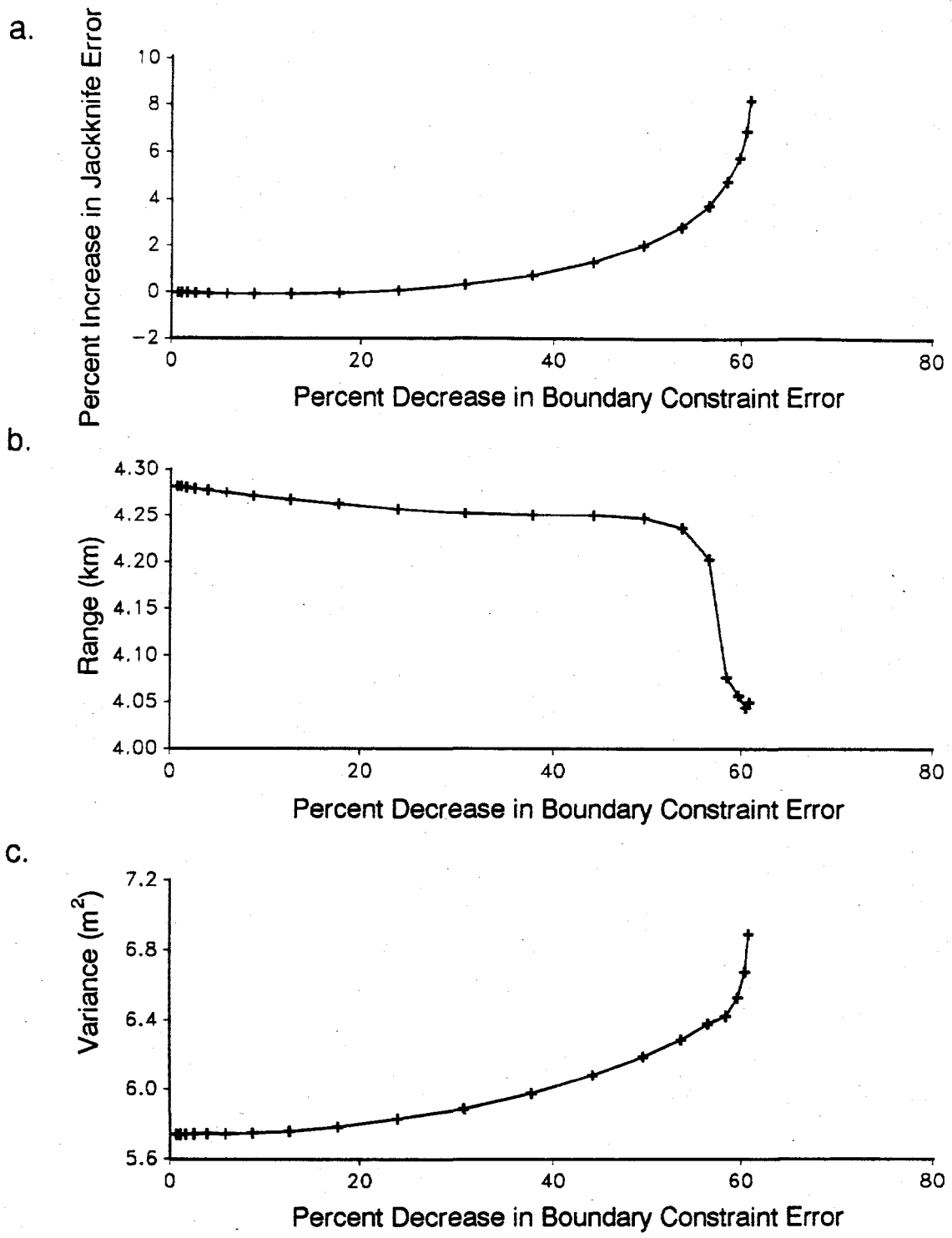

Figure 17. (a) Percent change in jackknifing error, (b) head residual range estimate, and (c) head residual variance verses the percent change in the boundary constraint error for fifth order drift solution.

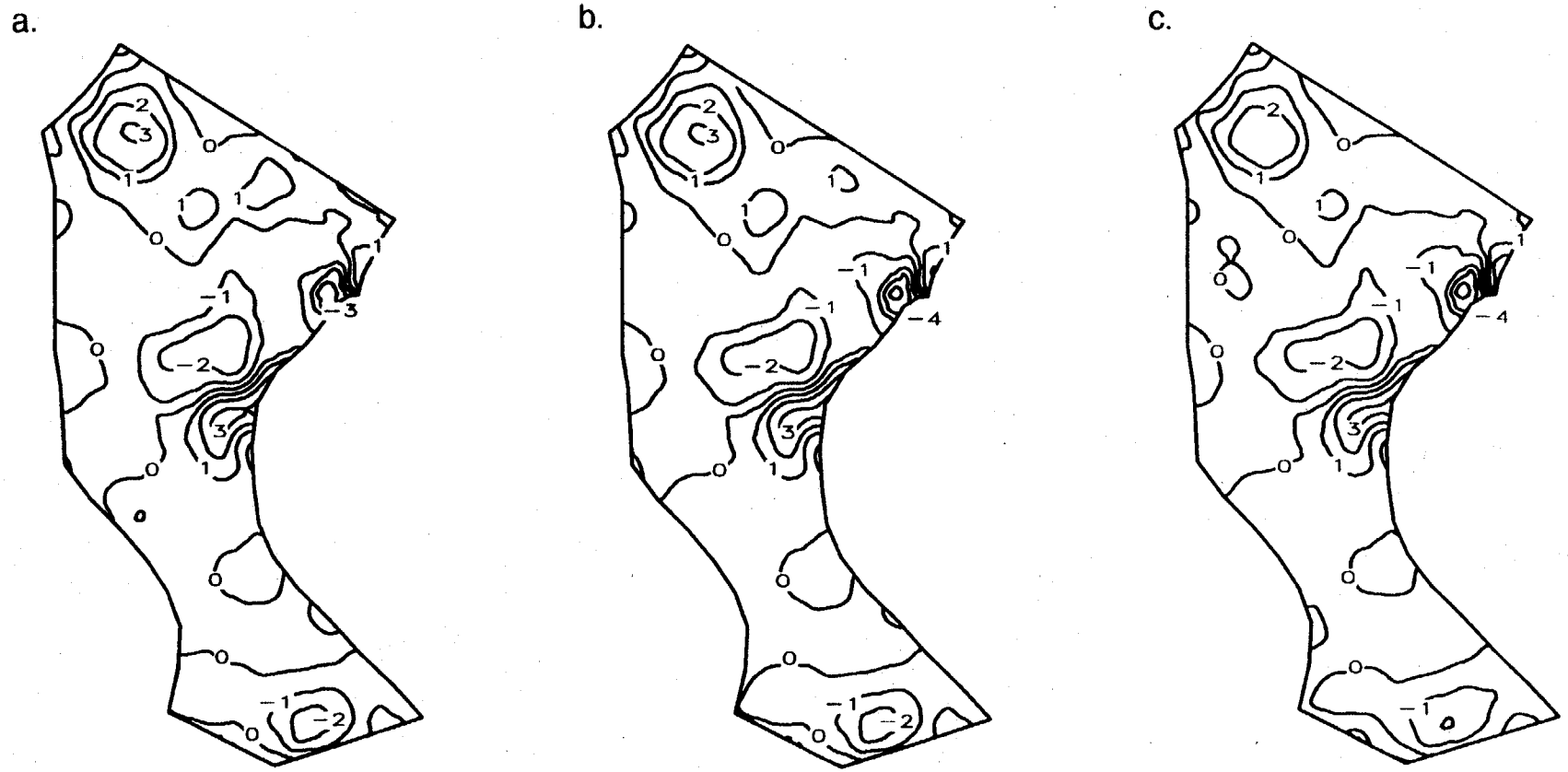

Figure 18. Head residuals in meters A.M.S.L. for fifth order drift solution using boundary constraint weightings of (a) 0.125, (b) 0.5, and (c) 2.0.

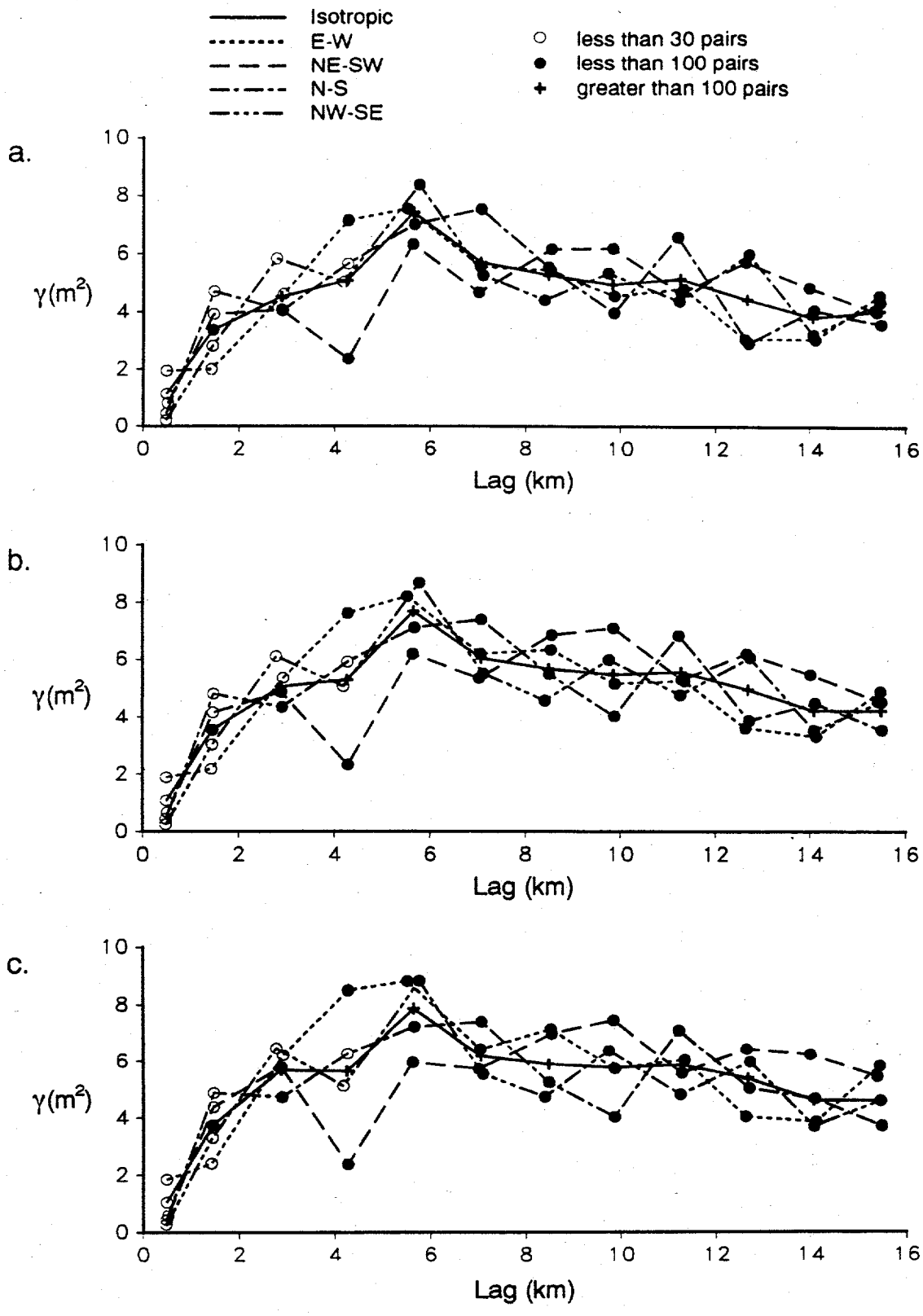

Figure 19. Sample semivariograms of head residuals for fifth order drift solution using boundary constraint weightings of (a) 0.125, (b) 0.5, and (c) 2.0.

boundary constraint residuals is not violated severely as the boundary constraint weighting is increased.

Figure 20 shows contour plots of estimated head values and boundary constraint errors along the no-flow boundaries for the fifth order solution with no boundary constraint weighting and with a boundary constraint weighting of 0.5. Figures 14 and 20 show that the fourth and fifth order drift solutions are affected similarly by the boundary constraints, especially along the west no-flow boundary. Along the east end of the north no-flow boundary and along the south end of the east no-flow boundary, the boundary constraint error for the fifth order drift solution is smaller than the fourth order drift solution with and without the boundary constraints. With the fifth order drift and a boundary constraint weighting of 0.5, the largest boundary constraint error is along the north end of the east no-flow boundary. This area is not affected much by the boundary constraints because of the abundance of hydraulic head measurements in the area.

Table 2 presents a summary of the estimated semivariogram parameters and errors for the fourth and fifth order drift solutions with boundary constraint weightings of 0, 0.125, 0.5, and 2. The jackknifing and boundary constraint errors with no weighting on the boundary constraints are considerably less for the fifth order solution than for the fourth order drift solution. This must be considered when comparing percent changes. Although the boundary constraint error for the fourth order drift solution can be reduced significantly by increasing the boundary constraint weighting, the sample semivariogram of the head residuals is severely affected at weightings of 0.5 or higher. The sample semivariogram of the head residuals for the fifth order drift solution is not nearly as sensitive to the high boundary constraint weightings.

Differences between the heads estimated with and without boundary constraints shown in Figure 20 are contoured in Figure 21a. As with the fourth order drift solution, the biggest differences are in the northeast and southeast corners where the head estimates are 12.4 and 8.1 m less, respectively, with the boundary constraints applied. The central section of the west no-flow boundary shows a considerable change of 5.3 m. Figure 21b shows the estimation errors calculated with a boundary constraint weighting of 0.5. The estimation errors in the northeast and southeast corners are reduced by about 50 percent with the boundary constraints as can be seen by comparing Figures 8b and 21b.

CONCLUSIONS

Inclusion of no-flow boundary constraints in the estimation of hydraulic head values in the Avra Valley case study was investigated for fourth and fifth order drift solutions. The semivariogram parameters of the head residuals that are used in the stepwise iterative regression and estimation error have been determined by a weighted least squares fit of the sample semivariogram and a jackknife

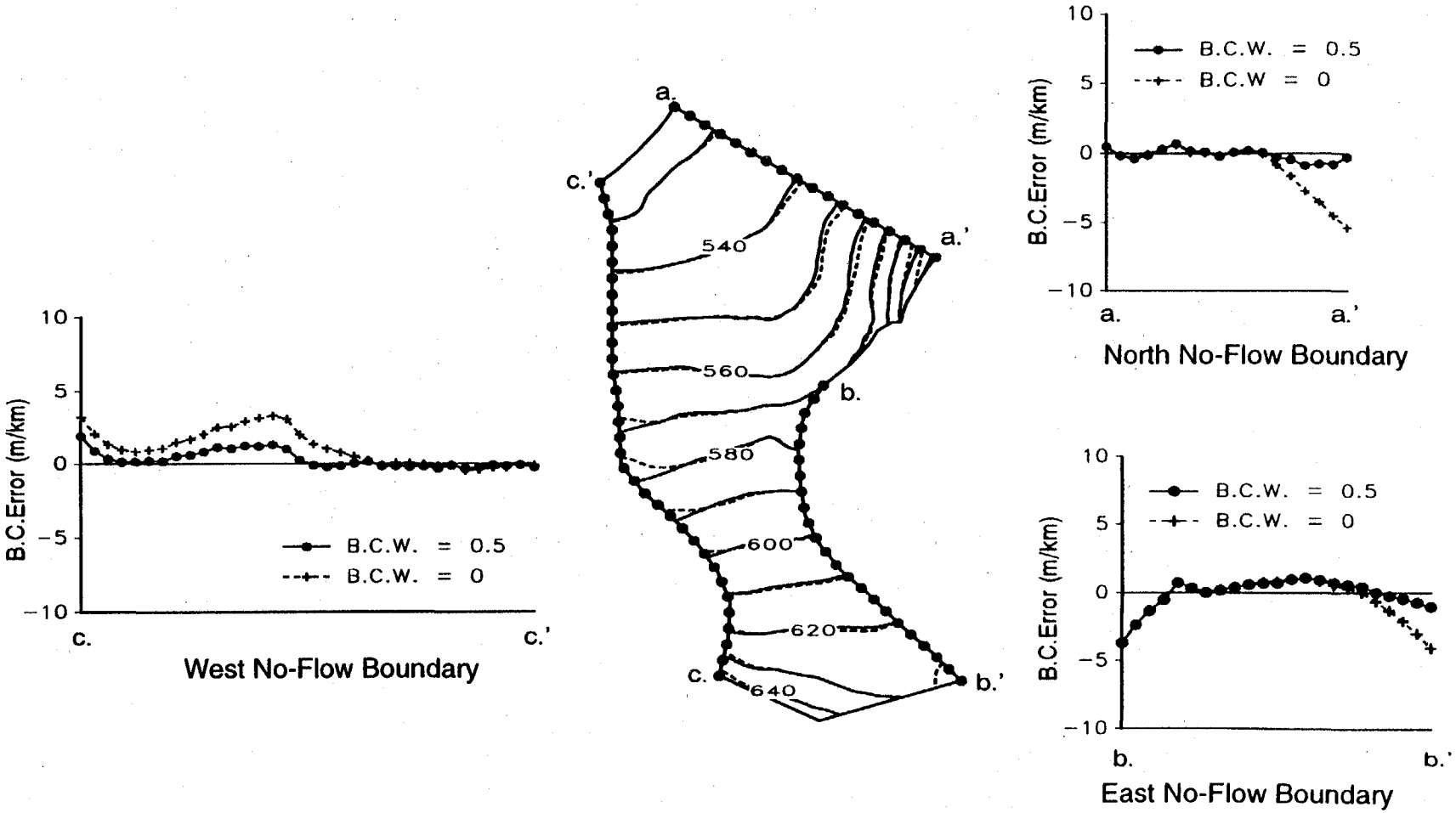

Figure 20. Estimated heads in meters A.M.S.L. and boundary constraint residuals with boundary constraint weightings of 0 and 0.5 for the fifth order drift solution. Heads estimated with boundary constraint weighting of 0.5 shown with solid line and heads estimated with no boundary constraint weighting shown with dashed line (B.C. Error is the boundary contratraint error).

Table 2. Estimated Semivariogram Parameters and Jackknife Kriging and Boundary Constraint Errors for the Fourth– and Fifth-Order Drift Solutions with Boundary Constraint Weightings of 0, 0.125, 0.5 and 2.

Order of Drift	Boundary Constraint Weight	Range (km)	Sill (m^2)	Jackknifing Error (m)	Boundary Constraint Error (m)
Fourth	0	4.46	8.58	2.27	4.65
	0.125	4.52	9.37	2.28	3.65
	(% change)	(+1%)	(+9%)	(0.4%)	(–22%)
	0.5	4.81	12.11	2.37	2.41
		(+8%)	(+41%)	(+5%)	(–48%)
	2	5.52	17.80	2.55	1.47
		(+24%)	(+107%)	(+12%)	(–68%)
Fifth	0	4.28	4.94	1.91	2.77
	0.125	4.25	5.27	1.92	1.76
		(–1%)	(+7%)	(0.6%)	(–37%)
	0.5	4.24	5.72	1.96	1.29
		(–2%)	(+16%)	(+3%)	(–53%)
	2	4.06	6.26	2.30	1.12
		(–5%)	(+27%)	(+20%)	(–60%)

error minimization method. When these two methods produce different results, a violation of the intrinsic hypothesis for the head residuals may be indicated. As the boundary constraint weightings are increased, changes in the range and sill of the head residuals and the tradeoff in fitting the head measurements and the boundary constraints are examined to determine an appropriate weighting level.

The fourth order drift solution with no boundary constraints produced an isotropic sample semivariogram head residual that exhibited a distinct sill at about 8.6 m^2, but the sills of the directional sample semivariograms varied from this by about 20 percent. The range value determined from the jackknife kriging method, 4.5 km, was much less than that determined by the weighted least squares method of 6.3 km. A contour plot of the head residuals showed certain areas where the residual values changed dramatically over short distances. These factors indicate that the head residuals for the fourth order drift solution may be non-intrinsic.

The fifth order drift solution with no boundary constraints produces similar range estimates using the weighted least squares and jackknife kriging methods of 4.36 and 4.28 km, respectively. The isotropic and directional sample semivariograms show less divergence than the fourth order solution. However, the sample semivariogram values peak at about 6.5 m^2 at a lag of about 5.5 km and then decrease to about 5 m^2 at longer lags. The fifth order drift solution could be overfitting the long lag values, in which case the true residuals are better characterized by the shorter lags. The fifth

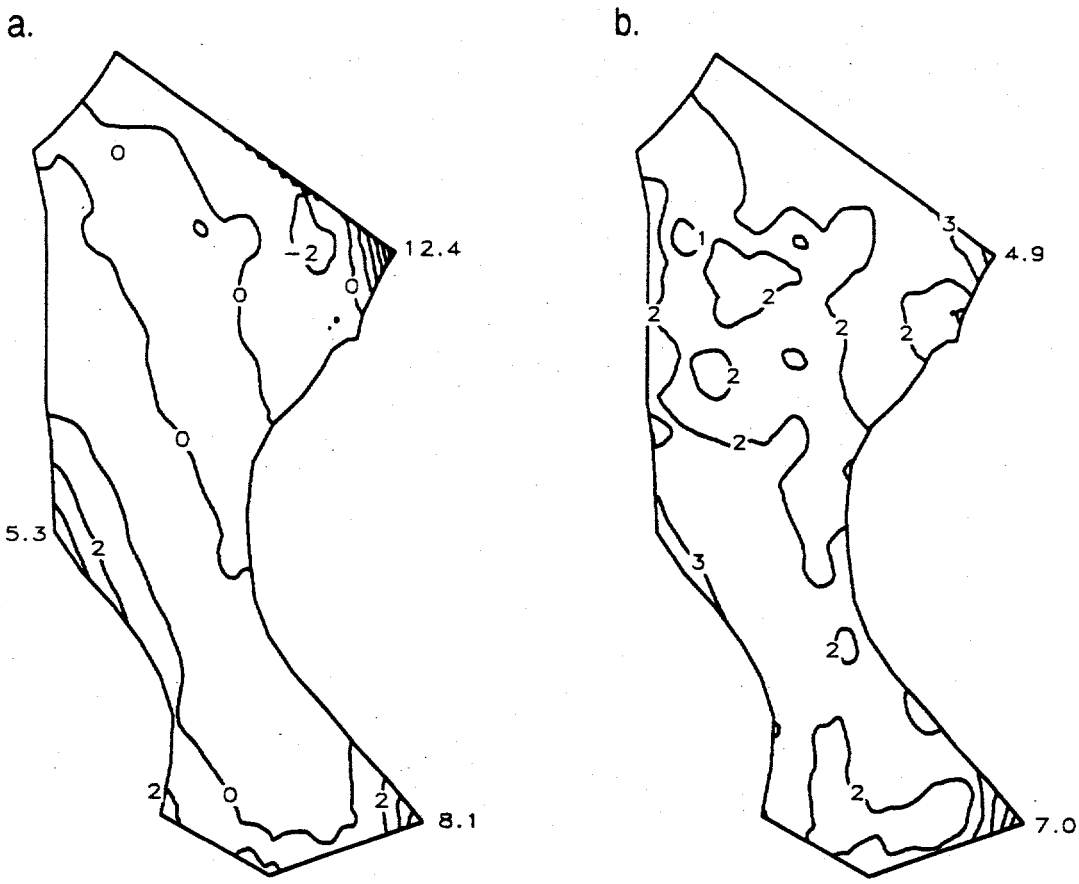

Figure 21. (a) Difference in meters of heads estimated with no boundary constraints and with boundary constraint weighting of 0.5 and (b) estimation error of heads estimated with boundary constraint weighting of 0.5 for fifth order drift solution.

order drift solution with no boundary cosntraints fit the no-flow boundary conditions much better than the fourth order drift solution.

Three configurations of boundary constraints were considered. Although the different configurations were sensitive to different relative levels of the boundary constraints weighting, they all showed very similar tradeoff between improvement in the boundary constraint fit and deterioration of the measured head fit. One of the boundary constraint configurations consisting of 75 constraints was chosen to examine the effects of different levels of boundary constraint weighting.

Three levels of boundary constraint weighting were examined in detail. These levels can be expressed as weighting the boundary constraints 0.125, 0.5, and 2 times the weight given to each head measurement. The 0.125 weighting represents weighting each of the 75 boundary constraints

one eighth as much as each of the 99 head measurements. This relatively low weighting resulted in significant improvement in the boundary constraint fit with a minimal effect on the jackknifing error of the heads and the semivariogram parameters of the head residuals for both fourth and fifth order drift solutions. The 0.5 weighting was chosen as a moderate weighting value and the weighting of 2 was investigated to examine the effects of a very severe boundary constraint weighting.

It was found that the sample semivariogram of the head residuals deteriorated as the boundary constraint weighting was increased for the fourth order solution. This indicates that the head residuals and the boundary constraint residuals may not be independent for the fourth order drift solution at boundary constraint weightings much over 0.125. The fifth order drift solution was much less sensitive to these changes when the boundary constraint weighting was increased. The boundary constraint weighting for the fifth order drift solution is limited more by the tradeoff in the jackknifing error and the boundary constraint error. A boundary constraint of 0.5 resulted in a reduction of over 50 percent in the boundary constraint error with only 3 percent increase in the jackknifing error. For both fourth and fifth order drift solutions, the biggest change in the head estimates with the boundary constraints are along the east end of the north no-flow boundary and along the south end of the east no-flow boundary, with some change along the central portion of the west no-flow boundary.

A new method to determine the estimation error of the heads was also presented that includes error from the drift and the residual components of the estimate. This method showed very high estimation errors, especially for the fifth order drift solution, in the northeast and southeast corners of the Avra Valley aquifer, regions where few head measurements are available. These errors were reduced significantly when the boundary constraint weighting was increased. Th estimation error of the heads in the interior regions of the aquifer, where the residual component of the error dominates, are lower for the fifth order drift solution.

The appropriate order for the drift and weighting for the boundary constraints are difficult to determine and should depend on how the estimated heads are to be used. Both fourth and fifth order drift solutions with light to moderate boundary constraint weightings produce reasonable results. The fourth order drift produces head residuals that may be non-intrinsic, while the head residuals from the fifth order drift solution are not normally distributed.

REFERENCES

Clifton, P.M., 1981. Statistical Inverse Modeling and Geostatistical Analysis of the Avra Valley Aquifer, M.S. Thesis, University of Arizona, Tucson.

Cressie, N., 1985. Fitting variogram models by weighted least square, *Mathematical Geology*, 17(5):563–586.

Cressie, N., 1993. Statistics for Spatial Data, John Wiley and Sons, New York.

Jacobson, E.A., 1985. A Statistical Parameter Estimation Method Using Singular Value Decomposition with Application to Avra Valley Aquifer in Southern Arizona, Ph.D. Thesis, University of Arizona, Tucson.

Jacobson, E.A., 1994. Estimation of aquifer parameters with measured and kriged hydraulic head data, accepted for publication in *Groundwater.*

Journel, A.G. and C.J. Huijbregts, 1978. Mining Geostatistics, Academic Press, New York.

Lamorey, G.W. and E.A. Jacobson, 1994. Estimation of semivariogram parameters and evaluation of the effects of data sparsity, accepted for publication in *Mathematical Geology*, included in this report as section 1.

Neuman, S.P. and E.A. Jacobson, 1984. Analysis of nonintrinsic spatial variability by residual kriging with application to regional groundwater levels, *Mathematical Geology*, 16(5):499–521.

Neuman, S.P. and S. Yakowitz, 1979. A statistical approach to the inverse problem of aquifer hydrology, 1 Theory. *Water Resources Research*, 15(4):845–860.

Press, W.H., B.P. Flannery, S.A. Teukolsky and W.T. Vetterling, 1986. The Art of Scientific Computing. Cambridge Numerical Recipes. Cambridge University Press.

APPENDIX A
CHEBYSHEV POLYNOMIAL

It may be necessary to increase the order of the hydraulic head drift when imposing boundary condition constraints. Neuman and Jacobson (1984) present semivariograms for first through fourth order drifts in their study of the Avra Valley. At higher than fourth order drifts, numerical problems are encountered when inverting the basis functions matrix, F, in the least squares solution. These problems are caused by the nearly linear behavior of the form of the basis functions at higher orders of drift. To alleviate these problems, the basis function can be written as a Chebyshev polynomial.

Chebyshev polynomials described by Press et al. (1986) are useful because they are orthogonal in the interval –1 to +1. When solving an undetermined problem, this orthogonality is useful because the best approximation of a polynomial of degree N by a polynomial of degree m where m << N is simply the Chebyshev polynomial truncated after m terms. For the determination of the drift and residuals for hydraulic head, which is a overdetermined problem, this orthogonality ensures that basis functions are not nearly linearly dependent. This results in a much lower condition number when inverting the basis functions, F. A Chebyshev polynomial of degree n in one dimension, x, can be written as:

$$T_n(x) = \cos(n \cdot arcos(x)) \tag{A1}$$

Using trigonometric identities, the Chebyshev polynomial can be expressed explicitly as:

$$\begin{aligned} T_0(x) &= 1 \\ T_1(x) &= x \\ T_2(x) &= 2x^2 - 1 \\ T_3(x) &= 4x^3 - 3x \\ T_4(x) &= 8x^4 - 8x^2 + 1 \\ &\cdots \\ T_{n+1}(x) &= 2xT_n(x) - T_{n-1}(x) \qquad \text{for } n \geq 1 \end{aligned} \tag{A2}$$

Chebyshev polynomials are usually used for one-dimensional data and must be extended to two dimensions to be used with hydraulic head measurement locations. The form of the basis function used by Neuman and Jacobson (1984) can be expressed in one dimension as:

$$F(x) = \sum_{k-0}^{n} a_i \, x^k \tag{A3}$$

where n is the order of the drift. Each increase in the order of drift results in an additional coefficient, a_n, multiplied by an increased power of x. In two dimensions, this function becomes:

$$F(x,y) = \sum_{i=0}^{n} \sum_{j=0}^{n-i} a_{i,j}\, x^i y^j \qquad \text{(A4)}$$

Here, the first term is a coefficient multiplied by the x to the n^{th} power and y to the zero power. Each successive term consists of an additional coefficient multiplied by a decreased power of x and an increased power of y until the final term, where y is raised to the n^{th} power and x to the zero power. The number of terms increases as $(n + 1)!$. In a similar way, the Chebyshev polynomial can be written in two dimensions as:

$$F(x,y) = \sum_{i=0}^{n} \sum_{j=0}^{n-i} c_{i,j}\, T_j(x) T_{i-j}(y) \qquad \text{(A5)}$$

For equal orders of drift, the Chebyshev polynomial gives the same results as the standard polynomial form used by Neuman and Jacobson (1984). The coefficients are different and the coordinates for x and y must be scaled from −1 to +1. However, implementation of the Chebyshev polynomial makes it possible to investigate much higher orders of drift.

APPENDIX B
DETERMINATION OF THE ESTIMATION ERROR FOR THE HYDRAULIC HEADS

Kriging Variance Method

The kriged estimate of the head residual, $\hat{R}_m$, is a linear combination of several of the observed data expressed as:

$$\hat{R}_m = \sum_{i=1}^{N_m} \alpha_{mi} R^*_{mi} \tag{B1}$$

where there are N_m observations, R^*_{mi}, to be used to estimate R at location m. The value of N_m at each location, m, often is set to be less than a specified maximum number of pairs and/or less than a specified separation distance. The difference between the observed and true values of R at location m is the measurement error, e_m, given by:

$$R^*_m = R_m - e_m \tag{B2}$$

The kriging coefficients, α_{mi}, are calculated to ensure that the variance of the estimation error is minimized, and that the kriged estimate is unbiased. To ensure that the kriged estimate is unbiased, a sufficient condition is:

$$\sum_{i=1}^{N_m} \alpha_{mi} = 1 \tag{B3}$$

The variance of the estimation error for the kriging variance method is the kriging variance given by:

$$Var[e_{Km}] = E[(R_m - \hat{R}_m)^2] \tag{B4}$$

where e_{Km} is the error in the head due to kriging.

Equations (B1), (B2), and (B4) can be combined and algebraically manipulated as follows:

$$\begin{aligned} Var[e_{Km}] &= E[(R_m - \sum_{i=1}^{N_m} \alpha_{mi} (R_{mi} - e_{mi}))^2] \\ &= E[R_m^2] \\ &\quad - 2\sum_{i=1}^{N_m} \alpha_{mi} \left\{E[R_m\ R_{mi}] - E[R_m\ e_{mi}]\right\} \\ &\quad + \sum_{i=1}^{N_m}\sum_{j=1}^{N_m} \alpha_{mi}\alpha_{mj} \left\{E[R_{mi}\ R_{mj}] - 2E[R_{mi}\ e_{mj}] + E[e_{mi}\ e_{mj}]\right\} \end{aligned} \tag{B5}$$

Equation (B5) can be simplified by the following assumptions concerning the measurement errors. The measurement errors are uncorrelated with each other:

$$E[e_m e_n] = O \qquad m \neq n \tag{B6}$$

The measurement errors are uncorrelated with the true residuals:

$$E[e_m R_n] = O \tag{B7}$$

The definition of the variance of the measurement errors is also used when simplifying equation (B5):

$$Var[e_m] = \sigma_m^2 \tag{B8}$$

Combining equations (B5), (B6), (B7), and (B8) yields:

$$Var[e_{Km}] = E[R_m^2] - 2\sum_{i=1}^{N_m} \propto_{mi} E[R_m R_{mi}] + \sum_{i=1}^{N_m}\sum_{j=1}^{N_m} \propto_{mi} \propto_{mj} E[R_{mi} R_{mj}] + \sum_{i=1}^{N_m} \propto_{mi} \sigma_{mi}^2 \tag{B9}$$

The equation for the semivariogram of equation (B5) can be written in terms of an expectation as:

$$\begin{aligned} \gamma(X_m, X_n) &= \tfrac{1}{2} E[(R_m - R_n)^2] \\ &= \tfrac{1}{2} E[R_m^2] + \tfrac{1}{2}[R_n^2] - E[R_m R_n] \end{aligned} \tag{B10}$$

Combining equations (B9) and (B10) yields an expression for the variance of the estimation errors in terms of the kriging weights, the semivariogram of the head residuals, and the measurement errors:

$$Var[e_{Km}] = 2\sum_{i=1}^{N_m} \propto_{mi} \gamma(x_{mi}, x_m) - \sum_{i=1}^{N_m}\sum_{j=1}^{N_m} \propto_{mi} \propto_{mj} \gamma(x_{mi}, x_{mj}) + \sum_{i=1}^{N_m} \propto_{mi}^2 \sigma_{mi}^2 \tag{B11}$$

The kriging weights are determined by minimizing equation (B11) subject to the unbiased condition of equation (B3).

The covariance of the estimation errors between estimates at locations m and n for the kriging variance method is given by:

$$\begin{aligned} Var[e_{Kmn}] &= E[e_{Km}\, e_{Kn}] \\ &= E[(R_m - \hat{R}_m)(R_n - \hat{R}_n)] \end{aligned} \tag{B12}$$

Equation (B12) can be expanded using equations (B1) and (B2) as follows:

$$Var[e_{Kmn}] = E[R_m - \sum_{i=1}^{N_m} \propto_{mi} (R_{mi} + e_{mi}) \tag{B13}$$

$$\cdot (R_n - \sum_{j=1}^{N_n} \propto_{nj} (R_{nj} + e_{nj}))]$$

$$= E[R_m R_n]$$

$$- \sum_{i=1}^{N_m} \propto_{mi} \left[E[R_n\ R_{mi}] + E[R_n\ e_{mi}]\right]$$

$$- \sum_{j=1}^{N_m} \propto_{nj} \left\{E[R_m\ R_{nj}] + E[R_n\ e_{nj}]\right\}$$

$$+ \sum_{i=1}^{N_m} \sum_{j=1}^{N_n} \propto_{mi} \propto_{nj} \left\{E[R_{mi}\ R_{nj}] + E[R_{mi}\ e_{nj}] + E[R_{nj}\ e_{mi}] + E[e_{mi}\ e_{nj}]\right\}$$

Equation (B13) can be simplified using equations (B6), (B7), and (B8):

$$Var[e_{Kmn}] = E[R_m\ R_n] - \sum_{i=1}^{N_m} \propto_{mi} E[R_{mi}\ R_n] \tag{B14}$$

$$- \sum_{j=1}^{N_n} \propto_{nj} E[R_m\ R_{nj}]$$

$$+ \sum_{i=1}^{N_m} \sum_{j=1}^{N_n} \propto_{mi} \propto_{nj} \left\{E[R_{mi}\ R_{nj}] + \delta_{mi,nj}\ \sigma_{mi}\ \sigma_{nj}\right\}$$

where: $\delta_{ni,mj} = 1$ if $x_{ni} = x_{mj}$ and $\delta_{ni,mj} = 0$ if $x_{ni} \neq x_{mj}$.

Combining equations (B10) and (B14) yields an expression for the covariance of the estimation errors in terms of the kriging weights, the semivariogram of the head residuals, and the measurement errors:

$$Var[e_{Kmn}] = -\gamma(x_m,\ x_n) + \sum_{i=1}^{N_m} \propto_{mi} \gamma(x_{mi},\ x_n) \tag{B15}$$

$$+ \sum_{j=1}^{N_n} \propto_{nj} \gamma(x_m,\ x_{nj})$$

$$- \sum_{i=1}^{N_m} \sum_{j=1}^{N_n} \propto_{mi} \propto_{nj} \left\{\gamma[x_{mi},\ x_{nj}] + \delta_{mi,nj}\ \sigma_{mi}\ \sigma_{nj}\right\}$$

Drift Plus Kriging Variance Method

The drift plus kriging method to determine the covariance of the estimation errors includes the error in the estimate of the drift given by:

$$E[(D_m - \hat{D}_m)(D_n - \hat{D}_n)] = \sum_{p=1}^{J_p} \sum_{q=1}^{J_p} f_p(x_m) V_{apq} f_q(x_n) \qquad \text{(B16)}$$

where $\hat{D}_m$ is the estimate of the drift, D_m, at location m. There are J_p coefficients of the drift polynominal, $f_i(x_m)$ represents the i^{th} term in the drift basis function at location m. V_a is the covariance matrix of the estimation errors on the drift coefficients given by:

$$V_a = (F^T V F)^{-1} \qquad \text{(B17)}$$

where F is the basis function matrix and V is the covariance matrix of the head residuals.

As shown in Figure B1 in the drift plus kriging variance method, the estimation error, e_{Dm}, at location m is given by:

$$e_{Dm} = D_m - \hat{D}_m + R_m - \hat{R}_m \qquad \text{(B18)}$$

At measurement locations, the sum of the true drift and true residual equals the sum of the estimated drift, residual, and measurement error. This leads to the following expression for the residual estimate at measurement location m:

$$\hat{R}'_m = D'_m - \hat{D}'_m + R'_m - e_m \qquad \text{(B19)}$$

where the primed superscript indicates that the location is a measurement location.

The covariance of the estimation errors between estimates at locations m and n for the drift plus kriging variance method, e_{Dmn}, is given by:

$$\begin{aligned} Var[e_{Dmn}] &= E[(D_m - \hat{D}_m + R_m - \hat{R}_m) \\ &\quad \cdot (D_n - \hat{D}_n + R_n - \hat{R}_n)] \\ &= E[(D_m - \hat{D}_m)(D_n - \hat{D}_n)] \\ &\quad + E[(D_m - \hat{D}_m)(R_n - \hat{R}_n)] \\ &\quad + E[(D_n - \hat{D}_n)(R_m - \hat{R}_m)] \\ &\quad + E[(R_m - \hat{R}_m)(R_n - \hat{R}_n)] \end{aligned} \qquad \text{(B20)}$$

The first term in equation (B20) is equivalent to equation (B16). The second term of equation (B20) can be expanded as follows:

$$E[(D_m - \hat{D}_m)(R_n - \hat{R}_n)] = E[(D_m - \hat{D}_m)R_n] - E[(D_m - \hat{D}_m)\hat{R}_n] \qquad \text{(B21)}$$

The second term of equation (B21) can be expanded further using equations (B1) and (B19):

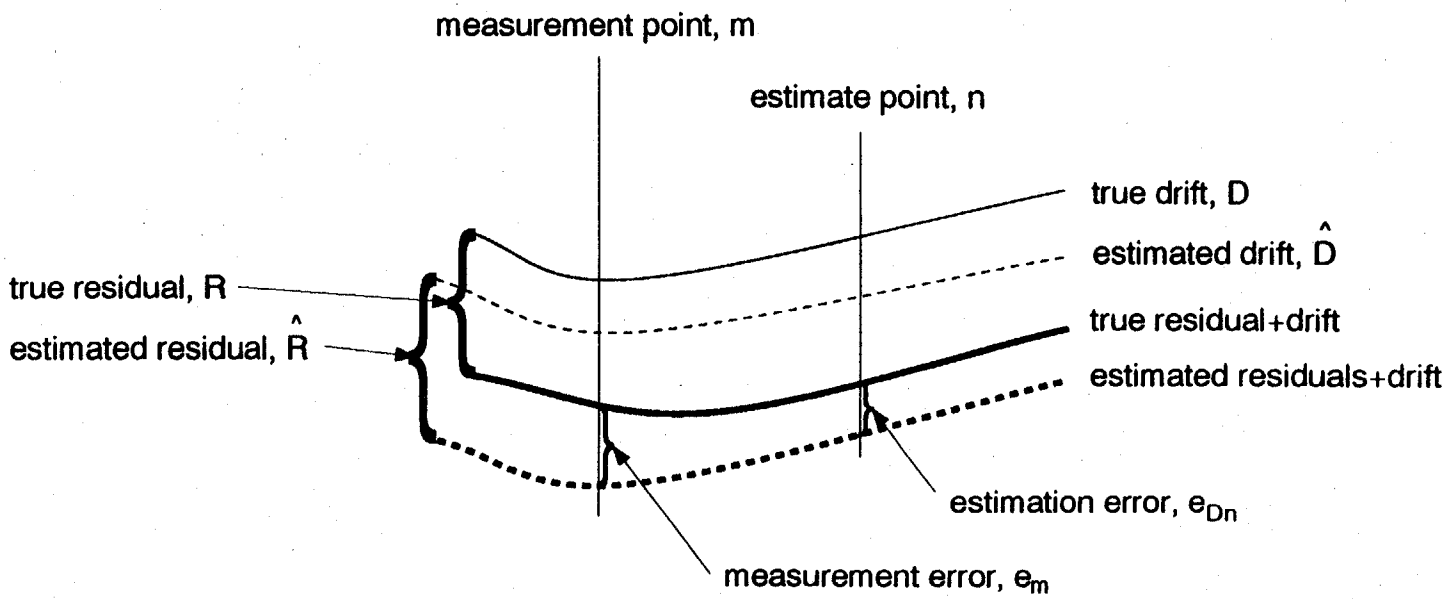

Figure B1. Configuration of the drift component error, residual component error, and measurement error.

$$E[(D_m - \hat{D}_m)\hat{R}_n] = E\left[\sum_{j=1}^{N_n} \propto_{nj} (D_m - \hat{D}_m)(D'_{nj} - \hat{D}'_{nj} + R'_{nj} - e_{nj})\right] \quad \text{(B22)}$$

$$= \sum_{j=1}^{N_n} \propto_{nj} \left\{E[(D_m - \hat{D}_m)(D'_{nj} - \hat{D}'_{nj})] + E[(D_m - \hat{D}_m)R'_{nj} - E[(D_m - \hat{D}_m)e_{nj}]\right\}$$

Equations (B21) and (B22) can be simplified by the following assumptions concerning the drift errors. The drift errors are not correlated with the true residuals:

$$E[(D_m - \hat{D}_m)R_n] = O \quad \text{(B23)}$$

The drift errors are not correlated with the measurement errors:

$$E[(D_m - \hat{D}_m)e_n] = O \quad \text{(B24)}$$

These are reasonable assumptions since the true residuals and the measurement errors are expected to be stochastic, while the drift errors are dependent on the location of the measurements and get large in regions where there are sparse data.

Combining equations (B16), (B21), (B22), (B23), and (B24) yields:

$$E[(D_m - \hat{D}_m)(R_n - \hat{R}_n)] = -\sum_{j=1}^{N_n}\sum_{p=1}^{J_p}\sum_{q=1}^{J_p} \propto_{nj} f_p(x_m)V_{apq}\, f_q(x_{nj}) \quad \text{(B25)}$$

The third term of equation (B20) is developed similar to the second term and becomes:

$$E[(D_n - \hat{D}_n)(R_m - \hat{R}_m)] = -\sum_{i=1}^{N_m}\sum_{p=1}^{J_p}\sum_{q=1}^{J_p} \propto_{mi} f_p(x_n)V_{apq}\, f_q(x_{mi}) \quad \text{(B26)}$$

The fourth and final term of equation (B20) is multiplied out into four more terms:

$$E[(R_m - \hat{R}_m)(R_n - \hat{R}_n)] = E[R_m R_n] - E[\hat{R}_m R_n] - E[R_m \hat{R}_n] + E[\hat{R}_m \hat{R}_n] \quad \text{(B27)}$$

The second term of equation (B27) is expanded using equations (B1) and (B19):

$$E[\hat{R}_m R_m] = E\left[\sum_{i=1}^{N_m} \propto_{mi} (D'_{mi} - \hat{D}'_{mi} + R'_{mi} - e_{mi})R_n\right] \quad \text{(B28)}$$

$$= \sum_{i=1}^{N_m} \propto_{mi} \left\{E[(D'_{mi} - \hat{D}'_{mi})R_n] + E[R'_{mi}\, R_n] + E[e_{mi}\, R_n]\right\}$$

Equation (B28) can be simplified by the assumptions of equations (B7) and (B23):

$$E[\hat{R}_m\, R_n] = \sum_{i=1}^{N_m} \propto_{mi} E[R'_{mi}\, R_n] \quad \text{(B29)}$$

The third term of equation (B27) is developed similar to the second term and yields:

$$E[R_m\ \hat{R}_n] \;=\; \sum_{j=1}^{N_n} \propto_{nj} E[R_m\ R'_{nj}] \tag{B30}$$

The fourth term of equation (B36) is expanded using equations (B1) and (B19):

$$\begin{aligned} E[\hat{R}_m\ \hat{R}_n] \;&=\; E\left[\left(\sum_{i=1}^{N_m} \propto_{mi} (D'_{mi} - \hat{D}'_{mi} + R'_{mi} - e_{mi})\right) \cdot \left[\sum_{j=1}^{N_n} \propto_{nj} (D'_{nj} - \hat{D}_{nj} + R'_{nj} - e_{nj})\right]\right] \\ &=\; \sum_{i=1}^{N_m}\sum_{j=1}^{N_n} \propto_{mi} \propto_{nj} \Big\{E[(D'_{mi} - \hat{D}'_{mi})(D'_{nj} - \hat{D}'_{nj})] \\ &+\; E[(D'_{mi} - \hat{D}'_{mi})R'_{nj}] - E[(D'_{mi} - \hat{D}'_{mi})e_{nj}] \\ &+\; E[(D'_{nj} - \hat{D}'_{nj})R'_{mi}] - E[(D'_{nj} - \hat{D}'_{nj})e_{mi}] \\ &-\; E[R'_{mi}\ e_{nj}] - E[R'_{nj}\ e_{mi}] \\ &+\; E[R'_{mi}\ R'_{nj}] + E[e_{mi}\ e_{nj}]\Big\} \end{aligned} \tag{B31}$$

The drift term in equation (B31) can be replaced by equation (B16), while the assumptions represented by equations (B6), (B7), (B23), and (B24) eliminate several terms in equation (B31) to obtain:

$$\begin{aligned} E[\hat{R}_m\hat{R}_n] \;=\; \sum_{i=1}^{N_m}\sum_{j=1}^{N_n} \propto_{mi} \propto_{nj} \Bigg\{&\sum_{p=1}^{J_p}\sum_{q=1}^{J_p} f_p(x_{mi}) V_{apq}\, f_q(x_{ni}) \\ &+\; E[R'_{mi}\ R'_{nj}] + \delta_{mi,nj}\, \sigma_{mi}\, \sigma_{nj}\Bigg\} \end{aligned} \tag{B32}$$

Equations (B29), (B30), and (B32) are substituted into equation (B27), which is substituted into equation (B20) along with equations (B16), (B25), and (B26) to produce:

$$Var[e_{Dmn}] = \sum_{p=1}^{J_p}\sum_{q=1}^{J_p} f_p(x_m)V_{apq}\, f_q(x_n) + E[R_m\, R_n] \qquad \text{(B33)}$$

$$- \sum_{j=1}^{N_n} \propto_{nj} \left\{ \sum_{p=1}^{J_p}\sum_{q=1}^{J_p} f_p(x_m)V_{apq}\, f_q(x_{nj}) + E[R_m\, R'_{nj}] \right\}$$

$$- \sum_{i=1}^{N_m} \propto_{mi} \left\{ \sum_{p=1}^{J_p}\sum_{q=1}^{J_p} f_p(x_n)V_{apq}\, f_q(x_{mi}) + E[R_n\, R'_{mi}] \right\}$$

$$+ \sum_{i=1}^{N_m}\sum_{j=1}^{N_n} \propto_{mi} \propto_{nj} \left\{ \sum_{p=1}^{J_p}\sum_{q=1}^{J_p} f_p(x_{mi})V_{apq}\, f_q(x_{nj}) \right\}$$

$$+ E[R'_{mi}\, R'_{nj}] + \delta_{mi,nj}\, \sigma_{mi}\, \sigma_{nj}$$

Until this point in the derivation of the covariance of the estimation errors between estimates at locations m and n for the drift plus kriging variance method, locations m and n could be the same or different. The fact that locations m and n are different or the same location results in a slightly different derivation, as shown below, when the expectation terms in equation (B33) are replaced by the semivariogram expression of equation (B10). For locations m and n that are different, equation (B33) becomes:

$$Var[e_{Dmn}] = \sum_{p=1}^{J_p}\sum_{q=1}^{J_p} f_p(x_m)V_{apq}\, f_q(x_n) - \gamma(x_m, x_n) \qquad \text{(B34)}$$

$$- \sum_{j=1}^{N_n} \propto_{nj} \left\{ \sum_{p=1}^{J_p}\sum_{q=1}^{J_p} f_p(x_m)V_{apq}\, f_q(x_{nj}) - \gamma(x_m, x_{nj}) \right\}$$

$$- \sum_{i=1}^{N_m} \propto_{mi} \left\{ \sum_{p=1}^{J_p}\sum_{q=1}^{J_p} f_p(x_{mi})V_{apq}\, f_q(x_n) - \gamma(x_{mi}, x_n) \right\}$$

$$+ \sum_{i=1}^{N_m}\sum_{j=1}^{N_n} \propto_{mi} \propto_{nj} \left\{ \sum_{p=1}^{J_p}\sum_{q=1}^{J_p} f_p(x_{mi})V_{apq}\, f_q(x_{nj}) - \gamma(x_{mi,}\, x_{nj}) + \delta_{mi,nj}\, \sigma_{mi}\, \sigma_{nj} \right\}$$

For the case where locations m and n are the same, equation (B33) can be rewritten as:

$$Var[e_{Dm}] = \sum_{p=1}^{J_p}\sum_{q=1}^{J_p} f_p(x_m)V_{apq}\, f_q(x_m) + E[R_m^2] \qquad \text{(B35)}$$

$$- 2\sum_{i=1}^{N_m} \propto_{mi} \left\{ \sum_{p=1}^{J_p}\sum_{q=1}^{J_p} f_p(x_m)V_{apq}\, f_q(x_{mi}) + E[R_m\, R'_{mi}] \right\}$$

$$+ \sum_{i=1}^{N_m}\sum_{j=1}^{N_m} \propto_{mi} \propto_{mj} \left\{ \sum_{p=1}^{J_p}\sum_{q=1}^{J_p} f_p(x_{mi})V_{apq}\, f_q(x_{mj}) + E[R'_{mi}\, R'_{nj}] \right\} + \sum_{i=1}^{N_m} \sigma_{mi}^2$$

When combined with the semivariogram expression of equation (B10), equation (B35) becomes:

$$Var[e_{Km}] = \sum_{p=1}^{J_p}\sum_{q=1}^{J_p} f_p(x_m)V_{apq}\, f_q(x_m) \qquad \text{(B36)}$$

$$- 2\sum_{i=1}^{N_m} \propto_{mi} \left\{ \sum_{p=1}^{J_p}\sum_{q=1}^{J_p} f_p(x_m)V_{apq}\, f_q(x_m) - \gamma(x_m, x_{mi}) \right\}$$

$$+ \sum_{i=1}^{N_m}\sum_{j=1}^{N_m} \propto_{mi} \propto_{mj} \left\{ \sum_{p=1}^{J_p}\sum_{q=1}^{J_p} f_p(x_{mi})V_{apq}\, f_q(x_{mj}) - \gamma(x_{mi}, x_{mj}) \right\} + \sum_{i=1}^{N_m} \sigma_{mi}^2$$

ESTIMATION OF AQUIFER PARAMETERS USING HYDRAULIC HEADS ESTIMATED WITH CONSTRAINTS ON THE HYDRAULIC HEAD GRADIENT ACROSS NO-FLOW BOUNDARIES

ABSTRACT

Transmissivities determined by an inverse groundwater model are dependent on the prior hydraulic heads used in the model. It is found in a case study that when gradients in the prior head distribution do not match assumed no-flow boundary conditions, the inverse model can produce low transmissivity values along these no-flow boundaries. These low transmissivities are a product of an attempt by the model to reconcile inconsistencies in the head gradient and the boundary conditions. Prior heads estimated at node points by a method that includes constraints on head gradients across no-flow boundaries did not produce the low transmissivities along no-flow boundaries in the inverse modeling. The constraints on the head gradient resulted in lower estimation errors on the prior heads and the subsequent estimation error of the transmissivities in regions of the aquifer in the vicinity of a no-flow boundary where few head measurements exist.

INTRODUCTION

In forward groundwater models, the hydraulic head distribution is calculated from aquifer parameters including transmissivities, pumping and recharge rates, and boundary conditions. However, there is usually a very limited number of measurements for these parameters available. Hydraulic head measurements are frequently available in more abundance than any measurement of the above parameters. Inverse groundwater models estimate aquifer parameters, primarily transmissivities, from the hydraulic heads. By using inverse groundwater models with prior information on the transmissivities, head measurements are used to check and improve upon previous estimates of transmissivities (Neuman and Yakowitz, 1979).

Transmissivity estimates from a inverse model can be very sensitive to noise in the hydraulic head data since derivatives of the hydraulic head are present in the governing equations (Neuman, 1973). Early efforts to alleviate this problem include optimizing the transmissivity zonation and imposing upper and lower bounds on the transmissivities in each zone (Emsellem and de Marsily, 1971; Yeh, 1975; Cooley, 1977; Yeh and Yoon, 1981). Neuman and Yakowitz (1979) developed a two-dimensional steady-state flow inverse method that utilizes prior information on the transmissivities to alleviate this problem. The method of Neuman and Yakowitz (1979) considers head estimates at nodes and transmissivity estimates for zones as well as the covariance matrices of the estimation error for the heads and transmissivities. This method allows flexibility in specifying how the hydraulic head and transmissivity data are weighted in the inverse model. Neuman (1980) presents a modification of this method that includes the ability to specify head data at any location in the aquifer.

Delhomme (1978) and Neuman (1982) recommend using geostatistical interpolation techniques, such as kriging, to obtain transmissivity and head estimates and the associated estimation errors. Simple kriging requires the mean of the data to be constant throughout the area of interest. This can be a problem for the hydraulic head data since the data obviously contain a trend. Neuman and Jacobson (1984) present a method to estimate the hydraulic heads and the covariance of the estimation errors at node locations by separating the heads into a polynomial drift component and a residual component. The residual component is kriged and added to the drift component at each estimation point. The appropriate order for the polynomial and the spatial characteristics of the residuals are obtained by examining the sample semivariogram of the residuals. The head estimation errors are determined from the kriging variance of the head residuals.

The extent to which estimates of transmissivity can be improved by considering hydraulic head data with an inverse model depends on the quality of the head estimates used. Use of only head measurements at well locations can leave large regions of the aquifer with no constraints on the head. Hand contouring of the hydraulic heads allows subjective knowledge to be included in the model concerning how the hydraulic heads should vary along the boundaries (Clifton and Neuman, 1982). However, it is difficult to accurately quantify the estimation error of the hand-contoured heads. The method of Neuman and Jacobson (1984) provides reasonable head estimates at nodes and their estimation errors. However, this method lacks constraints on the drift component of the head estimate in peripheral regions of the aquifer where few head data are available. This can lead to inappropriate hydraulic head gradients in these peripheral regions. These regions often are in the vicinity of no-flow boundaries since there are usually few wells located along these boundaries. Large head gradients across no-flow boundaries in the prior head distribution used in an inverse model will result in inconsistencies in the model.

It may be possible to improve an inverse model by using prior head estimates that more realistically reflect the boundary conditions. A modification of the Neuman and Jacobson (1984) method that includes constraints on the spatial drift across no-flow boundaries was presented by Lamorey and Jacobson (1994). They found in a case study of the Avra Valley aquifer in southern Arizona that as the weighting of the no-flow boundary constraints was increased, the gradient of the head estimates near the no-flow boundaries decreased at the expense of an increase in the misfit of the measured heads in the interior. Lamorey and Jacobson (1994) also describe a method to determine the head estimation errors that includes error in the drift and residual components of the head estimate. The head estimation error was found to increase slightly in the interior and decrease along the no-flow boundaries with increased weighting of the boundary constraints. These tradeoffs are investigated further here by examining the effect of heads estimated with no-flow boundary constraints on the transmissivities determined from an inverse model of the Avra Valley aquifer.

The Avra Valley aquifer has been the subject of several inverse modeling case studies. Clifton and Neuman (1982) examine an application of inverse method described by Neuman (1980) to the Avra Valley aquifer that uses hand-contoured hydraulic heads to estimate the nodal heads. Neuman and Jacobson (1984) demonstrate their method of estimating nodal heads on the Avra Valley aquifer and conclude that a fourth order polynomial drift is necessary to yield residuals that do not contain a trend. Jacobson (1994) applies Neuman's inverse method to the Avra Valley aquifer and compares results from using heads at measurement locations and heads at nodes determined by the method of Neuman and Jacobson (1984). Jacobson (1994) concludes that lower transmissivity estimation errors and a smoother flow pattern is obtained by using the heads estimated at nodes. However, Jacobson (1994) also found that the heads estimated at nodes from Neuman and Jacobson (1984) did not reflect the assumed no-flow boundary conditions in some regions where few head data were available.

STATISTICAL INVERSE THEORY

The following statistical inverse model for groundwater flow was developed by Neuman and Yakowitz (1979) and modified by Neuman (1980). Transmissivities are related to the hydraulic head by the following two-dimensional, steady-state groundwater flow equation for a heterogeneous isotropic aquifer:

$$\nabla \cdot (T\nabla h) - q = 0 \tag{1}$$

subject to either prescribed head or prescribed flux boundary conditions, where ∇ is the two-dimensional gradient operator, T is the aquifer transmissivity, h is the hydraulic head, and q is the rate of fluid generation per unit area of aquifer.

Equation (1) can be discretized by finite elements to produce the following matrix equation:

$$\underline{\underline{A}}\,\underline{h} = \underline{Q} \tag{2}$$

where $\underline{\underline{A}}$ is an N by N square matrix whose elements are calculated from the finite element mesh geometry and the transmissivity, $\underline{h}$ is a vector of the hydraulic heads at the N node points, and $\underline{Q}$ is a vector containing source and sink terms and the boundary flux at node points. The transmissivities are defined as constant values within zones. The hydraulic heads in equation (2) can be solved for by:

$$\underline{h} = \underline{\underline{A}}^{-1}\underline{Q} \tag{3}$$

The measured or estimated data can be expressed as the sum of the true, but unknown, value and an error for the hydraulic head and flux vectors:

$$\underline{h}^{*} = \underline{h} + \underline{\varepsilon} \tag{4}$$

$$\underline{Q}^{*} = \underline{Q} + \underline{\mu} \tag{5}$$

where $\underline{h}^*$ and $\underline{Q}^*$ are the measured or estimated head and flux vectors, and $\underline{\varepsilon}$ and $\underline{\mu}$ are error vectors, respectively.

Neglecting $\underline{\mu}$ in equation (5) (see Neuman, 1980, Appendix A) and substituting equations (4) and (5) into equation (3) yields:

$$\underline{h}^* - \underline{\underline{A}}^{-1}\underline{Q}^* = \underline{\varepsilon} \tag{6}$$

The mean of $\underline{\varepsilon}$ is assumed to equal zero and the covariance of $\underline{\varepsilon}$ is expressed as:

$$\underline{\underline{V}}(\varepsilon) = \sigma_h^2 \, \underline{\underline{V}}_h \tag{7}$$

where σ^2_h is a positive scalar that may or may not be known and $\underline{\underline{V}}_h$ is a known positive-definite symmetric matrix. The quantities $\underline{\underline{V}}_h$ and σ_h^2 can often be estimated with varying degrees of accuracy depending on the method used to specify the heads in the model. If the estimation error covariance of the hydraulic heads calculated in $\underline{\underline{V}}_h$ accurately reflect the true errors, then σ^2_h will equal one.

Equation (6) can be solved as a generalized nonlinear least squares regression problem. Neuman (1980) formulates the problem in terms of log transmissivities, $\underline{Y}=\log\underline{T}$, because this insures positive transmissivities and a log-normal distribution better describes the observed distribution of transmissivities. An estimate of the log transmissivities, $\hat{\underline{Y}}$, can be determined as the vector that minimizes the composite least-squares criterion, $J(\hat{\underline{Y}})$, defined as:

$$J(\hat{\underline{Y}}) = J_h(\hat{\underline{Y}}) + \lambda J_Y(\hat{\underline{Y}}) \tag{8}$$

where λ is a non-negative scalar defined as:

$$\lambda = \sigma_h^2 \, / \, \sigma_Y^2 \tag{9}$$

$J_n(\hat{\underline{Y}})$ is a criterion of model fit defined as:

$$J_h(\hat{\underline{Y}}) = [\underline{h}^* - \hat{\underline{h}}]^T \underline{\underline{V}}_h^{-1} [\underline{h}^* - \hat{\underline{h}}] \tag{10}$$

where $\underline{h}^*$ is a vector of hydraulic head estimates and $J_y(\hat{Y})$ is a criterion of parameter plausibility defined as:

$$J_Y(\hat{\underline{Y}}) = [\underline{Y}^* - \hat{\underline{Y}}]^T \underline{\underline{V}}_Y^{-1} [\underline{Y}^* - \hat{\underline{Y}}] \tag{11}$$

where $\underline{Y}^*$ is a vector of prior log transmissivity estimates for each of the zones. The log transmissivity estimates can be related to the true, but unknown, values as:

$$\underline{Y}^* = \underline{Y} + \underline{\upsilon} \tag{12}$$

where $\underline{\upsilon}$ is the estimation error of the log transmissivities. The mean of $\underline{\upsilon}$ is assumed to equal zero and the covariance of $\underline{\upsilon}$ is expressed as:

$$\underline{\underline{V}}(\upsilon) = \sigma_Y^2 \, \underline{\underline{V}}_Y \tag{13}$$

where σ^2_Y is a positive scalar that may or may not be known and $\underline{V}_Y$ is a known positive-definite symmetric matrix. As with the hydraulic head estimates, $\underline{V}_Y$ can often be estimated from the method used to estimate the prior log transmissivity values for each zone, such as block kriging (Clifton and Neuman, 1982). Again, if the estimation covariance of the log transmissivities calculated in $\underline{V}_Y$ accurately reflect the true errors, then σ^2_Y equals one.

If the covariance of the errors for the hydraulic heads and log transmissivities are known, then σ^2_h, σ^2_Y, and λ all equal one and equation (8) can be solved by minimizing $J(\underline{\hat{Y}})$. If either σ^2_h or σ^2_Y are unknown, or estimated with little confidence, a family of solutions can be generated by varying λ. Large λ values give more weight to the prior log transmissivity estimates, while small values give more weight to the measured or estimated head values. An optimum λ value should be between these two extremes.

The optimum value of λ may be indicated by considering various statistical aspects of the solution. Since the weighted hydraulic head residuals are assumed to have a zero mean normal distribution in the solution of equation (6), the mean value of the weighted hydraulic head residuals should be close to zero for an optimal solution. The weighted head residuals, z_h, are given by:

$$z_h = \underline{H}_h^{-1}(\underline{h}^* - \underline{\hat{h}}) \tag{14}$$

where H_h is an upper triangular matrix that satisfies $V_h=H_h{}^TH_h$. The weighted hydraulic head residuals should be normally distributed for an optimal solution. The χ^2 statistic goodness-of-fit test can be used to calculate a probability that the distribution of the weighted head residuals is normal.

Carrera and Neuman (1986) present a maximum likelihood approach to determine the optimum λ value by minimizing the log-likelihood criterion (ML):

$$ML = \frac{J_h}{\sigma_h^2} + \frac{J_Y}{\sigma_Y^2} + \ln|\underline{V}_h| + \ln|\underline{V}_Y| + L\ln\sigma_h^2 + M\ln\sigma_Y^2 + (L+M)\ln(2\pi) \tag{15}$$

where $|\underline{V}_h|$ and $|\underline{V}_Y|$ are the determinants of $\underline{V}_h$ and $\underline{V}_h$, respectively. For each λ value solution, a corresponding $\tilde{\lambda}$ value can be calculated as:

$$\tilde{\lambda} = \tilde{\sigma}_h^2/\tilde{\sigma}_Y^2 \tag{16}$$

where $\tilde{\sigma}^2_h$ and $\tilde{\sigma}^2_y$ can be approximated as $\tilde{\sigma}^2_h=J_h/L$ and $\tilde{\sigma}^2_y=J_Y/M$. For an optimal solution, values of λ and $\tilde{\lambda}$ should be equal.

In addition to examining statistical aspects of the inverse solution, it is important to examine how the hydraulic head and log transmissivity values change at different λ values. At large λ values, $\underline{\hat{Y}}$ will be close to the prior log transmissivity estimates but the head estimates may not match the prior

heads. As λ is reduced, the hydraulic heads should match better at the expense of the log transmissivities.

Estimation errors for the log transmissivities and hydraulic heads generated by the inverse model can be examined with a linearized error analysis (Schweppe, 1973). The inverse estimation error vector for the transmissivities, $\underline{e}_Y$, and for the hydraulic heads, $\underline{e}_h$, are defined as:

$$\underline{e}_Y = \hat{\underline{Y}} - \underline{Y} \tag{17}$$

$$\underline{e}_h = \hat{\underline{h}} - \underline{h} \tag{18}$$

If the estimation errors are sufficiently small, the true hydraulic head can be approximated by the linear portion of the Taylor series expansion about $\hat{\underline{Y}}$:

$$\underline{h} \cong \hat{h}(\hat{Y}) + \underline{\underline{Z}}(Y - \hat{Y}) \tag{19}$$

where $\underline{\underline{Z}}$ is the Jacobian matrix whose elements are $Z_{ni}=\delta\hat{h}/\delta\hat{Y}_i$. Equation (19) can be combined with equations (4), (7), (12), and (13) to form a linear model that can be analyzed by linear regression theory described by Seber (1977). The regression yields estimation errors for the transmissivities with a zero mean and a covariance matrix given by:

$$\underline{\underline{V}}(\underline{e}_Y) = \sigma_h^2(\underline{\underline{Z}}^T\underline{\underline{V}}_h^{-1}\underline{\underline{Z}} + \lambda\underline{\underline{V}}_Y^{-1})^{-1} \tag{19}$$

The estimation error vector of hydraulic heads can be expressed as:

$$\underline{e}_h \cong \underline{\underline{Z}}\,\underline{e}_Y \tag{20}$$

where the mean of $\underline{e}_h$ is equal to zero and the covariance matrix is given by:

$$\underline{\underline{V}}(\underline{e}_h) \cong \underline{\underline{Z}}\,\underline{\underline{V}}(\underline{e}_Y)\underline{\underline{Z}}^T \tag{21}$$

INVERSE MODELING OF THE AVRA VALLEY AQUIFER

Description of the Avra Valley Aquifer

Avra Valley, shown in Figure 1, is located in southern Arizona and contains an extensive alluvial aquifer as described in Clifton and Neuman (1982). The valley is oriented north to south and is about 50 km long and 10 to 20 km wide. Avra Valley is bounded by the Roskruge, Waterman, and Silverbell mountains on the west and the Tucson and Tortolita mountains on the east. The southern end of the valley is about 750 m above mean sea level, dropping off to about 550 m in the north. Two major intermittent watercourses cross the valley, the Santa Cruz River and the Brawley Wash, which becomes the Los Robles Wash in the north. The valley is arid with a mean annual rainfall of 24 cm.

The Avra Valley basin is a graben filled with Cenozoic alluvium and surrounded by Mesozoic and Tertiary volcanic rocks, Paleozoic sedimentary rocks, and Precambrian granites. The basin can be subdivided into a 2900-m-deep northern subbasin and a 760-m-deep southern basin. The fill

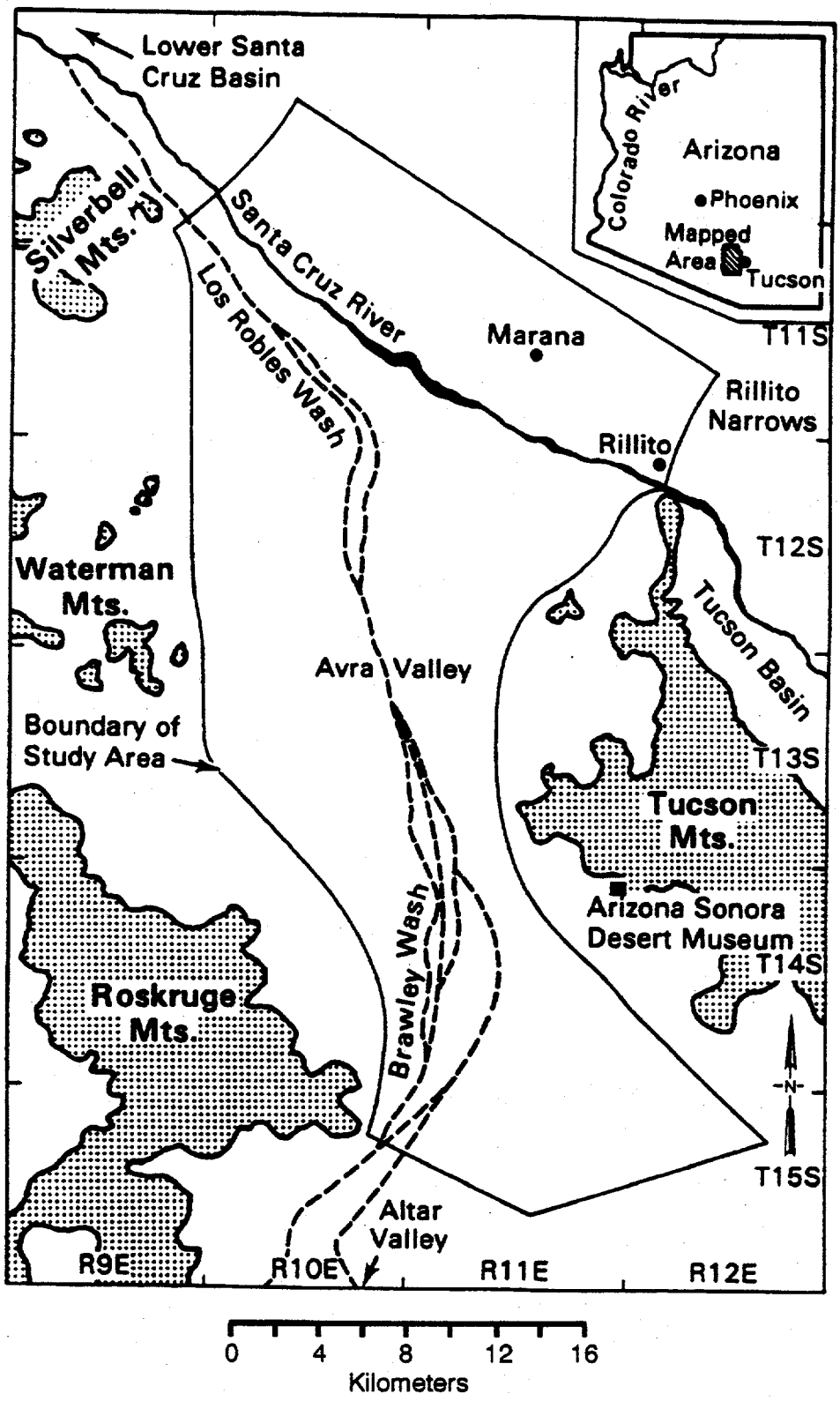

Figure 1. Location and physiographic setting of Avra Valley and study area boundary (from Clifton, 1981).

consists of sandy gravel, gravely sand, silt, and clay. The upper 180 to 210 m of the alluvium appear to be hydraulically connected and form a single unconfined aquifer with groundwater flowing to the north and northwest.

For an inverse model, Clifton (1981) used a finite-element grid with 176 nodes, shown in Figure 2. No-flow boundaries, also shown in Figure 2, were assumed along most of the mountain flanks except for a small amount of recharge through a pediment on the northwest side of the Tucson Mountains. An estimate of 6.2×10^5 m^3/yr for the recharge rate through this pediment is based on the mountain-front recharge rates along the Tucson Mountains determined by Osterkamp (1973). The northern boundary of the finite-element grid was placed to coincide with a streamline of Clifton's water-level contour map and represents another no-flow boundary. Prescribed head boundaries are assigned between the Avra Valley and its three adjoining groundwater basins: (1) the upper Santa Cruz Basin in the south, (2) the Tucson basin in the northeast, and (3) the lower Santa Cruz Basin in the northwest.

Transmissivity Data

Transmissivities based on recovery data from aquifer tests are available at 42 locations. An additional 106 transmissivity values have been estimated from specific capacities using a regression procedure described by Clifton and Neuman (1982). Transmissivities in the northern third of the aquifer have a geometric mean of about 2000 m^2/d, while in the south the geometric mean of the transmissivities is about 670 m^2/d. The higher transmissivities in the north may be due to channel deposition of sand by the Santa Cruz River according to Clifton and Neuman (1982).

For the inverse model, the Avra Valley has been divided into 122 zones, shown in Figure 3 (Clifton, 1981). The log transmissivity in each zone is determined by block kriging. However, the mean of the log transmissivity is not constant in space, which is a violation of one of the requirements for simple kriging. To alleviate this problem, Clifton (1981) divides the aquifer into two regions separated by the dashed line shown in Figure 3. Contour plots of the kriged log transmissivity estimates and the associated kriging errors are presented in Figure 4; the transmissivity values are expressed in m^2/day. The kriging errors of the log transmissivities are highest along boundaries where there are few measured data, especially in the southeast corner of the study area.

Hydraulic Head Data

Hydraulic head measurements were available at 99 locations inside or near the study area, as shown in Figure 2. Neuman and Jacobson (1984) apply their method to estimate the hydraulic head at node points and conclude that a fourth order drift is necessary to yield intrinsic residuals. Lamorey and Jacobson (1994) consider fourth and fifth order drift solutions for the Avra Valley hydraulic head data and find that the fourth order drift solution produces residuals with an anisotropic sill, thus a

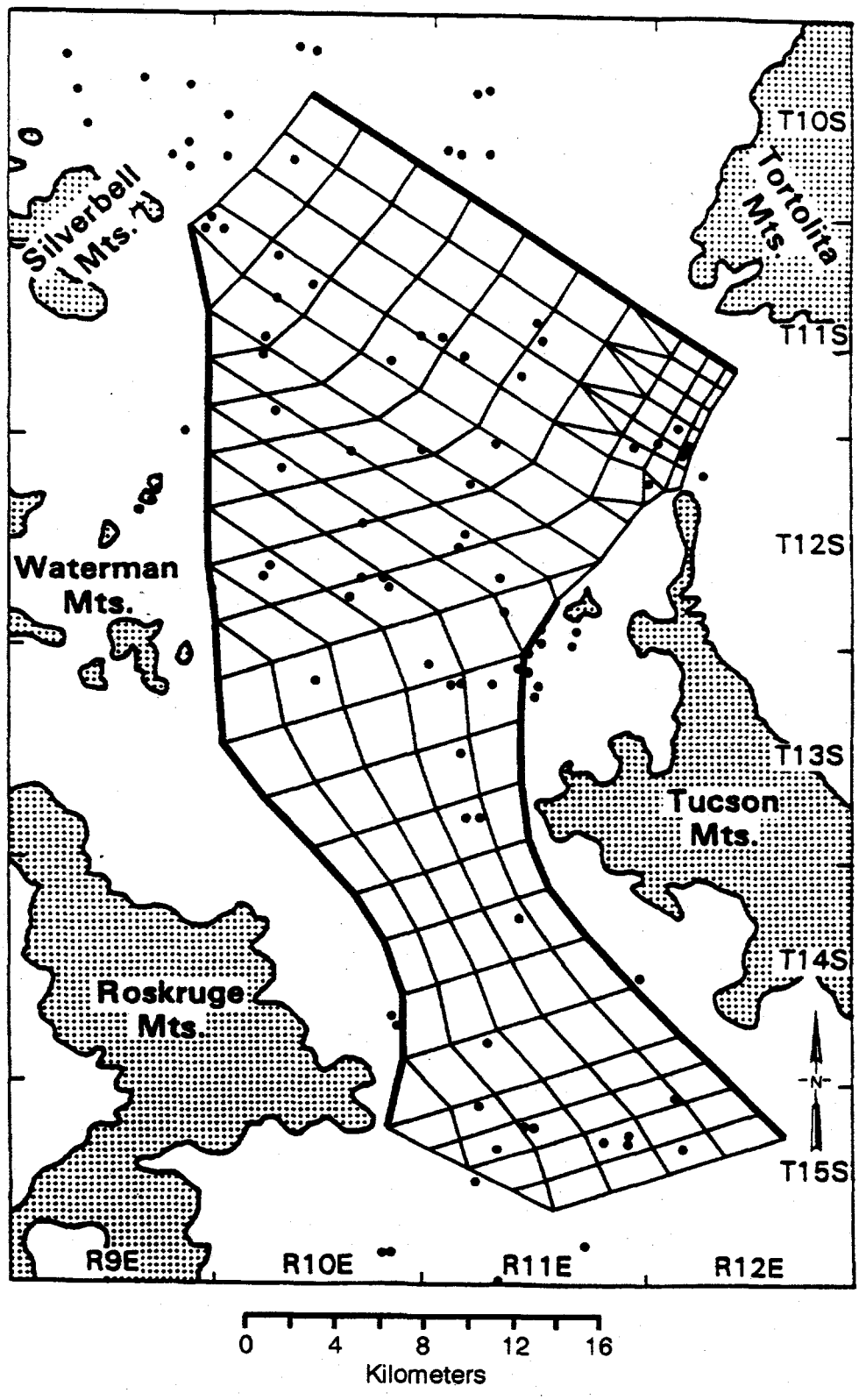

Figure 2. Location of wellbore water level data and finite element grid for hydraulic head estimates in Avra Valley including no-flow boundary (bold line) (from Clifton, 1981).

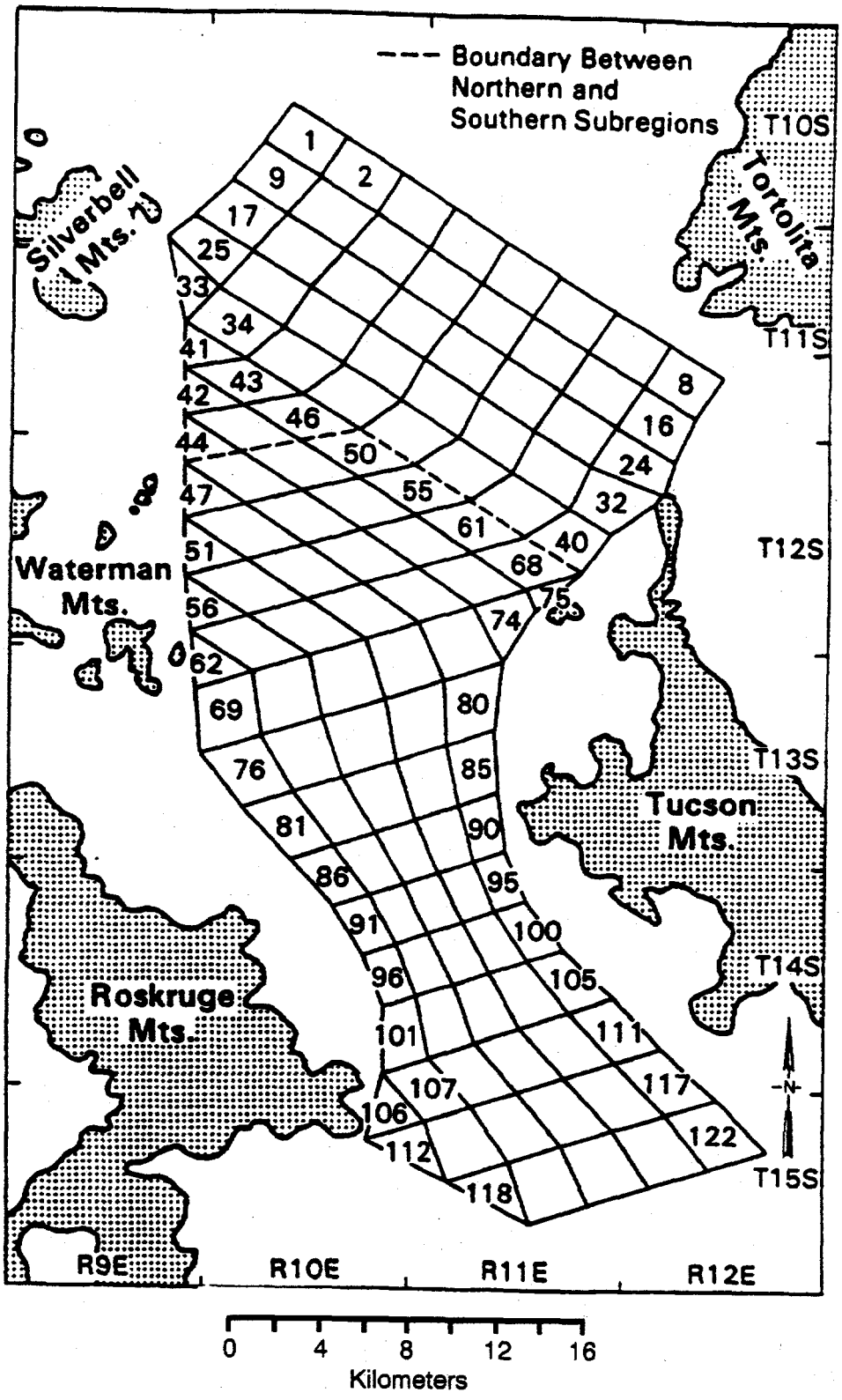

Figure 3. Zonation pattern for estimation of log transmissivities in the Avra Valley (from Clifton, 1981).

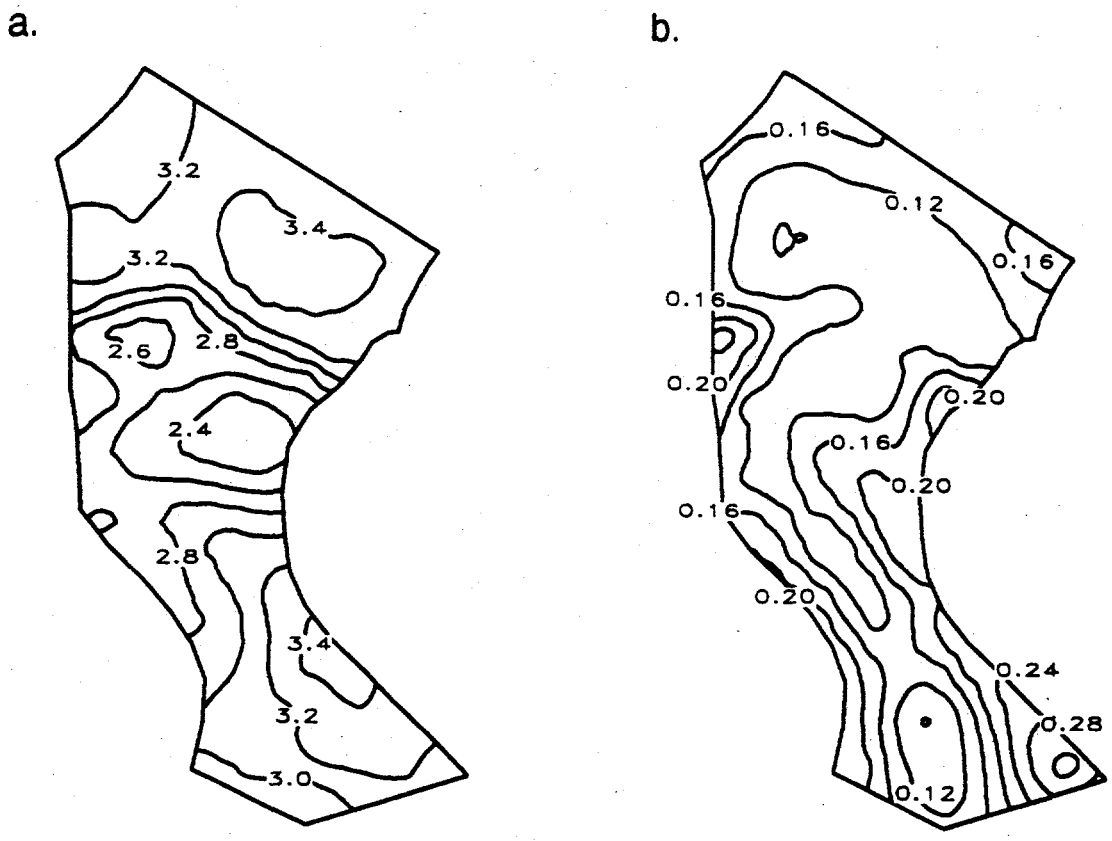

Figure 4. Contour plots for (a) prior estimates of the log transmissivities and (b) the associated estimation errors (after Clifton, 1981).

fifth order drift solution may be necessary to obtain intrinsic residuals. However, the fifth order drift solution produces residuals that are not normally distributed, indicating that the fifth order solution could be overfitting the head data.

Lamorey and Jacobson (1994) apply no-flow boundary constraints to both the fourth and fifth order drift solutions for the drift of the hydraulic head. They found that the sample semivariogram of the head residuals from a fourth order drift solution was much more sensitive to the no-flow boundary constraints than the fifth order drift solution. They also found that the tradeoff between fitting the head measurements and fitting the no-flow boundary constraints was much more favorable for the fifth order drift solution. Lamorey and Jacobson (1994) could not conclude if the fourth or fifth order drift was more appropriate, since the fifth order drift solution showed indications that it overfit the data, while the fourth order drift solution produced head residuals that contain a trend.

The hydraulic head estimates and estimation errors determined by Lamorey and Jacobson (1994) for fourth and fifth order drift solutions without boundary constraints and with boundary

constraints are used in the Avra Valley aquifer inverse model. Initially, fourth and fifth order drift solutions without boundary constraints for the prior head values are implemented. Then hydraulic heads estimated with various levels of no-flow boundary constraint weightings for both the fourth and fifth order solutions are considered. Results from the inverse model, including estimated log transmissivities, log transmissivity estimation errors, and other model statistics, are examined to identify the most appropriate drift order and no-flow boundary constraints weighting for estimating the hydraulic heads.

Inverse Model Results Using Hydraulic Heads Estimated without Boundary Constraints

Hydraulic head values estimated using fourth and fifth order drift solutions are shown in Figures 5a and 5b. The head estimation errors using the method described by Lamorey and Jacobson (1994) for the fourth and fifth order drift solutions are shown in Figures 5c and 5d. For the fourth order drift, the head values and estimation errors were calculated with a head residual range of 4.46 km and a sill of 8.58 m^2. For the fifth order drift, a head residual range of 4.28 km and sill of 4.94 m^2 was used. The two solutions yield similar head distributions with the largest differences in the southern end of the aquifer. The head estimation error distribution from the two solutions are also similar with high values in the northeast and southeast corners of the aquifer. The fifth order drift solution has slightly lower head estimation error values in the interior due to the lower sill, but much higher values in peripheral regions with few head measurements. These values for the head estimates and estimation errors are used in the inverse model with the prior transmissivity estimates and estimation errors shown in Figure 4. Resulting model statistics for various values of λ are summarized in Figure 6. As previously discussed, the optimum λ should be indicated by a value of $\tilde{\lambda}$ approaching λ, a small value of J_h, a small absolute value of $\bar{z}_h$, a minimum in the log likelihood criterion (ML), and a high χ^2 statistic indicating a normal distribution of the weighted hydraulic head residuals.

Plots of $\tilde{\lambda}$, J_h, $\bar{z}_h$, ML, and the χ^2 statistic shown in Figure 6 for the prior heads determined from fourth and fifth order drift solutions are similar. The maximum likelihood and χ^2 statistic for the two prior heads differ the most, but still show similar trends. The fifth order drift solution for prior heads reaches higher χ^2 values over a smaller range of λ values, indicating an optimum λ around 1 or slightly less. The χ^2 values for the prior heads estimated with the fourth order drift has two major local maximums at λ values of about 5 and 0.5. The maximum likelihood criterion reaches a minimum at a λ of about 0.2. The $\tilde{\lambda}$ plot shows optimums at λ equal to about 50 and 0.05 for both fourth and fifth order drift prior heads. The J_h decreases with decreasing λ, as expected, with no distinct inflection to indicate an optimum λ. Values of $\bar{z}_h$ are close to zero for values of λ less than or equal to 1. Jacobson (1994) obtained similar results for prior heads estimated with a fourth order drift using the kriging variance method to determine the head estimation errors. If the estimation errors of

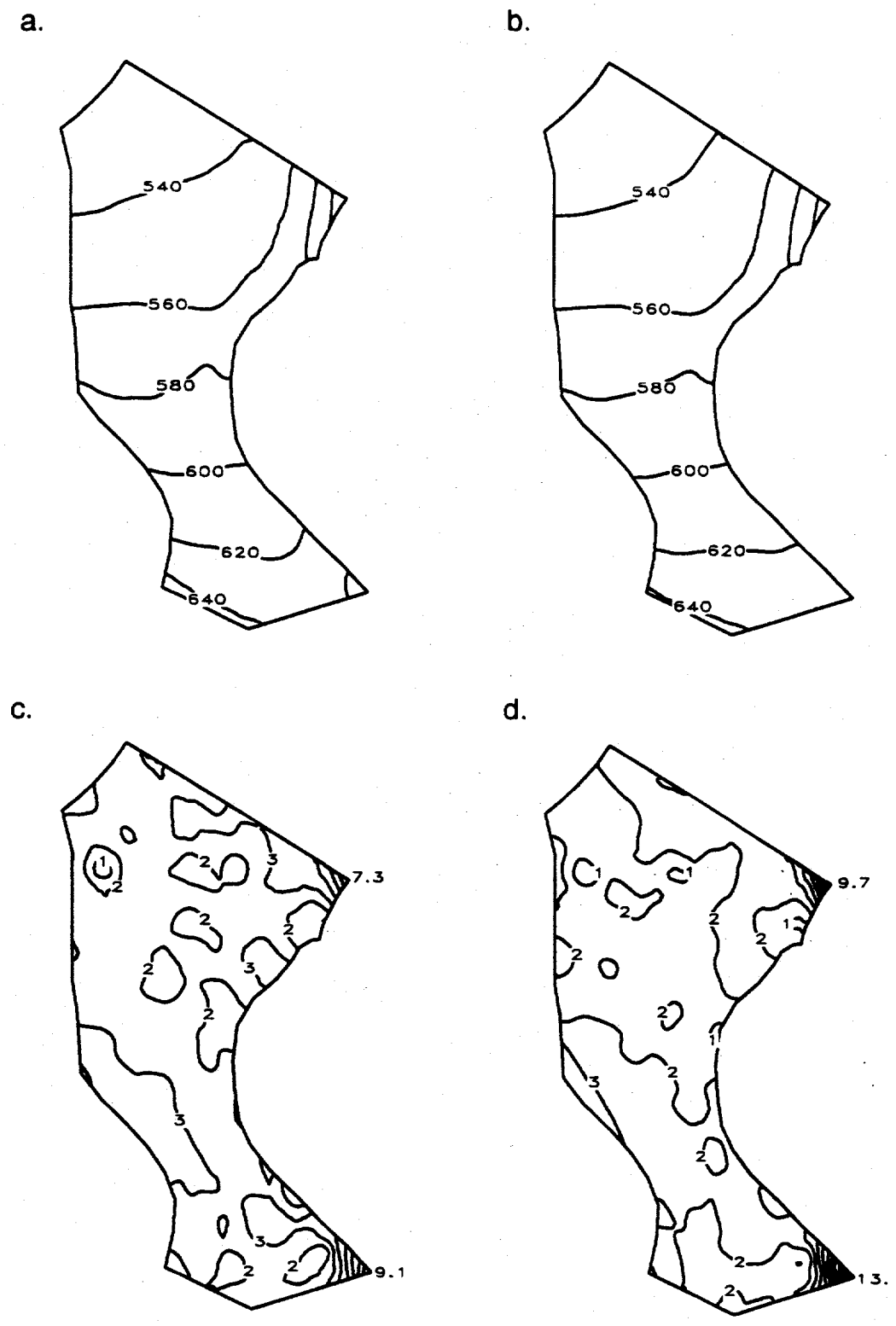

Figure 5. Contour plots for prior heads in meters A.M.S.L. estimated with (a) fourth and (b) fifth order drift solutions and associated estimation errors in meters for the prior heads estimated with (c) fourth and (d) fifth order drift solutions.

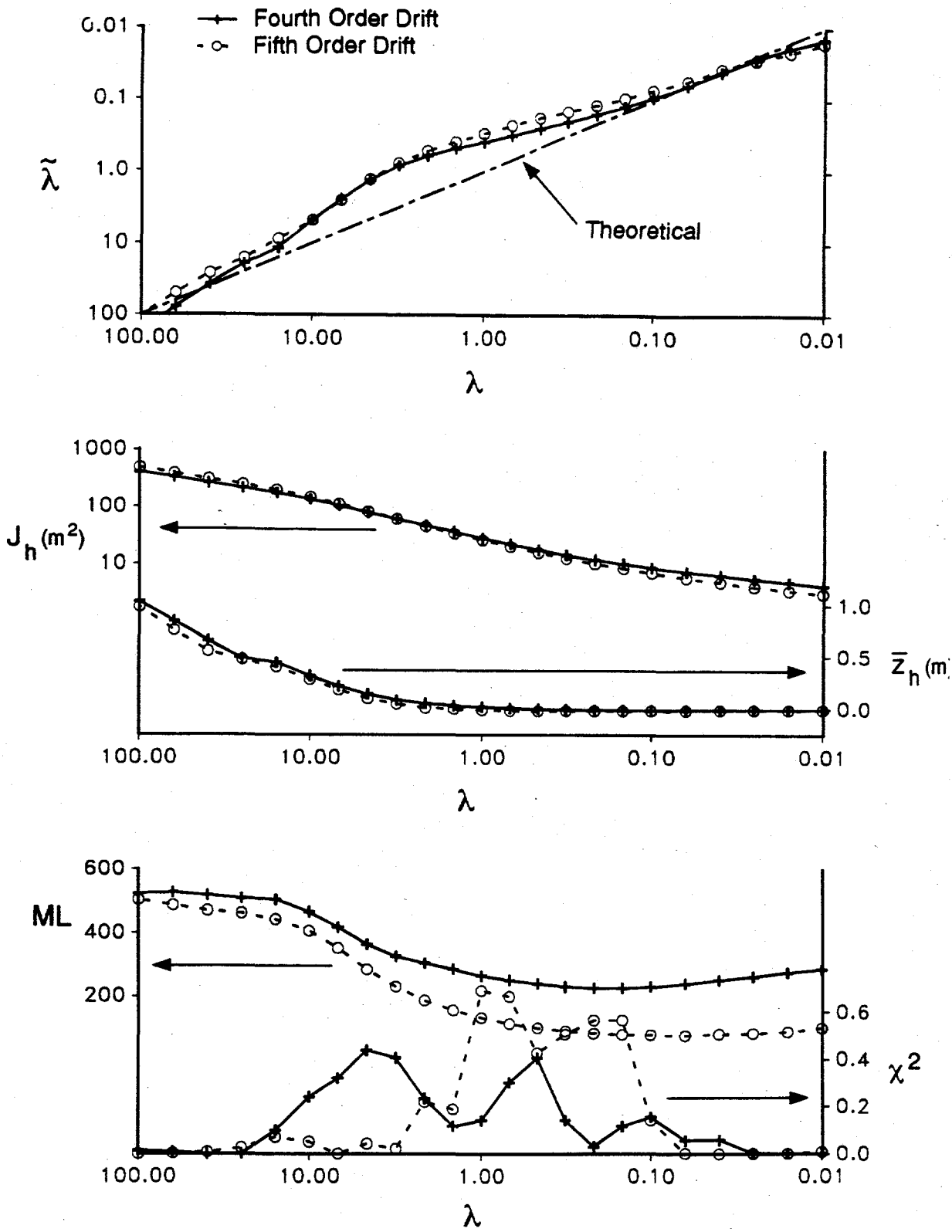

Figure 6. Plots of $\tilde{\lambda}$, J_h, $\bar{z}_h$, ML, and a statistic based on the χ^2 test verses λ for inverse model using prior heads estimated with a fourth and fifth order drift solutions.

the prior log transmissivities and heads have been accurately specified, the optimum λ should be one. Although the plots in Figure 6 do not indicate a clear optimum, a λ value of one is a reasonable choice. This choice is supported by the $\bar{z}_h$ plot and the χ^2 plot; it is also the choice of Jacobson (1994).

The log transmissivities from the inverse model for λ equal to one are shown in Figures 7a and 7b for prior heads determined from the fourth and fifth order drift solutions, respectively. One way to examine the effects of an inverse model on the prior transmissivities is to subtract the log transmissivities estimated by the inverse model from the prior log transmissivity estimates. Contour plots of these differences for the fourth and fifth order drift solutions are presented in Figures 7c and 7d, respectively. The fourth and fifth order drift prior heads produce similar transmissivity distributions with the largest changes in the transmissivities in the northeast and southeast corners. However, the fourth order drift solution shows a much greater change in the southeast corner and a large gradient in the estimated transmissivities along the south end of the east no-flow boundary. It appears that the prior heads determined with the fourth order drift solution produce a zone of low transmissivity along the south end of the east no-flow boundary to try and reconcile the no-flow boundary condition and the gradient in the hydraulic heads. Lamorey and Jacobson (1994) found that the fifth order drift solution produced prior head estimates that fit the no-flow boundary much better in the southeast corner of the aquifer.

The log transmissivity estimation errors from the inverse model with λ equal to one and prior heads determined from fourth and fifth order drift solutions are shown in Figures 8a and 8b, respectively. The transmissivity estimation errors can also be examined by subtracting the log transmissivity estimation errors determined from the inverse model from the prior log transmissivity estimation errors. The resulting contour plots, shown in Figures 8c and 8d, for fourth and fifth order drift solutions, indicate how much the estimation error of the transmissivities is reduced by the inverse model. Caution must be exercised when comparing the transmissivity estimation errors since the inverse estimation errors are calculated assuming the correct optimum λ. The fourth and fifth order drift solutions show the largest reductions in the transmissivity estimation error in remote regions of the aquifer where there are few head or transmissivity measurements. The fifth order solution shows more of a reduction in the estimation error than the fourth order solution. However, this could be due to the lower head residual sill of the fifth order drift solution since the sill is used to calculate the prior head estimation error. The lower head residual sill of the fifth order drift solution could represent an actual reduction in the head estimation error or be a product of overfitting the data as discussed by Lamorey and Jacobson (1994).

Inverse Model Results Using Hydraulic Heads Estimated with Boundary Constraints

Prior heads calculated with two levels of uniform weighting of the no-flow boundary constraints are considered here. A weighting of 0.125 gives each of the 75 boundary constraints one

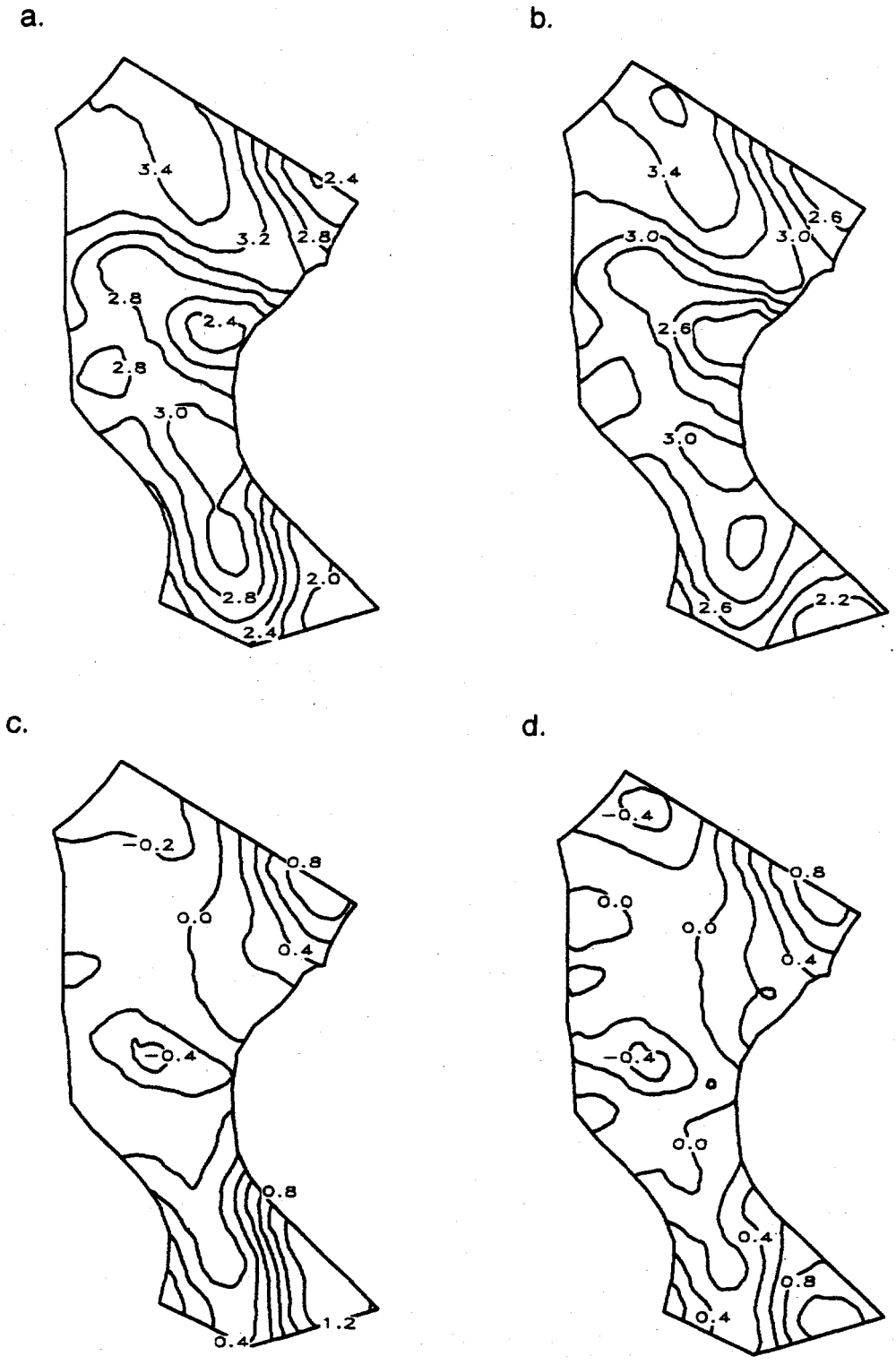

Figure 7. Contour plots of log transmissivities from inverse model using a (a) fourth and (b) fifth order drift solution to estimate the prior heads. Contour plots of estimated log transmissivities subtracted from the prior log transmissivities using a (c) fourth and (d) fifth order drift solution to estimate the prior heads.

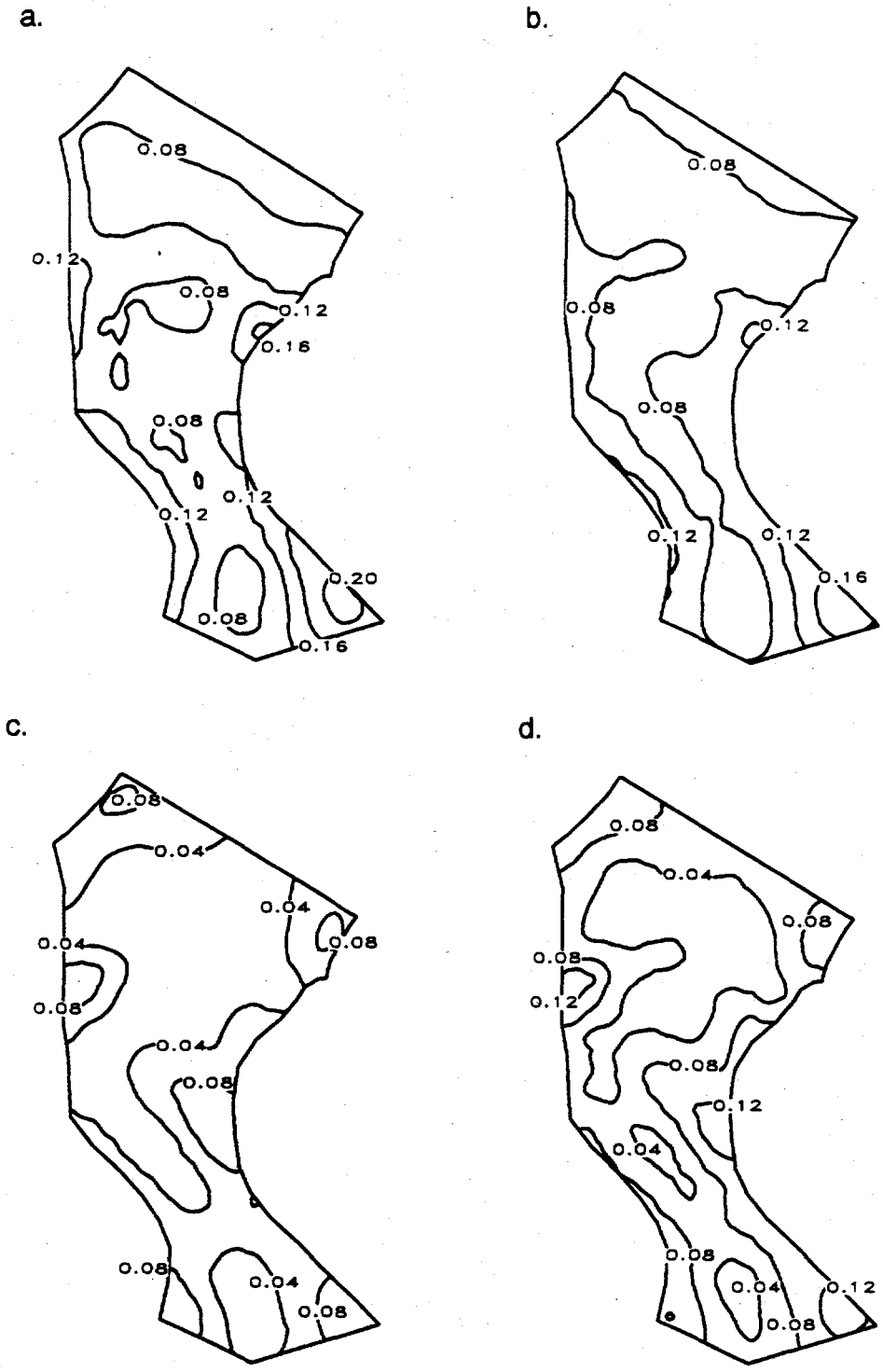

Figure 8. Contour plots of log transmissivity estimation errors from inverse model using a (a) fourth and (b) fifth order drift solution to estimate the prior heads. Contour plots of log transmissivity estimation errors subtracted from the prior log transmissivity estimation error using a (c) fourth and (d) fifth order drift solution to estimate the prior heads.

eighth of the weighting of each of the 99 head measurements. A heavier weighting of 0.5 gives each of the boundary constraints one half the weight given to each head measurement. These two levels of boundary constraint weighting were examined in detail by Lamorey and Jacobson (1994) and represent light to moderate boundary constraint weighting.

Boundary constraints are considered first for the fourth order drift solution for the prior heads. As the weighting of the boundary constraints was increased from 0 to 0.125 to 0.5, the range of the prior head residuals was found to increase from 4.46 to 4.81 to 5.52 km, while the sill increased from 8.58 to 9.37 to 12.11 m^2 for the fourth order drift solution. The sill increases as the boundary constraint weighting is increased because of the increased misfit of the measured heads.

The effect of the boundary constraints on the prior heads can be examined by subtracting the heads estimated with the boundary constraints from the heads estimated without the boundary constraints. These differences are presented for the fourth order drift solution with boundary constraint weightings of 0.125 and 0.5 in Figures 9a and 9b, respectively. For the 0.125 weighting, the differences in the head values is small except in the northeast and southeast corners where the change is 10.3 and 7.0 m, respectively. For the 0.5 weighting, the difference in the northeast and southeast corners increases to 22.1 and 18.4 m, respectively, and there is a change of 4.3 m along the central portion of the west no-flow boundary.

The head estimation error for the prior heads estimated by a fourth order drift solution with boundary constraint weightings of 0.125 and 0.5 are shown in Figures 9c and 9d, respectively. These plots can be compared to the head estimation errors without boundary constraints shown in Figure 5c. As the weighting on the boundary constraints is increased, the head estimation errors in the northeast and southeast corners decreases, while in most other areas there is a slight increase due to the larger sill of the head residuals.

Inverse model statistics for prior heads estimated with a fourth order drift solution and boundary constraints of 0.125 and 0.5 are plotted as a function of λ in Figure 10. Statistics obtained with no boundary constraint weighting are included in Figure 10 for comparison. The plots of $\bar{\lambda}$, J_h, z_h, ML, and the χ^2 statistic show similar trends with and without boundary constraints on the prior head estimates. The maximum likelihood criterion decreases for prior heads estimated with higher weighting on the boundary constraints, but the location of the minimum remains at a λ value of about 0.2. The χ^2 statistic changes with the different boundary constraints weightings with no clear optimum at any weighting. Again, the plots do not indicate a clear optimum λ value and a λ of one is a reasonable and consistent choice.

The log transmissivities calculated with a λ value of one and boundary constraint weightings of 0.125 and 0.5 are shown in Figures 11a and 11b, respectively. These log transmissivities are

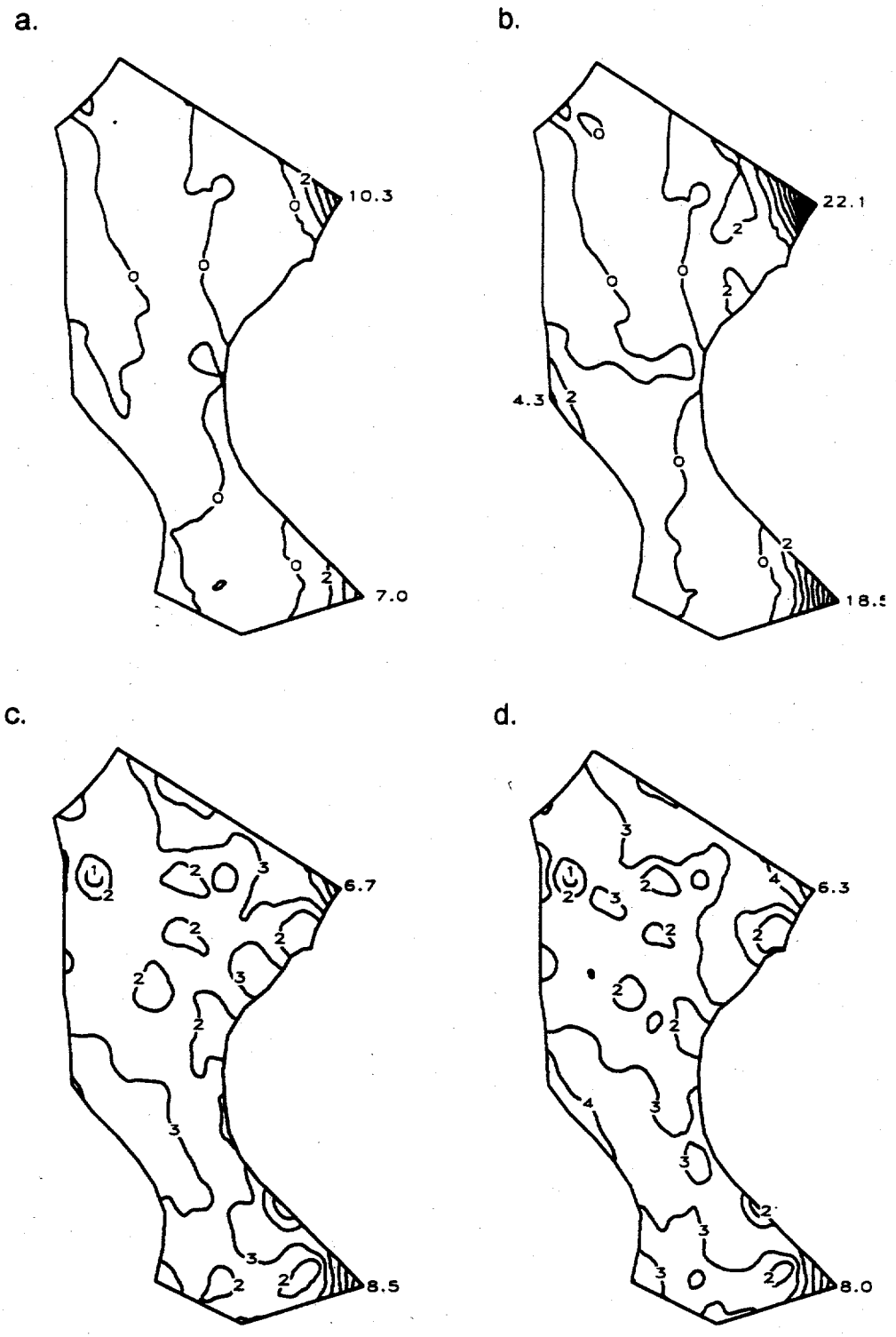

Figure 9. Contour plots of the difference between prior heads in meters estimated with a fourth order drift solution and no boundary constraints and (a) 0.125 boundary constraint weighting and (b) 0.5 boundary constraint weighting. Contour plots of prior head estimation errors in meters for a fourth order drift solution and (c) 0.125 boundary constraint weighting and (d) 0.5 boundary constraint weighting.

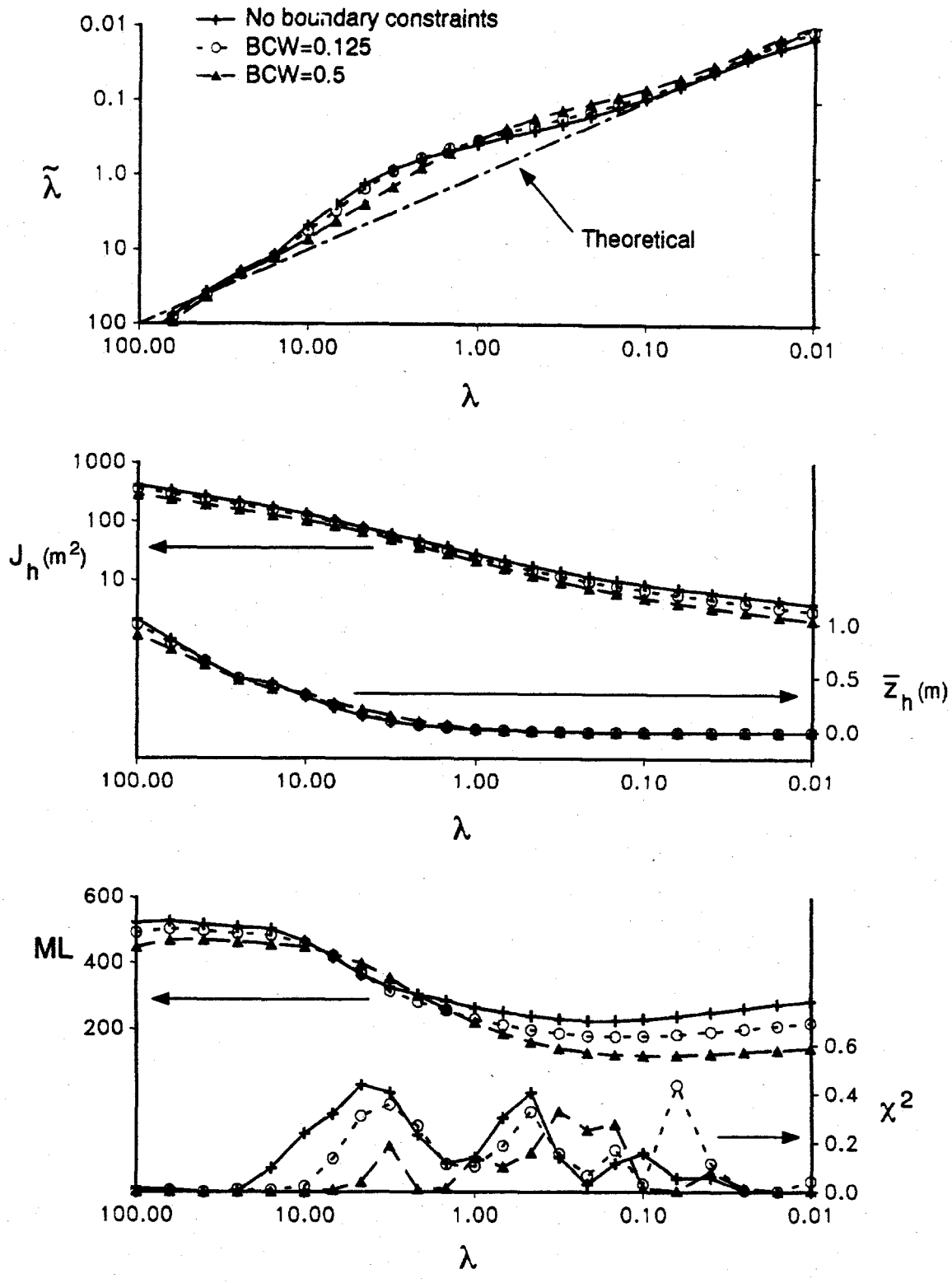

Figure 10. Plots of $\tilde{\lambda}$, J_h, $\bar{z}_h$, ML, and a statistic based on the χ^2 test verses λ for inverse model using prior heads estimated with a fourth order drift solution and boundary constraint weighting (BCW) of 0, 0.125 and 0.5.

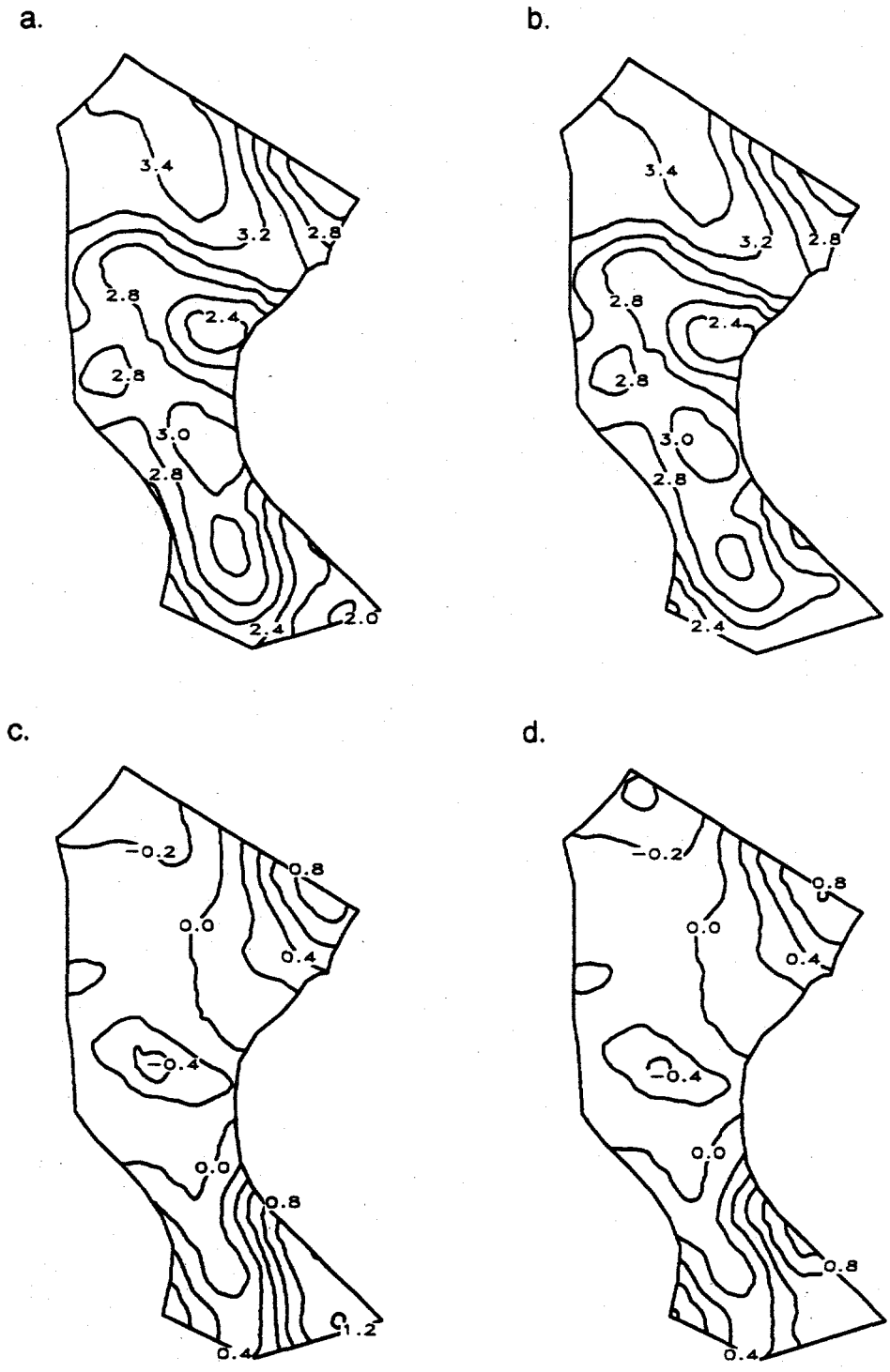

Figure 11. Contour plots of log transmissivities estimated with prior heads determined using fourth order drift solution and (a) boundary constraint weighting of 0.125 and (b) 0.5 for head estimates. Contour plots of differences between prior log transmissivities and log transmissivities estimated with prior heads determined using fourth order drift solution and (c) boundary constraint weighting of 0.125 and (d) 0.5.

subtracted from the prior log transmissivities and the differences are plotted in Figures 11c and 11d for the 0.125 and 0.5 weightings, respectively. The contour plots in Figure 11 can be compared to results with no boundary constraints shown in Figures 7a and 7c. The only region of the aquifer where the boundary constraints on the prior heads result in significantly different transmissivities in the southeast corner. Higher log transmissivities in the southeast corner counteract the previously discussed tendency for the inverse model to try and reconcile the no-flow boundary and the head gradient. There is also much less of a gradient in the calculated log transmissivities along the southern end of the east boundary as the weighting on the boundary constraints is increased. However, even with the higher boundary constraint weighting on the prior heads, the differences in prior and estimated log transmissivities in the southeast corner are strongly aligned with the no-flow boundary. Although the biggest difference in the prior heads when boundary constraints are applied occurs in the northeast corner, the log transmissivities are affected much less here than in the southeast corner.

Estimation errors for the log transmissivities shown in Figure 11 are presented in Figures 12a and 12b. Figures 12a and 12b are very similar and show the same pattern of estimation errors obtained without the boundary constraints on the prior heads shown in Figure 8a. Again, the contour plots for differences between the prior log transmissivity estimation errors and the log transmissivity estimation errors from the inverse model are presented in Figures 12c and 12d. As the weighting on the boundary constraints are increased, there is a slight decrease in the estimation errors throughout the aquifer with the largest decrease in the southeast corner. As previously discussed, the differences in the log transmissivity estimation errors are dependent on the correct determination of the optimum λ.

The fifth order solution for the prior heads with boundary constraints of 0.125 and 0.5 are also considered in the inverse model. The range and sill of the head residuals from the fifth order solution were less sensitive to the boundary constraints than the heads from the fourth order drift solution. As the weighting of the boundary constraints was increased from 0 to 0.125 to 0.5, Lamorey and Jacobson (1994) found that the range of the head residuals changed only slightly, from 4.28 to 4.25 to 4.24 km, while the sill increased from 4.94 to 5.27 to 5.72 m^2.

Differences between prior heads estimated using the fifth order drift solution with boundary constraint weightings of 0.125 and 0.5 and those estimated without boundary constraints are presented in Figures 13a and 13b, respectively. The estimation errors associated with the fifth order drift prior heads estimated with boundary constraints are presented in Figures 13c and 13d. As with the fourth order drift solution, the largest changes in the prior head estimates and estimation errors due to the weighting of the boundary constraints are in the northeast and southeast corners of the study area. However, the fifth order drift solution shows smaller changes in the prior head values and larger changes in the estimation error when compared to the fourth order drift solution.

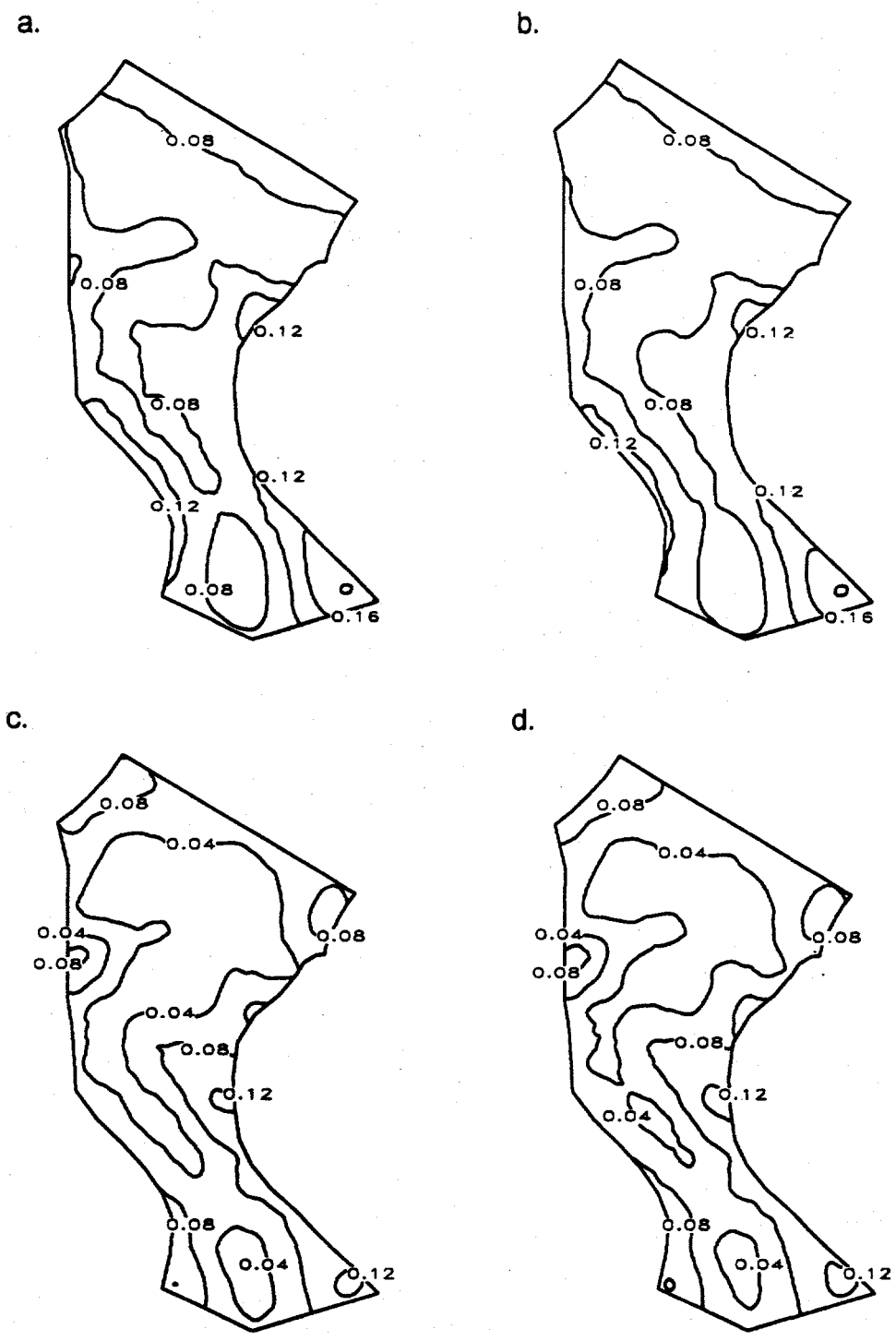

Figure 12. Contour plots of log transmissivity estimation errors with prior heads determined using fourth order drift solution and (a) boundary constraint weighting of 0.125 and (b) 0.5 for head estimates. Contour plots of differences between prior log transmissivity estimation errors and log transmissivity estimation errors from prior heads determined using fourth order drift solution and (c) boundary constraint weighting of 0.125 and (d) 0.5.

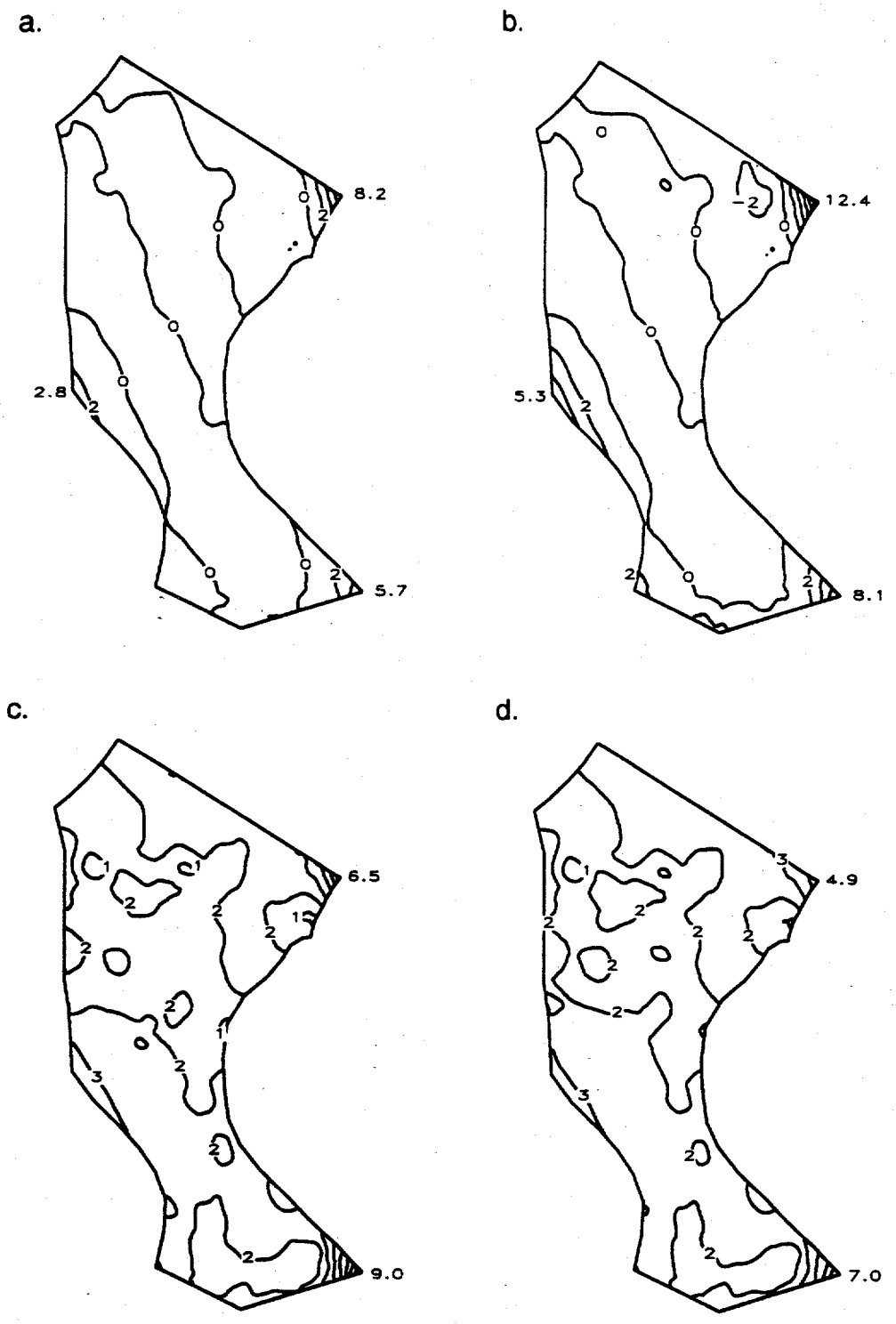

Figure 13. Contour plots of the difference between prior heads in meters estimated with a fifth order drift solution and no boundary constraints and (a) 0.125 boundary constraint weighting and (b) 0.5 boundary constraint weighting. Contour plots of head estimation errors in meters for a fifth order drift solution and (c) 0.125 boundary constraint weighting and (d) 0.5 boundary constraint weighting.

Inverse model statistics for prior heads estimated with a fifth order drift solution and boundary constraint weightings of 0, 0.125, and 0.5 are plotted as a function of λ in Figure 14. The inverse model statistics using prior heads estimated with a fifth order drift solution and boundary constraints follow the same trends as observed without the boundary constraints. The χ^2 statistic with the boundary constraint weighting of 0.5 is below 0.2 for all values of λ, indicating that the weighted head residuals from the inverse model are not normally distributed and that a lower weighting of the boundary constraints may be preferred.

The log transmissivities calculated with a λ value of 1 and boundary constraint weightings of 0.125 and 0.5 are shown in Figures 15a and 15b, respectively. Differences between the prior log transmissivities and the inverse log transmissivities in Figures 15a and 15b are presented in Figures 15c and 15d. When these contour plots are compared to contour plots without boundary constraints, shown in Figures 7b and 7d, the largest differences in the log transmissivities are found in the southeast corner of the aquifer. As with the fourth order drift solution results, these changes in log transmissivities in the southeast corner of the aquifer counteract the tendency for the model to produce low transmissivities along the no-flow boundary.

Estimation errors for the log transmissivities shown in Figure 15 are presented in Figures 16a and 16b. The plots for differences between prior log transmissivity estimation errors and log transmissivity estimation errors determined from the inverse model are presented in Figures 16c and 16d. The transmissivity estimation errors are reduced slightly when the boundary constraint weighting is 0.125. The transmissivity estimation errors for the 0.5 boundary constraint weighting are slightly greater than those calculated without using the boundary constraints to estimate the prior heads, especially in the southeast corner. This, together with the low χ^2 values for the 0.5 weighting, indicates that this level of boundary constraint weighting may be too high for the fifth order drift solution.

Evaluation and comparison of transmissivity estimates and estimation errors for the different prior heads depends on the correct determination of the optimum λ. A λ of 1 assumes that the prior transmissivity and head estimation errors have been accurately determined. When the inverse model statistics were used to identify an optimum λ, the mean of the weighted head residuals, $\bar{z}_h$, approached zero at λ values of about 1 for fourth and fifth order drift prior heads with and without boundary constraints. Figure 17 presents a closer view of $\bar{z}_h$ for the different prior heads at values of λ between 10 and 0.1. The fifth order drift prior heads produced $\bar{z}_h$ values that approach zero at slightly lower λ values than the fourth order drift prior heads, indicating a lower optimum λ. The prior heads with increased boundary constraint weightings also produced $\bar{z}_h$values that indicate a slightly lower optimum λ. If the sill of the prior head residuals is overestimated due to the presence of a trend, then

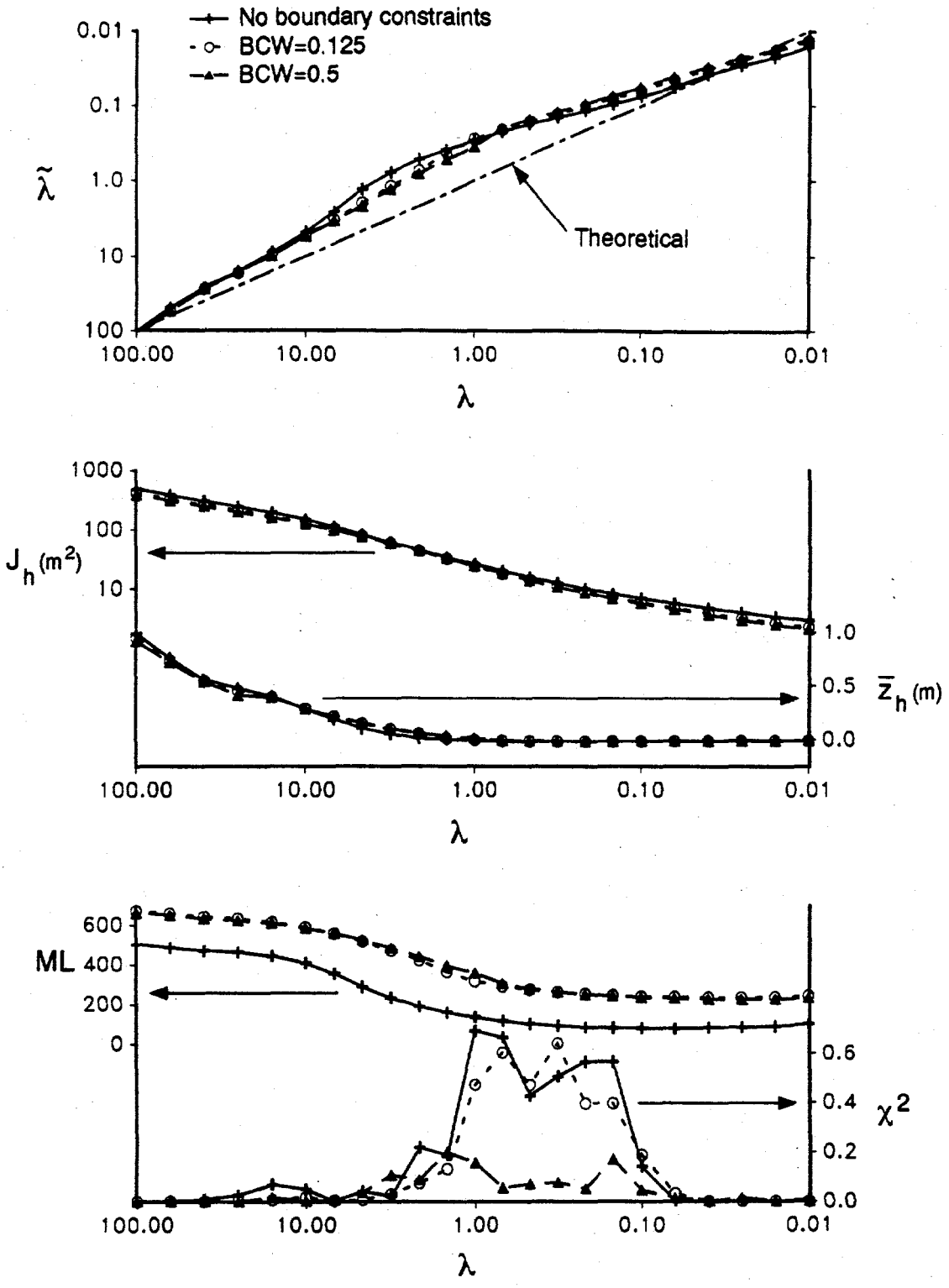

Figure 14. Plots of $\tilde{\lambda}$, J_h, $\bar{z}_h$, ML, and a statistic based on the χ^2 test verses λ for inverse model using prior heads estimated with a fifth order drift solution and boundary constraint weighting (BCW) of 0, 0.125 and 0.5.

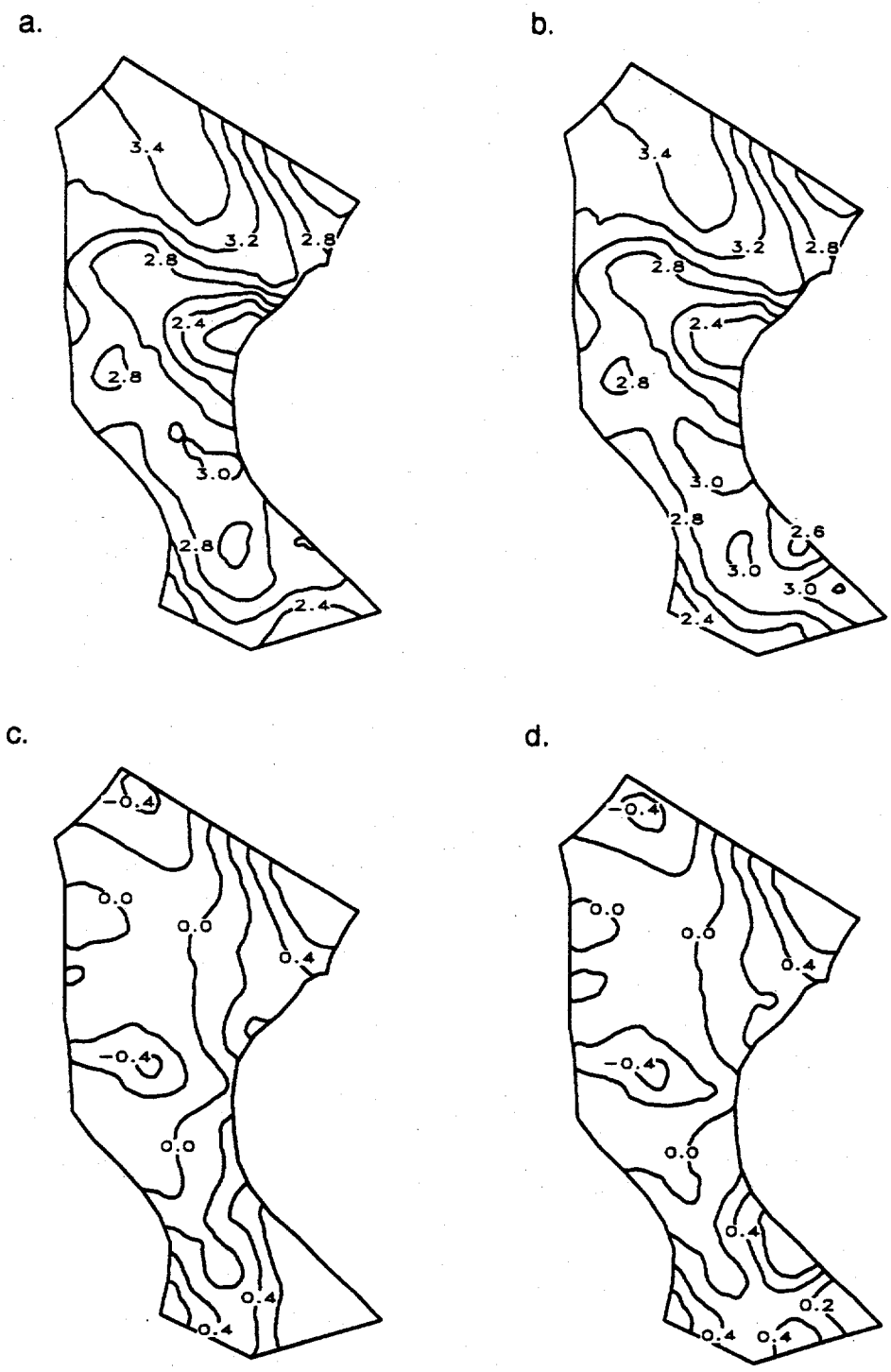

Figure 15. Contour plots of log transmissivities estimated with prior heads determined using fifth order drift solution and (a) boundary constraint weighting of 0.125 and (b) 0.5 for head estimates. Contour plots of differences between prior log transmissivities and log transmissivities estimated with prior heads determined using fifth order drift solution and (c) boundary constraint weighting of 0.125 and (d) 0.5.

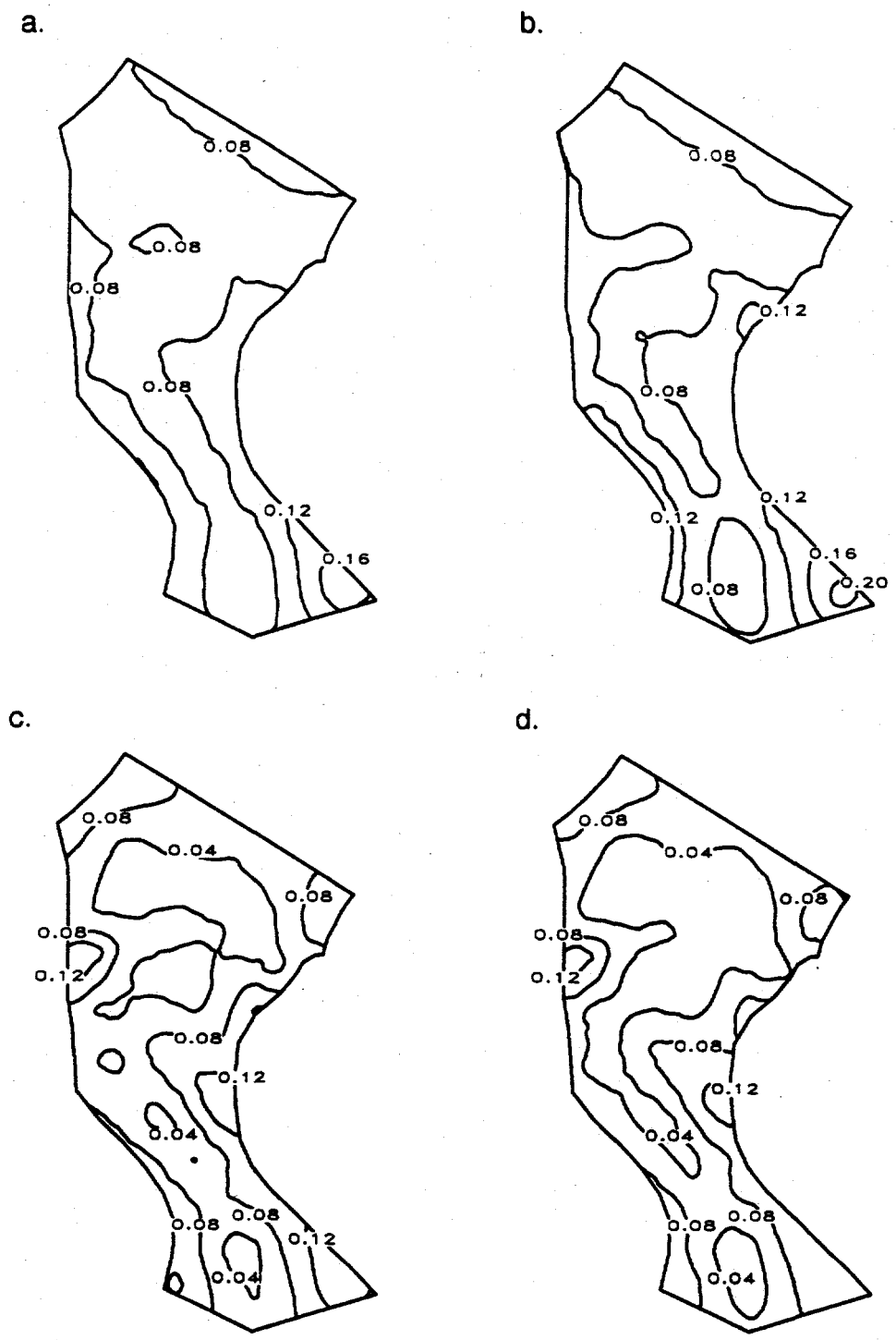

Figure 16. Contour plots of log transmissivity estimation errors with prior heads determined using fifth order drift solution and (a) boundary constraint weighting of 0.125 and (b) 0.5 for head estimates. Contour plots of differences between prior log transmissivity estimation errors and log transmissivity estimation errors from prior heads determined using fifth order drift solution and (c) boundary constraint weighting of 0.125 and (d) 0.5.

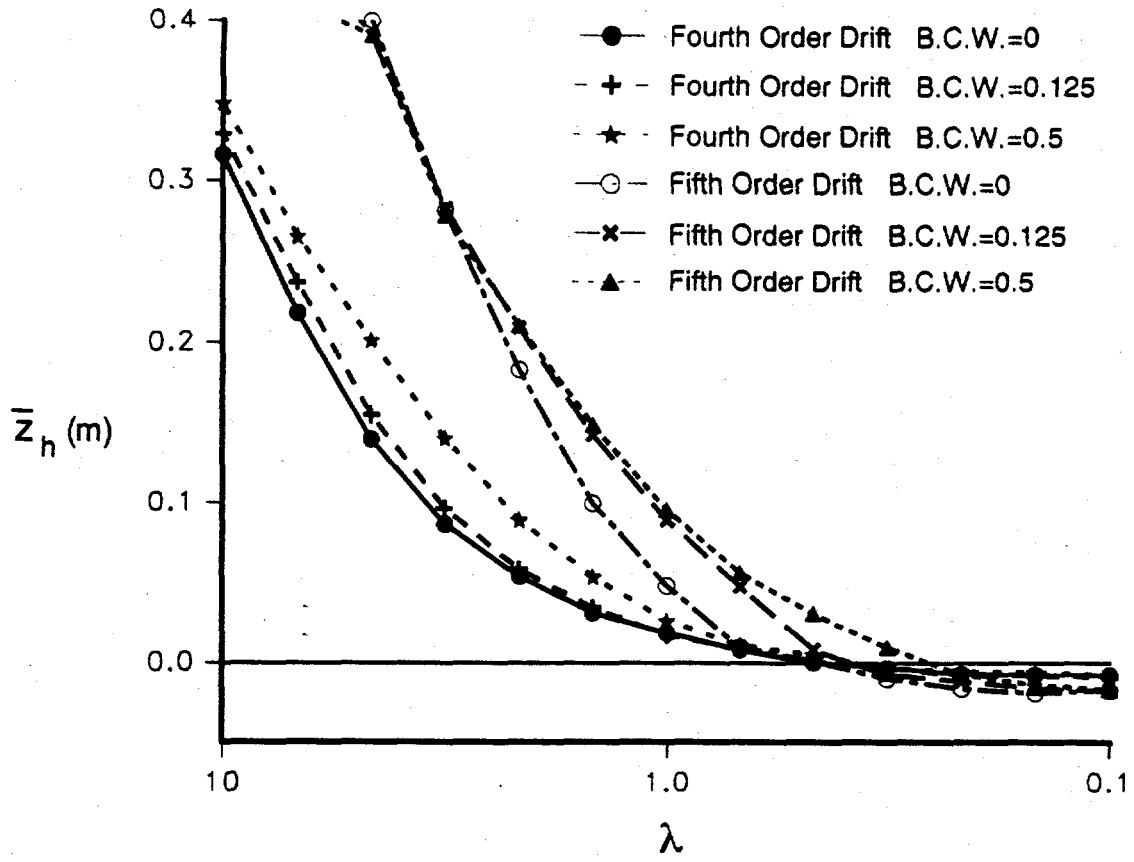

Figure 17. Plot of $\bar{z}_h$ verses λ for inverse model using fourth and fifth order drift prior heads with various boundary constraint weighting (BCW).

the prior heads will be weighted too little at λ = 1 because the estimation errors for the prior heads are too large. In this case, the optimum λ will be less than 1 to increase the weighting of the prior heads. This can explain the change in $\bar{z}_h$ values as the boundary constraint weighting is increased. However, this does not explain the difference of the $\bar{z}_h$ curves between the fourth and fifth order drift prior heads. If the fourth order drift prior heads residuals contain a trend, then the $\bar{z}_h$ curve should be displaced towards smaller λ values compared to the fifth order prior heads and it is not. The differences between the $\bar{z}_h$ curves for the fourth and fifth order drift prior heads could be due to basically different z_h distributions.

CONCLUSIONS

Prior heads estimated from fourth and fifth order drift solutions were considered in an inverse model of the Avra Valley aquifer. Inverse model statistics used to determine the optimum weighting

of prior heads relative to prior log transmissivities, or optimum λ value, were very similar for the fourth and fifth order drift prior heads. Neither indicated a clear optimum, but a λ of 1 was a reasonable choice for both cases. An optimum λ value of 1 is expected if the estimation errors on the prior log transmissivities and prior heads are accurate.

With a λ of 1, the fourth and fifth order drift prior heads produced similar log transmissivities except in the southeast corner of the aquifer. In this region, the fourth order drift solution resulted in low log transmissivities along the no-flow boundary as the inverse model attempted to try and reconcile the no-flow boundary and the hydraulic head gradient. Although the fifth order drift prior heads produced log transmissivity estimates lower than the prior log transmissivities in the southeast corner, the changes in the log transmissivities are not aligned along the no-flow boundary as with the fourth order drift prior heads.

The fifth order drift prior heads produced lower transmissivity estimation errors than the fourth order drift prior heads throughout the aquifer. However, the fifth order drift solution may be overfitting the head data and producing head residuals with a semivariogram sill that is too low. This would help to reduce the transmissivity estimation errors, but it would also imply that the optimum λ is not 1.

The boundary constraints were included in the fourth and fifth order drift solutions for the prior heads used in the inverse model. The inverse model statistics used to identify an optimum λ changed little with the boundary constraints applied to the prior heads. The χ^2 statistic used to determine if the weighted head residuals produced by the inverse model are normally distributed dropped dramatically for all values of λ with the fifth order drift prior heads at the higher boundary constraint weighting. This could indicate that the lower boundary constraint weighting is more appropriate for the fifth order drift prior heads.

For both fourth and fifth order drift solutions, the boundary constraints on the prior heads resulted in little difference in the estimated transmissivities, except in the southeast corner of the aquifer. Here, the heads estimated with the boundary constraints fit the no-flow boundary condition better and did not produce as low transmissivities values as without the boundary constraints. However, the fourth order drift prior heads with boundary constraints still produced lower log transmissivity estimates that were strongly aligned with the no-flow boundary. The fourth order drift prior heads required higher boundary constraint weightings than the fifth order drift prior heads to produce significant changes in the estimated log transmissivities. This could be because the fourth order drift does not have the flexibility needed to accommodate the boundary condition in the southeast corner of the aquifer.

The boundary constraints weightings of 0.125 and 0.5 applied to the fourth order drift prior heads reduced the log transmissivity estimation errors in the southeast corner of the aquifer with little change elsewhere. The boundary constraints weighting of 0.125 applied to the fifth order drift prior heads reduced the log transmissivity estimation errors slightly throughout the aquifer. With a boundary constraint weighting of 0.5 applied to the fifth order drift prior heads, the log transmissivity estimation error is slightly greater than with no boundary constraints on the prior heads. These small changes in the log transmissivity estimation errors should be interpreted with care since they assume the correct optimum λ. However, the increase in the log transmissivity estimation errors for the fifth order drift prior heads with the higher boundary constraint weighting could be another indication that this level of weighting is too high.

The northern two thirds of the aquifer shows little change in log transmissivities or their estimation errors for the fourth or fifth order drift prior heads with or without boundary constraints. Even where the boundary constraints produce different prior head estimates and estimation errors, such as in the northeast corner, the estimated inverse log transmissivities are not very sensitive to these differences.

The prior heads estimated with a fourth order drift solution produce log transmissivities in the southeast corner that appear to be affected by inconsistencies between the head gradient and the no-flow boundary, even when boundary constraints are applied to the prior head estimates. This implies that the fifth order drift is necessary to accommodate the boundary conditions in this region. The fifth order drift prior heads with the lower boundary constraint weighting of 0.125 produced the most reasonable solution for the log transmissivities as determined by examining statistics from the inverse model and the resulting log transmissivities and estimation errors.

REFERENCES

Carrera, J. and S.P. Neuman, 1986. Estimation of aquifer parameters under transient and steady-state conditions: 1. Maximum likelihood method incorporating prior information, *Water Resources Research*, 22(2):199–210.

Clifton, P.M., 1981, Statistical Inverse Modeling and Geostatistical Analysis of the Avra Valley Aquifer, M. S. Thesis, University of Arizona, Tucson.

Clifton, P.M. and S.P. Neuman, 1982. Effects of kriging and inverse modeling on conditional simulation of the Avra Valley aquifer in southern Arizona, *Water Resources Research*, 18(4):1215–1234.

Cooley, R.L., 1977. A Method of estimating parameters and assessing reliability for models of steady-state groundwater flow, 1, Theory and numerical properties, *Water Resources Research*, 13(2):318–324.

Delhomme, J.P., 1978. Kriging in the hydrosciences, *Advances in Water Resources*, 1(5):251–266.

Emsellem, Y. and G. de Marsily, 1971. An automatic solution for the inverse problem, *Water Resources Research*, 7(5):1264–1283.

Jacobson, E.A., 1985. A Statistical Parameter Estimation Method Using Singular Value Decomposition with Application to Avra Valley Aquifer in Southern Arizona, Ph.D. Thesis, University of Arizona.

Jacobson, E.A., 1994. Estimation of aquifer parameters with measured and kriged hydraulic head data, accepted for publication in *Groundwater*.

Lamorey, G.W. and E.A. Jacobson, 1994. Incorporation of constraints on hydraulic head gradients near no-flow boundary conditions in the determination of spatial drift, to be submitted to *Water Resources Research*, included in this dissertation as Chapter 2.

Neuman, S.P., 1973. Calibration of distributed parameter groundwater flow models viewed as a multiple-objective decision process under uncertainty, *Water Resources Research*, 9(4):1006–1021.

Neuman, S.P., 1980. A statistical approach to the inverse problem of aquifer hydrology, 3, Improved Solution method and added perspective, *Water Resources Research*, 16(2):331–346.

Neuman, S.P., 1982. Statistical Characterization of Aquifer Heterogeneities: An Overview, Recent Trends in Hydrogeology, G.S.A. Special Paper 189, pp. 81–102, Geological Society of America, Boulder, CO.

Neuman, S.P. and E.A. Jacobson, 1984. Analysis of nonintrinsic spatial variability by residual kriging with application to regional groundwater levels, *Mathematical Geology*, 16(5):499–521.

Neuman, S.P. and S. Yakowitz, 1979. A statistical approach to the inverse problem of aquifer hydrology, 1, Theory, *Water Resource Research*, 15(4):845–860.

Osterkamp, W.R., 1973. Ground–water Recharge in the Tucson, Arizona, U.S. Geological Survey Miscellaneous Series, Map I–844–E, 1 sheet.

Schweppe, F., 1973. Uncertain Dynamic Systems, Prentice–Hall, Englewood Cliffs, New Jersey.

Seber, G.A.F., 1977. Linear Regression Analysis, John Wiley, New York.

Yeh, W.W–G., 1975. Optimal identification of parameters in an inhomogeneous medium with quadratic programming, *Society of Petroleum Engineering Journal*, 15(5):371–375.

Yeh, W.W–G. and Y.S. Yoon, 1981. Parameter identification with optimum dimension in parameterization, *Water Resources Research*, 17(3):664–672.